MULTIPLE ENZYMATIC FUNCTIONS OF SIRT2 AND ITS INVOLVEMENT IN CANCER

A Dissertation

Presented to the Faculty of the Graduate School

of Cornell University

In Partial Fulfillment of the Requirements for the Degree of

Doctor of Philosophy

by

Hui Jing

December 2017

MULTIPLE ENZYMATIC FUNCTIONS OF SIRT2 AND ITS INVOLVEMENT IN CANCER

Hui Jing, Ph. D.

Cornell University 2017

SIRT2 belongs to the mammalian sirtuin or NAD-dependent lysine deacylase family. Growing evidence suggests that SIRT2 plays important roles in cell cycle regulation, stress response, metabolism and differentiation by deacetylating a wide variety of substrates. Targeting SIRT2 for cancer treatment has been a topic of debate due to conflicting reports and lack of potent and specific inhibitors.

I began the project with the development and mechanistic study of SIRT2 inhibitors. From a collection of mechanism-based small molecule inhibitors mimicking different lysine acyl modifications, I characterized that a thiomyristoyl lysine compound (TM), a potent SIRT2-specific inhibitor, has broad anticancer effect in various human cancer cells and mouse models of breast cancer. Mechanistically, I demonstrated that SIRT2 inhibition promotes c-Myc ubiquitination and degradation and that the anticancer effect of TM correlates with its ability to decrease c-Myc level. This study suggests that SIRT2 inhibition could be utilized to target c-Myc and that potent and selective SIRT2 inhibitors are promising anticancer agents.

SIRT2 has been reported to have lysine defatty-acylase activity in addition to the previously known deacetylase activity. However, whether the defatty-acylase activity is physiologically relevant has not been investigated. I identified the oncoprotein K-Ras4a as a SIRT2 defatty-acylase substrate. I further elucidated that SIRT2-mediated lysine defatty-acylation promotes endomembrane localizaiton of K-Ras4a, enhances its interaction with A-Raf, and thus promotes cellular transformation. This study not only highlights lysine fatty

acylation as a previously unknown regulatory mechanism for the Ras family of GTPases that is distinct from cysteine fatty acylation, but also unveils a new mechanism by which SIRT2 is involved in cancer by defatty-acylating K-Ras4a. This finding also provides further support that SIRT2 is a promising target for cancer treatment.

BIOGRAPHICAL SKETCH

Hui Jing was born in Shanxi province, China. She earned her Bachelor's degree in Science in 2009 and Master's degree in Pharmacology in 2012 from Zhejiang University in China. She joined the Department of Chemistry and Chemical Biology at Cornell University as a graduate student in 2013. Under Prof. Hening Lin's guidance, she studies the multiple enzymatic functions of SIRT2 and its relevance to cancer. She won Bayer Teaching Excellence Award as a chemistry teaching assistant in 2015 and is a Howard Hughes Medical Institute international student research fellow since 2016.

Dedication

To

My beloved parents and grandparents

My lovely husband and little daughter

ACKNOWLEDGMENTS

First and foremost, I would like to express the deepest appreciation to my advisor, Professor Hening Lin. He is both a mentor and role model for me in my endeavor to become a scientist. He has allowed me freedom to formulate my research project while still provide guidance when needed. I am and will be always grateful to him for the immense support and great opportunities he has provided me.

I would like to thank my thesis committee: Professor Robert Weiss and Professor Richard Cerione for their guidance and support. Their advice on my project, ranging from experimental details to broader scope and vision, has been invaluable.

My thanks to the people who have contributed to my project through collaboration and who have provided consultation for my work. These include Professor Robert Weiss and his lab members, Jack Stupinski, Yashira Negron for the collaboration on the in vivo study of SIRT2 inhibitors; Professor Paraskevi Giannakakou and her lab member, Dr. Keren Weiser and Dr. Marisa Carbonaro for the collaboration on the cellular effects of TM on SIRT2; Dr. Zhenglong Gu and his lab members, Dr. Xuepeng Sun and Ruoyu Wang for the collaboration on RNA-sequencing and data analysis; Professor Quan Hao and his lab member, Dr. Yan-bin Teng for the collaboration on the defatty-acylation activity of SIRT2; Professor Maurine Linder for her invaluable advice and support on the K-Ras4a lysine fatty acylation project.

I would like to thank the members of the Lin lab, past and present, for providing an enjoyable and collaborative environment to work in. And I would like to specifically acknowledge those who I have been fortunate to work closely with during my time in the lab. Dr. Jing Hu has helped me immensely with the SIRT2 inhibitor project and taught me a lot of biochemical techniques during my first year. Dr. Bin He and Dr. Jing Hu have done much pioneer work on SIRT2 inhibitor, without which I would not have

been able to work on the project. Dr. Ying-ling Chiang and Nicole Spiegelman have also spent a lot of effort on synthesizing SIRT2 inhibitor and Alk14 probe, which have ensured my project to proceed smoothly. Dr. Hong Jiang, Dr. Bin He and Dr. Ji Cao have also helped me with many experimental details and provided helpful discussion on my project. And many thanks to our lab manager, Xuan Lu, for her tireless dedication to everyone in the lab, and for her generous help both inside and outside of the lab. I have also had the opportunity to work with an undergraduate student, Stephanie Wisner. She has been a great asset and has made great contributions to my project. It has always been a pleasure to work with and learn from everyone in the lab.

Many thanks to Cornell Chemistry and Chemical Biology program for their training and support, and Howard Hughes Medical Institute International Student Research Fellowship for supporting my last year of graduate study.

Finally, I would like to thank my friend and family for the selfless support along my way. Special thanks go to my husband, Xiaoyu Zhang, for his continuous and unfailing love, support, understanding and help. He has worked closely with me on identifying K-Ras4a as a SIRT2 substrate, and provided immense help and support to my work. He helps me to keep things in perspective and encourages me to go forward. His unwavering love has made the years with him the best time of my life. I appreciate my baby, my little girl, Chloe Zhang, for coming to my life and being the light of my life. She has given me extra strength to move forward. The last word of acknowledgement goes to my parents for showing faith in me and the unconditional support. I am deeply grateful to the selfless care and sacrifice they did to shape my life.

TABLE OF CONTENTS

LIST OF FIGURES

LIST OF TABLES

CHAPTER 1

INVOLVEMENT OF SIRT2 IN CANCER: AN OVERVIEW [a]

1. Introduction

Sirtuins are a family of enzymes with nicotinamide adenine dinucleotide (NAD)-dependent protein lysine deacylase. Yeast Sir2, the founding member of all sirtuins, was initially found to be important for calorie restriction-induced life span extension in yeast [1]. Subsequent biochemical studies demonstrate that it is an NAD-dependent deacetylase that regulates histone acetylation [2]. This connection between aging and metabolism (the fact that it uses a metabolic important molecule, NAD, as a co-substrate) attracted great interest into this class of enzymes.

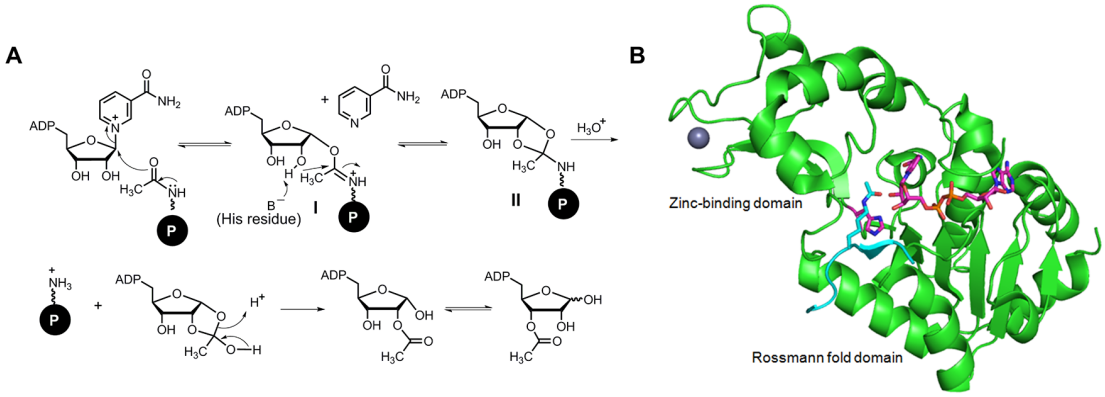

Figure 1.1 The enzymatic function of sirtuins. (A) The enzymatic reaction mechanism of sirtuins. (B) The structure of a ternary sirtuin-NAD-acetyl peptide complex (PDB ID 2H4F). NAD, acetyl lysine, and the key catalytic His residue are shown in stick representation. The bound zinc is shown in grey sphere. The protein structure picture is generated using PyMol.

The enzymatic reaction mechanism for sirtuin-catalyzed NAD-dependent protein lysine deacetylation has been well understood through a series of elegant biochemical and structural studies (Figure 1.1) [3,4]. The conserved catalytic core of sirtuins consists of a zinc-binding domain and a Rossmann fold domain (Figure 1.1B) [5-7]. The active site lies at the interface of the

[a] This is a revised version of our published review articles: Hu, J., Jing, H. & Lin, H. Sirtuin inhibitors as anticancer agents. *Future Med Chem* **6**, 945-66 (2014); Jing, H. & Lin, H. Sirtuins in epigenetic regulation. *Chem Rev* **115**, 2350-75 (2015).

two domains. It was thought that the acetyl lysine peptide binds first, followed by the binding of NAD [8]. Once the tertiary complex is formed, the carbonyl oxygen of the acetyl group attacks the C1'-position of the nicotinamide ribose, displacing nicotinamide and forming the alkylamidate intermediate (intermediate I, Figure 1.1A) [3]. A conserved histidine residue then serves as a general base to deprotonate the ribose 2'-OH, which then attacks intermediate I at the carbonyl carbon, generating the 1',2'-cyclic intermediate (intermediate II, Figure 1.1A). Intermediate II is then hydrolyzed to produce 2'-O-acetyl-ADP-ribose (2'-O-Ac-ADPR), which can be non-enzymatically isomerized to 3'-O-Ac-ADPR [3,4].

In mammals, there are seven sirtuins (SIRT1-7) that localize in different subcellular compartments, such as cytoplasm (SIRT1 and SIRT2), nucleus (SIRT1, SIRT2, SIRT6, and SIRT7) and mitochondria (SIRT3, SIRT4 and SIRT5) [9,10]. By regulating the activity of various substrate proteins, sirtuins are involved in many biological pathways, including transcriptional regulation, genome stability, metabolic regulation, and cell survival [11]. Among the seven sirtuins, SIRT2 is the only predominantly cytosolic member [12,13]. SIRT2 has thus far been characterized primarily as an NAD-dependent deacetylase. It was originally reported to co-localize with microtubules and deacetylate α-tubulin at lysine 40 [13]. Later SIRT2 was also found to be enriched on chromatin and regulate chromatin condensation by deacetyating histone H4 lysine 16 (H4K16) during G2/M transition and mitosis [14]. It was found that SIRT2 actively shuttles between cytoplasm and nucleus during interphase, while it accumulates on mitotic structures during mitosis [15]. As more of SIRT2 substrate proteins (summarized in Table 1.1) have been identified, it has been intimately connected with multiple physiological processes, including cell cycle [16], oxidative stress response [17], metabolism [18,19], microtubule dynamics [13], apoptosis [20], differentiation [21,22] and aging [23]. Therefore, there is growing research interest in exploring the potential of SIRT2 as a therapeutic target for treatment of cancer. Many SIRT2 inhibitors have been reported to have anticancer activities. Research in the past decade, however, has also

disclosed that SIRT2 possesses dual roles in tumorigenesis – they could have both tumor-promoting and tumor-suppressing functions.

Table 1.1 SIRT2 deacetylation substrates

Substrate	Full name	Site of modifications	Function of SIRT2-catalyzed deacetylation
Histones			
H4	Histone H4	K16	Regulates chromatin condensation during metaphase [14]; regulates H4K20 methylation, promotes cell cycle progression and genome stability [24]; suppresses transcription of certain genes [25].
H3	Histone H3	K18	*L. monocytogenes* InlB triggers SIRT2 nuclear localization to suppress gene transcription [26].
		K56	Involved in DNA replication and DNA damage repair [27,28].
Chromatin modifying enzymes			
PR-Set7	N-lysine methyltransferase KMT5A	K90	Promotes PR-Set7 chromatin localization and the establishment of H4K20me1 by PR-Set7 during G2/M phase [24].
Transcription factors			
P300		Many	Promotes binding of p300 to preinitiation complex [29].
FOXO3	Forkhead box protein O3	Unknown	Increases FOXO3 DNA binding and target gene transcription [17]; Increases FOXO3 ubiquitinylation and degradation [30].
FOXO1	Forkhead box protein O1	Unknown	Promotes FOXO1 interaction with PPARg and represses PPARg target genes [21]; Inhibits FOXO1 interaction with ATG7 and autophagic cell death [31].
HIF-1α	Hypoxia-inducible factor 1α	K709	Promotes hydroxylation and degradation of HIF-1α [32].
RelA/p65	RelA/p65 subunit of nuclear factor-κB	K310	Suppresses NF-κB dependent gene expression [33].
PGC-1α	Peroxisome proliferator-activated receptor-γ coactivator 1α	Unknown	Decreases expression of β-oxidation and mitochondrial genes [34].
NRF2	Nuclear factor erythroid-derived 2-related factor 2	K506, 508	Destabilizes NRF2, which leads to reduced ferroportin 1 expression and consequently decreased cellular iron export [35].
Cell cycle related			
BubR1	Mitotic checkpoint serine/threonine-protein kinase BUB1 β	K668	Stabilizes BubR1 and improves cardiac function and extends lifespan in vivo [23].
CDK9	Cyclin dependent kinase 9	K48	Increases CDK9 kinase activity and decrease sensitivity to hydroxylurea-induced replication stress response [36].

CDH1/ CDC20	Fizzy/cell division cycle 20 related 1/ Cell division cycle protein 20	K69 and 159 (CDH1), K66 (CDC20)	Activates the E3 ubiquitin ligase activity, leading to decreased Aurora A level [37].
ATRIP	ATR-interacting protein	K32	Promotes ATR-ATRIP binding to replication protein A-coated single-stranded DNA (RPA-ssDNA) to drive ATR activation and thus facilitate recovery from replication stress [38].
Metabolic enzymes			
LDH-A	Lactate dehydrogenase A	K5	Activates LDH-A [39].
PEPCK	Phosphoenolpyruvate carboxykinase	K70, 71	Inhibits the ubiquitinylation and degradation of PEPCK [18].
ACLY	ATP-citrate lysase	K540, 546, 554	Promotes ATP-citrate lyase degradation [40].
G6PD	Glucose-6-phosphate dehydrogenase	K403	Promotes the formation of active G6PD dimer and increase NADPH production [19,41,42].
PGAM	Phosphoglycerate mutase	K100	Activates PGAM activity [43].
ALDH1A1	Aldehyde dehydrogenase 1A1	K353	Activates ALDH1A1 activity and promote breast cancer stem cells [44].
GKRP	Glucokinase regulatory protein	K5	Destabilizes GFRP, which results in nuclear export of glucokinase and cytosolic glycolysis [45].
PKM2	Pyruvate Kinase 2	K305	Activates PKM2 activity by promoting its tetramerization [46].
Cell signaling related			
PRLR	Prolactin receptor	Many	Facilitates prolactin receptor dimerization and activation of STAT5 [47].
K-Ras	Kirsten rat sarcoma viral oncogene homolog	K104	Promotes K-Ras activity [48].
		K147	Decreases K-Ras activity [49].
PAR-3	Partitioning defective 3 homolog	K831, 848, 881, 1327	Decreases the activity of aPKC and regulates myelin formation [50].
TIAM1	T-cell lymphoma invasion and metastasis 1	K1420	Promotes activation of DVL/TIAM1/Rac axis and cell migration in cancer cells [51].
MKP-1	Mitogen-activated protein kinase phosphatase-1	Unknown	Inhibits MKP-1 activity and consequently activates mitogen-activated protein kinases, which aggravates postischemic liver injury [52].
Structural proteins			
α-tubulin	α-tubulin	K40	Destabilizes microtubule [13].
Keratin 8	Keratin 8	K207	Affects its phosphorylation and filament organization [53].
ANKLE2	Ankyrin repeat and LEM domain containing 2	K302	Regulates ANKLE2 acetylation and phosphorylation dynamics, which is essential for normal nuclear envelope reassembly [54].

I will next discuss the roles of SIRT2 in cancer obtained from genetic studies (knockout, knockdown, and overexpression), the development of sirtuin inhibitors with anticancer activity, and then I will highlight the recent progress on identifying SIRT2 as a versatile lysine deacylase. Finally, I will discuss the rationale behind my doctoral study, which is to establish SIRT2 inhibition as an anticancer strategy and to understand the role of SIRT2 in cancer.

2. Tumor-suppressing roles of SIRT2

The tumor-suppressing role of SIRT2 may come from its ability to maintain genome stability. *Sirt2*$^{-/-}$ mice look grossly normal, but starting from 10 months of age, they tend to have more tumors than the wild type. This effect was attributed to the role of SIRT2 in regulating the genome integrity by deacetylating APC/C (CDH1/CDC20) [55]. The hypothesis was that SIRT2 is important for the mitosis and thus without SIRT2, abnormal cell division occurs and thus tumor arises. However, the increased spontaneous tumor formation in *Sirt2*$^{-/-}$ mice may be strain-dependent and was not seen in another study [24]. Serrano and coworker reported that SIRT2 affects H4K20 methylation by deacetylating H4K16 and histone methyltransferase PR-Set7. *Sirt2*$^{-/-}$ cells have increased H4K16 acetylation levels, decreased H4K20 methylation levels during G2/M transition and M phase. *Sirt2*$^{-/-}$ cells exhibit increased DNA damage and aberrant cell cycle progression compared with wildtype cells. Although no increased spontaneous tumorigenesis was observed in the *Sirt2*$^{-/-}$ mice up to one year of age, increase in tumorigenesis was observed in an induced skin tumor model [24]. A latter study by Zhang et al. defined a function for SIRT2 in regulating replication stress response and genome integrity through deacetylation of CDK9 [36]. SIRT2 interacts with and deacetylates CDK9 in response to replication stress, thereby stimulating CDK9 kinase activity and promoting recovery from replication arrest. More recently, Naini et al. reported that SIRT2 blocks mitotic entry under mitotic stress. Phosphorylation of SIRT2 by cyclin A/CDK2 complex inhibits its activity and its binding affinity to centrosomes and mitotic spindles, promoting G2/M phase transition [56].

The tumor-suppressing role of SIRT2 may come from its ability to deacetylate or inactivate certain transcription factors, kinases, metabolic enzymes or oncoproteins involved in tumorigenesis. SIRT2 deacetylates Hypoxia-inducible factor-1α (HIF-1α), which leads to hydroxylation and degradation of HIF-1α [32]. Loss of SIRT2 increases MEK acetylation and confers resistance to BRAF and MEK inhibitors in BRAF mutant melanoma and K-RAS mutant colon cancers[57,58]. SIRT2 has been shown to inhibit Wnt signaling in nonmalignant cells by directly binding to β-catenin, and thus attenuate cell mobility and invasion [59]. Song et al. recently reported that SIRT2 deletion promotes K-RAS-induced tumorigenesis *in vivo* by regulating K-RAS K147 acetylation status[49]. However, another study by Yang et al. showed that SIRT2 and HDAC6 may promote growth properties of cancer cells by deacetylating K-RAS at K104[48]. Therefore, the regulation of K-RAS by SIRT2 still remains obscure. SIRT2 has been shown to deacetylate and promote the degradation of ATP-citrate lyase (ACLY), which is important for lipid biosynthesis and thus tumor growth. Inhibition of SIRT2 promotes ATP-citrate lyase stability and thus may promote tumor growth [40]. Deacetylation of pyruvate kinase 2 (PKM2) by SIRT2 alters glycolytic metabolism and inhibits malignant growth in cancer cells [46]. Moreover, SIRT2 deacetylates and inhibits the peroxidase activity of peroxiredoxin (Prdx-1) in breast cancer cells, thereby sensitizing breast cancer cells to reactive oxygen species (ROS)-induced DNA damage and cytotoxicity [60].

Consistent with a tumor suppressor role, SIRT2 levels decreased in glioma cells and overexpression of SIRT2 decreased the colony formation of glioma cells [61]. SIRT2 was also found to be downregulated in skin cancer as compared with normal skin. Deletion of SIRT2 increased tumor growth induced by 7,12-dimethylbenz(a)anthracene (DMBA) and 12-O-tetradecanoylphorbol-13-acetate (TPA) [62]. In addition, decreased expression of SIRT2 has also been observed in ovarian carcinoma[63] and colorectal cancer[64] compared with the adjacent non-cancerous tissues.

3. Tumor-promoting roles of SIRT2

In contrast to the tumor suppressor role of SIRT2, SIRT2 has been demonstrated to be tumor-promoting through various mechanisms. One mechanism is that SIRT2 helps to stabilize or activate oncogenes, such as *MYC*, *FOXO and K-RAS*. Thus, inhibiting SIRT2 will destabilize or inactivate these oncogenes and inhibit cancer. SIRT2 inhibition and knockdown have recently been shown to down regulate the C-MYC and N-MYC oncoproteins in neuroblastoma and pancreatic cancer cells [25]. This is achieved by releasing the inhibition of SIRT2 (via its histone deacetylase activity) on the transcription of the ubiquitin ligase NEDD4. SIRT2 has also been reported to deacetylate and decrease the level/activity of FOXO1 [65] and FOXO1 can increase cell death by activating autophagy [66]. Thus, SIRT2 inhibition can promote cell death by increasing FOXO1 activity. SIRT2 can deacetylate K-RAS and promotes it activity and cancer cell growth [67]. SIRT2 has recently been shown to be an AKT binding partner and critical for its activation by insulin [68]. Moreover, SIRT2 deacetylates and stabilizes Slug to promote malignancy of basal-like breast cancer. Slug is well known to promote tumor progression through epithelial-mesenchymal transition (EMT). Therefore, depletion or inhibition of SIRT2 could destabilize Slug and inhibit tumor growth[69].

SIRT2 inhibition has been shown to increase the levels of tumor suppressor genes, such as p53 and p21 [70-72]. Increased p53 level is achieved through deacetylation of p53, but the mechanism for increased p21 level is not clear. Additionally, Soung et al. recently indicated that SIRT2 suppresses the expression of the tumor suppressor Arrestin domain-containing 3 (ARRDC3) in basal-like breast cancer cells by binding and increasing acetylation levels at ARRDC3 promoter [73].

SIRT2 may exert tumor-promoting function by regulating cancer cell metabolism. SIRT2 can deacetylate and activate lactate dehydrogenase A (LDH-A) [74], which is over-expressed in many cancer cells and is responsible for the increased production of lactate in cancer cells.

SIRT2-mediated deacetylation and activation of glucose-6-phosphoate dehydrogenase (G6PD) stimulates pentose phosphate pathway (PPP) to supply cytosolic NADPH in response to oxidative damage[19]. It has been shown that activation of G6PD by SIRT2 promotes glioma cell[42] and leukaemia cell proliferation[41]. Oxidative stress could also activate the glycolytic enzyme phosphoglycerate mutase (PGAM) by SIRT2-dependent deacetylation[43]. Since PGAM plays an important role in NADPH homeostasis and inhibition of PGAM attenuates cell proliferation and tumor growth, SIRT2 may promote tumor growth by regulating PGAM. Moreover, Zhao et al. found that NOTCH signaling activates aldehyde dehydrogenase 1A1 (ALDH1A1) through the induction of SIRT2, leading to ALDH1A1 deacetylation and enzymatic activation to promote breast cancer stem cells[44].

In line with the tumor promoting role of SIRT2, elevated SIRT2 expression in human cancer samples compared with their non-transformed counterparts has been correlated with worse prognosis and poor survival in various cancer types, including acute myeloid leukemia[75], prostate cancer[76], non-small lung cancer[77], breast cancer[69], liver cancers[78] and melanoma[79]. In many cancer cell lines, it has been demonstrated that SIRT2 knockdown or pharmacological inhibition can inhibit cancer cell proliferation and growth [47,71,78,80-86]. For example, expression of SIRT2 has been shown to be crucial for the survival of rhabdomyosarcoma cells[47]. SIRT2 activity has also been demonstrated to be essential for the survival of C6 glioma cells[87].

4. SIRT2 inhibitors

As growing evidence shows that SIRT2 plays a role in many biological processes, there has been sustained interest in developing small molecules that target SIRT2. Below I provide a summary of SIRT2 inhibitors, with a focus on those that have been shown to have anticancer effect.

4.1. Nicotinamide and its analogues

Nicotinamide (Table 1, entry 1) is one of the earliest sirtuin inhibitors discovered. Nicotinamide inhibits SIRT1, SIRT2, SIRT3, SIRT5 and SIRT6 with IC_{50} varying from 50 to 184 μM [88-90]. It has been shown that nicotinamide can block proliferation and promote apoptosis in leukemic cells, and inhibit the growth and viability of human prostate cancer cells [91,92].

Analogues of nicotinamide and benzamide (a nicotinamide mimic) have been sought as sirtuin inhibitors. Two 3'-phenethyloxy-2-anilino benzamide analogues (Table 1.2, entries 2 and 3) were discovered as potent and selective SIRT2 inhibitors with IC_{50} value of 1 μM and 0.57 μM, respectively. Selective SIRT2 inhibition by 3'-phenethyloxy-2-anilinobenzamide leads to increase in α-tubulin acetylation in human colon cancer HCT116 cells [93]. Fragment-based approach led the design of the (5-benzamidonaphthalen-1/2-yloxy) nicotinamide derivatives, among which one compound (Table 1.2, entry 4) shows potent and selective SIRT2 inhibition *in vitro* and in cells [94]. But whether this compound exerts anticancer activity was not further pursued.

AK-1 and AK-7 (Table 1.2, entries 5 and 6), another two benzamide-containing compounds, also exhibit selective SIRT2 inhibition [95]. It has been shown that AK-1 induces cell cycle arrest by promoting degradation of the Snail transcription factor through inactivation of the NF-κB/CSN2 pathway in HCT116 cells[96]. Later, AK-1 was also shown to destabilize HIF-1α under hypoxia in a von Hippel–Lindau tumor suppressor (VHL)-dependent manner in various cancer cell lines[97]. Interestingly, different from SIRT2 inhibition by AK-1, depletion of SIRT2 upregulates HIF-1α[97], suggesting that SIRT2 protein depletion may produce different outcome from activity inhibition or that AK-1 may have off-target effect. Moreover, both AK-1[98] and AK-7[99] have been demonstrated to exert neuroprotection effects *in vitro* and *in vivo* by decreasing sterol biosynthesis. Later, based on computational docking of AK-7 with SIRT2 crystal structure, more benzamide derivatives were designed and synthesized, which led to the discovery of compound 17k (Table 1.2, entry 7) [100]. 17k is selective for SIRT2 (IC_{50} = 0.60 μM)

over SIRT1 and SIRT3 (IC_{50} > 100 μM). However, its biological activity was not further investigated.

AEM1 (Table 1.2, entry 8) was recently identified as a selective SIRT2 inhibitor [101]. It has an IC_{50} value of 18.5 μM against SIRT2, while showing only weak effects on SIRT1 and SIRT3. Addition of a 3-methyl-pridyl group to the carboxamide group of AEM1 (compound AEM2, Table 1.2, entry 8) resulted in an improved IC_{50} value of 3.8 μM against SIRT2. Both of AEM1 and AEM2 sensitize non-small cell lung cancer cells to DNA-damaging agent etoposide-induced apoptosis in a p53-dependent manner [101].

Table 1.2 Nicotinamide and structurally similar analogs

Entry #	Structure	IC_{50}	Biology Activity
1	Nicotinamide 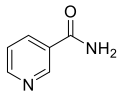	SIRT1: 120 μM[88] SIRT2: 100 μM[90] SIRT3: 50 μM[88] SIRT5: 150 μM[88] SIRT6: 184 μM[89]	Blocks proliferation and promoted apoptosis selectively in leukemic and oral squamous cell carcinoma (OSCC) cells[91,102]; Inhibits the growth and viability of human prostate cancer cells through inhibiting SIRT1[92].
2	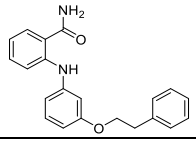	SIRT1: >300 μM SIRT2: 1 μM SIRT3: >300 μM[93]	
3	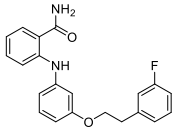	SIRT1: >300 μM SIRT2: 0.57 μM SIRT3: >300 μM[93]	
4	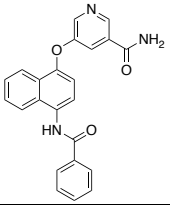	SIRT1: 10.2 μM SIRT2: 0.048 μM SIRT3: 44.2 μM [94]	Induces hyperacetylation of α-tubulin in cells [94].
5	AK-1 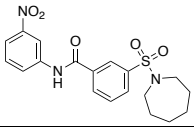	SIRT1: ND SIRT2:12.5 μM[103] SIRT3: ND	Induces cell cycle arrest in HCT116 colon cancer cells[96]; Destabilizes HIF-1α under hypoxia in various cancer cell lines[97];

			Neuroprotective in cellular and invertebrate Huntington's disease model[98].
6	AK-7 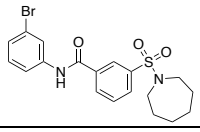	SIRT1: ND SIRT2: 15.5 μM[103] SIRT3: ND	With brain-permeability but limited metabolic stability[95] ; Neuroprotective in Huntington's disease mouse models[99].
7	Compound 17k 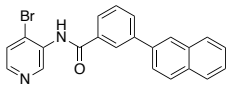	SIRT1: >100 μM SIRT2: 0.6 μM SIRT3: >100 μM	
8	AEM1 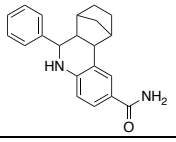	SIRT1: 118.4 μM SIRT2: 18.5 μM SIRT3: 20% inhibition at 50 μM [101]	Sensitize non-small cell lung cancer cells to DNA-damaging agent etoposide-induced apoptosis in a p53-dependent manner [101].
8	AEM2 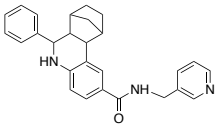	SIRT1: >100 μM SIRT2: 3.8 μM SIRT3: ND [101]	

4.2. Mechanism-based thioacyllysine-containing compounds

Compounds containing N^{ε}-thioacetyllysine (Table 1.3, entries 1-7) can form a covalent ADP-ribose-adduct (1'-S-alkylimidate intermediate) during the first step of the sirtuin-catalyzed deacetylation reaction [104,105]. This intermediate is relatively stable and does not readily undergo the normal downstream reactions. Thus, the intermediate occupies the sirtuin active site and inhibits the enzymatic activity of the sirtuin. Both mass spectrometry and crystal structures support this suicide substrate inhibition mechanism [104,105]. N^{ε}-thioacetyl-lysine was first incorporated into a peptide derived from the C-terminal region of the human p53 protein (amino acid residue 372–389) mimicking the substrate (Table 1.3, entry 1), which shows 2 μM IC_{50} value towards SIRT1 [106]. Since then, a lot of efforts have been invested to further improve this type of mechanism-based inhibitors, including incorporating the N^{ε}-thioacetyl-lysine into tri-,

tetra-, and pentapeptides [107], using various N-acyl group [108-113], changing the lysine side chain [114] as well as the C-terminal of the peptide [109]. However, peptide-based inhibitors are generally not very appealing as they may be unstable and not cell permeable for cellular or *in vivo* studies. Thus, non-peptide N-thioacetyllysine analogs have been developed [115-117]. All these inhibitors show some selectivity for SIRT1 over SIRT2 (Table 1.3, entries 2-6). Some of the non-peptide analogs inhibit SIRT1 and cell proliferation in cancer cells [115-117]. However, it remains unclear whether SIRT2 inhibition also contributes their anticancer effects.

Trifluoroacetyl lysine-containing peptides have also been developed as mechanism-based sirtuin inhibitors [118]. Several cyclic and linear peptides containing trifluoroacetyl lysine (Table 2, entries 7-8) can inhibit SIRT2 selectively with low nM IC_{50} values. However, whether these compounds can inhibit cancer cell proliferation and growth has not been reported.

Table 1.3 Sirtuin inhibitors: *N*-thiocarbamoyl lysine and *N*-Tfa lysine

Entry #	Structure	IC_{50}	Biology Activity
1	H_2N-KKGQSTSRHKK (N-thioacetyl)LMFKTEG-OH	SIRT1: 2 μM[106]	
2	KK(N-thioacetyl)L	SIRT1: 0.57 μM SIRT2: 151 μM[107]	
3	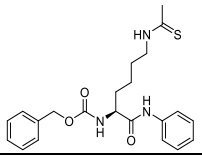	SIRT1: 2.7 μM SIRT2: 23 μM SIRT3: >100 μM[115]	Causes a dose-dependent increase in p53 acetylation in human colon cancer HCT116 cells [115].
4	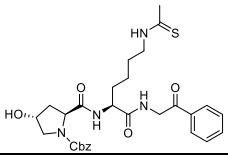	SIRT2: 0.24 μM SIRT2: 1.8 μM SIRT3: 3.9 μM[117]	
5	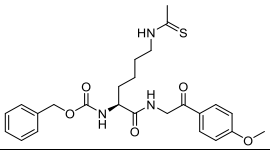	SIRT1: 0.89 μM SIRT2: 2.5 μM SIRT3: 8.4 μM[117]	Antiproliferative effects on A549 lung carcinoma and MCF-7 breast carcinoma cells at μM concentrations; Causes cell cycle arrest at the G1 phase [117]
6	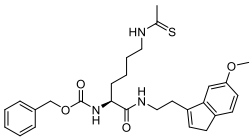	SIRT1: 5.98 μM SIRT2: 25.8 μM SIRT3: 29.4 μM[117]	

7	S2iL8  	SIRT1: 47 nM SIRT2: 3.2 nM SIRT3: 480 nM[118]	
8	S2iD7  	SIRT1: 32 nM SIRT2: 3.7 nM SIRT3: 240 nM[118]	
9	lin-S2iL8 Ac[L]YSNFRIK[Tfa]RYSNSSC[R]—NH2	SIRT1: ND SIRT2: 6.1 nM SIRT3: ND[118]	
10	lin-S2iD7 Ac[D]YHDYRIK[Tfa]RYHTYPC[R]—NH2	SIRT1: ND SIRT2: 5.5 nM SIRT3: ND[118]	
11	RIK[Tfa]RY AcRIK[Tfa]RY—NH2	SIRT1: 280 nM SIRT2: 31 nM SIRT3: 1000 nM[118]	

4.3. β-naphthol-containing inhibitors

Sirtinol. Sirtinol (Table 1.4, entry 1) is identified from a high throughput cell-based screen of more than 1000 compounds [119]. It inhibits human SIRT1 and SIRT2 with IC_{50} values of 131 μM [120] and 38 μM [119] in vitro, respectively, but it does not increase global acetylation levels of histones and tubulin in mammalian cells. Structure–activity relationship (SAR) study shows that the hydroxyl-napthaldehyde moiety is important for the inhibition [119].

Sirtinol is reported to have anticancer activity. It induces senescence-like growth arrest with reduced activation of RAS-MAPK pathway in human breast cancer MCF7 cells and lung cancer H1299 cells [121]. In another study, sirtinol induces cell apoptosis in MCF-7 cells in a process that requires p53 [72]. Sirtinol inhibits the growth of PC3 and Du145 cells and increases sensitivity of the cells to camptothecin and cisplatin [122]. Sirtinol and cisplatin also showed synergistic effect at inhibiting Hela cell proliferation [123]. More recently, it was found to impair cell growth and induce apoptosis in primary chronic lymphocytic leukemia (CLL)[124]. It destabilizes Slug and attenuates basal-like breast cancer (BLBC) growth by SIRT2 inhibition[69].

Salermide. Salermide (Table 1.4, entry 2), a reversed amide based on the structure of sirtinol has stronger *in vitro* inhibitory effect on SIRT1 and SIRT2 than sirtinol [125]. It induces apoptosis in a wide range of human cancer cell lines but not in normal cells through inhibition

of SIRT1 in a p53-independent manner. It shows much more significant inhibition of leukemia cell lines (MOLT4 and KG1A)，colon cancer (SW480) and lymphoma primary tumors than the breast cancer cell line MDA-MB-231[125]. Salermide also induces apoptosis in non-small cell lung cancer (NSCLC) cells through up-regulation of death receptor 5 (DR5) [126]. Similar to sirtinol, the cytotoxic effect of salermide is dependent on the presence of functional p53 in the breast cancer cell line MCF-7 [72]. Several salermide analogs have also been developed and shown to possess anti-proliferative effects in cancer cells (Table 1.4, entries 3 and 4) [127].

Splitomicin and its derivatives. Splitomicin (Table 1.4, entry 5) was identified from a cell-based screening for inhibitors of Sir2 and Hst1 from yeast [128]. About 100 splitomicin derivatives were screened and found to have different selectivity towards the two yeast sirtuins [129]. Splitomicin has no effect on mammalian sirtuins. However, a series of compounds based on β-aryl splitomicins (Table 1.4, entries 6-8) were synthesized and several SIRT2 inhibitors were further identified with low micromolar IC_{50} values [130]. β-(4-Methyl) phenyl-8-bromo-splitomicin (Table 1.4, entry 7) and the R-enantiomer of β-(4-methyl) phenyl-8-methyl-splitomicin (Table 1.4, entry 8) inhibit SIRT2 with an IC_{50} of 1.5 μM and 1.0 μM, repectively. These compounds inhibit the proliferation of MCF-7 breast cancer cells only modestly, which was attributed to their high lipophilicity. These compounds induce tubulin hyperacetylation in cells, suggesting that they target SIRT2 in cells [130].

Table 1.4 Sirtinol, salermide, Splitomicin and their analogues

Entry #	Structure	IC_{50}	Biology Activity
1	Sirtinol 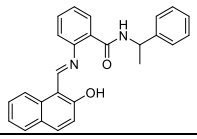	SIRT1: 131 μM [120] SIRT2: 38 μM [119]	Inhibits viability of breast, lung, prostate, cervical, oral, basal-like breast cancer cells and CLL[69,92,102,121-124].
2	Salermide 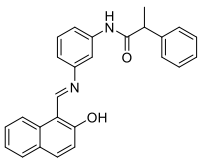	SIRT1: 76.2 μM SIRT2: 45 μM[72,125]	No apparent toxicity in mice at concentrations of 100 μM[125]; Induces apoptosis in MOLT4, KG1A, K562, SW480, Raji and NSCLC cells[125,126]; Potent antiproliferative on MDA-MB-231 and colon RKO cancer cell lines, and colorectal carcinoma CSCs[127].
3	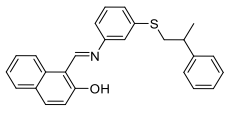	SIRT1: 40.3 μM SIRT2: 19.2 μM[127]	Antiproliferative in MOLT4, MDA-MB-231 and colon RKO cancer cell lines, and glioblastoma multiforme CSCs [127]

4	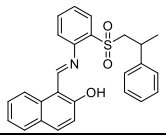	SIRT1: 40.3~67.3 μM SIRT2: 24.2 μM[127]	Inhibits glioblastoma multiforme CSCs[127]
5	Splitomicin 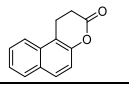	60 μM for Sir2[128]. No inhibition against mammalian sirtuins [131]	
6	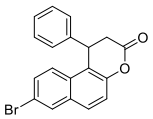	SIRT2: 5.2 μM[130]	
7	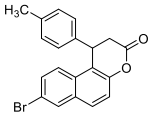	SIRT2: 1.5 μM[130]	Weak anti-proliferative properties in MCF7 breast cancer cells; Increases tubulin acetylation in MCF7 breast cancer cells[130]
8	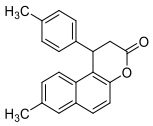	SIRT2: 1.5 μM (racemic) 1.0 μM (R); 35.1% at 100μM (S)[130]	

4.4. Tenovin and its analogues

A cell-based screen designed to detect small molecules that activate the tumor suppressor p53 led to the discovery of tenovin-1 (Table 1.5, entry 1) and its water-soluble analogue tenovin-6 (Table 1.5, entry 2) [132,133]. Biochemical assays suggest that the targets of the tenovins are SIRT1 and SIRT2. At low micromolar concentrations, tenovin-1 shows cytotoxic effects to BL2 Burkitt's lymphoma cells and ARN8 melanoma cells expressing wild type p53, and reduce tumor growth derived from those cells [132]. It is likely that p53 contributes to the cytotoxicity of tenovin-1 but is not essential for the long-term killing effect [132]. Tenovin-6 is more active than tenovin-1 to ARN8 melanoma cells and it delays the growth of ARN8-derived xenograft tumors [132]. Treatment with tenovin-6 eliminates leukemic stem cells in a mouse model for chronic myelogenous leukemia [134]. Further modification of tenovins gave a SIRT2 inhibitor named tenovin-D3 (Table 1.5, entry 3), which promotes expression of p21 in a p53-independent manner, increases acetylation of α-tubulin, and reduces cell migration in MDA-MB-468 breast cancer cells [71].

Table 1.5 Tenovin and its analogues

Entry #	Structure	IC_{50}	Biology Activity

1	Tenovin-1 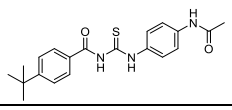	Not determined due to lack of water solubility[133]	Cytotoxic to the BL2 Burkitt's lymphoma cells and ARN8 melanoma cells; reduced tumor growth in the BL2 and ARN8 mouse xenograft model [132].
2	Tenovin-6 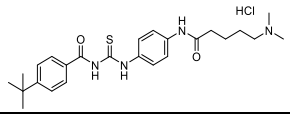	SIRT1: 37.5 μM SIRT2: 10.4 μM[133]	Cytotoxic to ARN8 melanoma cells; delayed the growth of xenograft tumors derived from ARN8 cells [132]; deterred the disease progression of chronic myelogenous leukemia in mice model [134].
3	Tenovin-D3 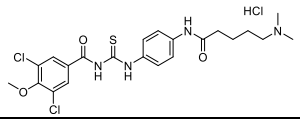	SIRT1: >90 μM SIRT2: 21.8 μM[71]	Promotes expression of p21 in a p53-independent manner, increases acetylation of α-tubulin, and reduces cell migration in MDA-MB-468 breast cancer cells [71].

4.5. Other sirtuin inhibitors

Many other types of compounds have been reported as sirtuin inhibitors (Table 9, entries 1-10). Several of these are worth commenting. AGK2 (Table 1.6, entry 1) is discovered from a focused compound library as a selective SIRT2 inhibitor which rescues α-synuclein toxicity and protects against Parkinson's disease in a cellular model [135]. This study suggests that SIRT2 may be a good target for Parkinson's disease. AGK2 has been widely used as a tool compound to inhibit SIRT2 in various studies. However, unlike other SIRT2 specific inhibitors above, to date its anticancer effect was only demonstrated in C6 glioma cells [127].

ICL-SIRT078 (Table 1.6, entry 2) was identified as a SIRT2 selective inhibitor by pharmacophore screening. It acts as a substrate-competitive SIRT2 inhibitor (K_i = 0.62 μM, IC_{50} = 1.45 μM) with more than 50-fold specificity against SIRT1, 3 and 5. Treating MCF-7 breast cancer cells with ICL-SIRT078 upregulates acetylation of α-tubulin and suppression of cell proliferation[136].

Table 1.6 Other sirtuin inhibitors

Entry #	**Structure**	**IC_{50}**	**Biology Activity**
1	AGK2 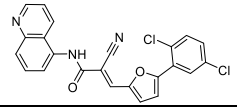	SIRT1: >50 μM SIRT2: 3.5 μM SIRT3: >50 μM[135]	Protective against Parkinson's disease[135,137]; Potent against C6 glioblastoma cells [127].

2	ICL-SIRT078 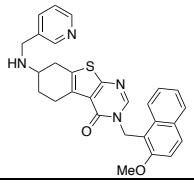	SIRT1: >100 μM SIRT2: 1.45 μM SIRT3: >100 μM[136]	Upregulates acetylation of α-tubulin and suppression of cell proliferation in MCF-7 cells[136].
3	SirReal2 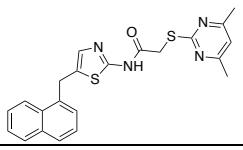	SIRT1: >100 μM SIRT2: 0.14 μM SIRT3: >100 μM[135]	Causes increase in acetylation of α-tubulin [138].
4	Tanikolide Dimer 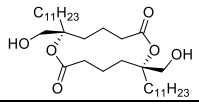	SIRT1: 36.4 μM SIRT2: 3.3 μM[139]	
5	6,8-dibromo-2-pentylchroman-4-one 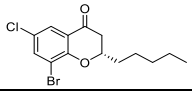	SIRT1: >200 μM SIRT2: 1.5 μM SIRT3: >200 μM [140]	
6	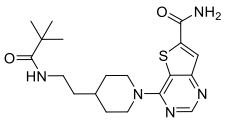	SIRT1: 15 nM SIRT2: 10 nM SIRT3: 33 nM [141]	
7	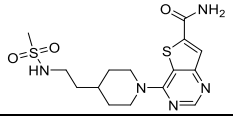	SIRT1: 4.3 nM SIRT2: 1.1 nM SIRT3: 7.2 nM [141]	

From a compound library screening for discovering sirtuin inhibitors, SirReal2 (Table 1.6, entry 3) was found to selectively inhibit SIRT2 (IC_{50} = 140 nM) over SIRT1 and SIRT3 [138]. It belongs to a family of aminothiazoles that are termed sirtuin-rearranging ligands (SirReals). The crystal structure of SIRT2 in complex with SirReal2 revealed that the potency and selectivity are based on a ligand-induced structural rearrangement of the active site, exploiting an adjacent binding pocket. Treatment of HeLa cells with SirReal2 leads to hyperacetylation of α-tubulin, indicating inhibition of SIRT2 in cells.

Tanikolide dimer (Table 1.6, entry 4) was isolated from the Madagascar marine cyanobacterium Lyngbya majuscule and was identified as a SIRT2 selective inhibitor. Among a series of substituted chromone/chroman-4-one derivatives, 6,8-dibromo-2-pentylchroman-4-one (Table 1.6, entry 5) was found to be most potent and selective against SIRT2 *in vitro*. The

most potent sirtuin inhibitors reported to date are thieno[3,2-*d*]pyrimidine-6-carboxamides (Table 1.6, entries 6 and 7) that are developed using encoded library screen technology. These compounds inhibit SIRT1-3 with low nM IC_{50} values [141]. In spite of the high potency and selectivity of these compounds above, the biological activities of these compounds have not been reported. It would be of great interest to see whether these compounds exhibit anticancer activity.

5. Novel SIRT2 enzymatic activities

The seven sirtuins share a conserved NAD-binding and catalytic core domain, but possess distinct N- or C-terminal extensions. Among them, only SIRT1, 2, and 3 exert robust deacetylase activity *in vitro*. SIRT4-7, in contrast, have very weak deacetylase activity *in vitro* [142,143]. It has been proposed that some of them may function as ADP-ribosyltransferases [143-145]. However, this activity is also very weak *in vitro* and its physiological significance is still under debate [146,147]. Recently, SIRT4-7 were shown to hydrolyze other acyl groups more efficiently than acetyl group (Table 1.7). For example, it was demonstrated that SIRT5 functions to remove negatively charged acyl groups, such as succinyl and malonyl, from protein lysine residues [148]. SIRT6 has more efficient activity in removing long chain fatty acyl groups, such as myristoyl and palmitoyl [149]. Similar to SIRT6, SIRT1-3 could hydrolyze long-chain fatty acyl groups efficiently [150-152]. These findings demonstrate that different class of sirtuins may have different acyl lysine substrate specificity.

Table 1.7 Acyl group specificity for mammalian SIRT1-7

Sirtuins	Acyl group specificity
SIRT1	Acetyl[153], Fatty-acyl[150]
SIRT2	Acetyl[13], Fatty-acyl[150,151], 4-Oxononanoyl[154,155]
SIRT3	Acetyl[156], Fatty-acyl[150]
SIRT4	Lipoyl[157], Biotinyl[157], methylglutaryl[158], hydroxymethylglutaryl[158], 3-methylglutaconyl[158]
SIRT5	Acetyl[159], Malonyl[160], Succinyl[160], Glutaryl[161]
SIRT6	Acetyl[162-164], Fatty-acyl[165]

SIRT7	Acetyl[166], Fatty-acyl[167]

After SIRT6 being identified as a lysine defatty-acylase, SIRT1, 2, 3 were also shown to have efficient lysine defatty-acylase activity [150-152]. Regarding SIRT2, it was found to hydrolyze propionyl, butyryl, crotonyl, hexanoyl, decanoyl, dodecanoyl, myristoyl, and lipoyl lysine *in vitro*. SIRT2 exerts comparable steady-state rates of deacetylation, dedodecanoylation, and demyristoylation [150]. Later, we further found that SIRT2 is able to remove myristoyl groups with catalytic efficiency comparable to that of removing acetyl groups from lysine residues (Table 1.8) [151]. We have also resolved the crystal structure of SIRT2 in complex with a thiomyristoyl peptide BHJH-TM1, showing that the myristoyl group is accommodated by a pocket formed by multiple hydrophobic amino acid residues. More recently, SIRT2 was identified to remove lysine 4-oxononanoylation (4-ONylation) from histones and other proteins in cells [154,155]. SIRT2 removes 4-ONylation in stimulated macrophages, which could be involved in cytoprotective signaling responses. These newly discovered activities suggest that SIRT2 may be involved in cancer through not only deacetylase but also other deacylase activities, which merits further investigation.

Table 1.8 Kinetics data for SIRT2 on acetyl and myristoyl H3K9 peptides

Acyl peptide	k_{cat} **(s^{-1})**	K_m **(μM)**	k_{cat}/K_m **($s^{-1}M^{-1}$)**
H3K9 acetyl	0.275 ± 0.014	19.00 ± 0.85	14500
H3K9 myristoyl	0.018 ± 0.003	0.24 ± 0.03	74000

Promoted by the findings that SIRT5 is an efficient demalonylase and desuccinylase and that SIRT6 is an efficient defatty-acylase, mechanism-based SIRT5 [168] and SIRT6 [152] inhibitors have been developed. Taking the advantage of SIRT5's unique acyl group preference, a

thiosuccinyl H3K9 peptide is synthesized and shown to be SIRT5-specific inhibitors with an IC_{50} of 5 μM. The thiosuccinyl peptide does not inhibit SIRT1-3 even at 100 μM. In contrast, the thioacetyl H3K9 peptide inhibits SIRT1-3 potently, but does not inhibit SIRT5 [88]. Likewise, thiomyristoyl peptides are shown to be potent and cell-permeable SIRT6 inhibitors. The thiomyristoyl peptides exert potent inhibition activity for SIRT1, 2 and 3 [152], which agrees with the efficienty defatty-acylation activity for SIRT1, 2, and 3. These proof-of-principle study suggests that the mechanism-based inhibitors can be a simple approach to develop inhibitors specific for a particular sirtuin. Specifically, by changing the chain length of acyl groups in the thioacyl lysine compounds, we may obtain inhibitors specific for different sirtuins.

6. Summary

It seems that the biological data and the SIRT2 inhibitor studies described above do not completely agree with each other. One of the most striking differences between the biological data and pharmacological data is that while the former points to conflicting (both tumor-suppressing and tumor-promoting) roles of SIRT2, the majority of SIRT2 inhibitors studies suggest that inhibiting SIRT2 is a promising anticancer strategy. The discrepancy suggests that a clear understanding of SIRT2's function is still lacking and that more studies are needed to further delineate the precise roles of SIRT2 in cancer.

Inhibiting an enzyme with a small molecule could lead to different outcome from knocking down or knocking out the corresponding gene. The enzyme concentration generally remains unchanged in cells with a small molecule inhibitor, while the concentration is lower when the gene is knocked out or knocked down. In one simple scenario, if the enzyme also has other roles (e.g. mediating protein-protein interactions) that are not dependent on its enzymatic activity, using small molecule inhibitors likely will not affect these other roles. Therefore, highly potent and selective SIRT2 inhibitors will help to directly test whether inhibiting SIRT2 is a good strategy for treating cancers.

However, several caveats exist in the previous SIRT2 inhibitor studies. First, most of the SIRT2 inhibitors reported are still not potent enough with IC_{50} values in the μM range. Although inhibitors with low nM IC_{50} values have been reported [141], their bioavailability and biological activity have not been demonstrated. Second, most of the SIRT2 inhibitors that show anticancer effects are not very selective. It is possible that the anticancer effects of the SIRT2 inhibitors are due to the inhibition of multiple sirtuins. Peck et al. have proposed that inhibiting both SIRT1 and SIRT2 is important for the anticancer effect of salermide and sirtinol [72]. Last, in most sirtuin inhibitor studies, no experiments were carried out to carefully examine whether the anticancer effect of sirtuin inhibitors was due to sirtuin inhibition or not. In Chapter 2, I will summarize my doctoral research to establish SIRT2 inhibition as a strategy to treat certain *Myc*-driven cancer by using a highly specific and potent SIRT2 inhibition in combination with genetic approaches.

Although several lysine deacylase activities have been identified for SIRT2, the physiological substrates and significance of these activities remains largely unknown. To date, the known biological functions of SIRT2 have been attributed to its ability to deacetylate various substrate proteins. Therefore, it will be of great interest to study the physiological relevance and especially the cancer involvement of novel SIRT2 activities. In Chapter 3, I will summarize my work to identify a Ras protein as SIRT2 defatty-acylation target and to elucidate the function of SIRT2-dependent defatty-acylation in cancer.

7. Reference

1. Lin, S.-J., Defossez, P.-A. & Guarente, L. Requirement of NAD and SIR2 for life-span extension by calorie restriction in Saccharomyces cerevisiae. *Science* **289**, 2126-2128 (2000).
2. Imai, S.-i., Armstrong, C.M., Kaeberlein, M. & Guarente, L. Transcriptional silencing and longevity protein Sir2 is an NAD-dependent histone deacetylase. *Nature* **403**, 795-800 (2000).
3. Sauve, A.A. et al. Chemistry of gene silencing: the mechanism of NAD+-dependent deacetylation reactions. *Biochemistry* **40**, 15456-63 (2001).
4. Sauve, A.A., Wolberger, C., Schramm, V.L. & Boeke, J.D. The biochemistry of sirtuins. *Annu. Rev. Biochem.* **75**, 435-465 (2006).
5. Finnin, M.S., Donigian, J.R. & Pavletich, N.P. Structure of the histone deacetylase SIRT2. *Nat. Struct. Mol. Biol.* **8**, 621-625 (2001).
6. Avalos, J.L. et al. Structure of a Sir2 enzyme bound to an acetylated p53 peptide. *Mol. Cell* **10**, 523-535 (2002).
7. Zhao, K., Chai, X. & Marmorstein, R. Structure of the yeast Hst2 protein deacetylase in ternary complex with 2'-*O*-acetyl ADP ribose and histone peptide. *Structure* **11**, 1403-1411 (2003).
8. Borra, M.T., Langer, M.R., Slama, J.T. & Denu, J.M. Substrate specificity and kinetic mechanism of the Sir2 family of NAD+-dependent histone/protein deacetylases. *Biochemistry* **43**, 9877-9887 (2004).
9. Frye, R.A. Phylogenetic classification of prokaryotic and eukaryotic Sir2-like proteins. *Biochem. Biophys. Res. Commun.* **273**, 793-798 (2000).
10. Michishita, E., Park, J.Y., Burneskis, J.M., Barrett, J.C. & Horikawa, I. Evolutionarily conserved and nonconserved cellular localizations and functions of human SIRT proteins. *Mol. Biol. Cell* **16**, 4623-4635 (2005).
11. Haigis, M.C. & Sinclair, D.A. Mammalian Sirtuins: Biological Insights and Disease Relevance. *Annu. Rev. Pathol.* **5**, 253-295 (2010).
12. Perrod, S. et al. A cytosolic NAD-dependent deacetylase, Hst2p, can modulate nucleolar and telomeric silencing in yeast. *EMBO J* **20**, 197-209 (2001).
13. North, B.J., Marshall, B.L., Borra, M.T., Denu, J.M. & Verdin, E. The human Sir2 ortholog, SIRT2, is an NAD+-dependent tubulin deacetylase. *Mol Cell* **11**, 437-44 (2003).
14. Vaquero, A. et al. SirT2 is a histone deacetylase with preference for histone H4 Lys 16 during mitosis. *Genes Dev* **20**, 1256-61 (2006).
15. North, B.J. & Verdin, E. Interphase nucleo-cytoplasmic shuttling and localization of SIRT2 during mitosis. *PLoS One* **2**, e784 (2007).
16. Dryden, S.C., Nahhas, F.A., Nowak, J.E., Goustin, A.S. & Tainsky, M.A. Role for human SIRT2 NAD-dependent deacetylase activity in control of mitotic exit in the cell cycle. *Mol Cell Biol* **23**, 3173-85 (2003).
17. Wang, F., Nguyen, M., Qin, F.X. & Tong, Q. SIRT2 deacetylates FOXO3a in response to oxidative stress and caloric restriction. *Aging Cell* **6**, 505-14 (2007).
18. Jiang, W. et al. Acetylation regulates gluconeogenesis by promoting PEPCK1 degradation via recruiting the UBR5 ubiquitin ligase. *Mol Cell* **43**, 33-44 (2011).
19. Wang, Y.P. et al. Regulation of G6PD acetylation by SIRT2 and KAT9 modulates NADPH homeostasis and cell survival during oxidative stress. *EMBO J* **33**, 1304-20 (2014).
20. Li, Y. et al. SIRT2 down-regulation in HeLa can induce p53 accumulation via p38

MAPK activation-dependent p300 decrease, eventually leading to apoptosis. *Genes Cells* **16**, 34-45 (2011).
21. Jing, E., Gesta, S. & Kahn, C.R. SIRT2 regulates adipocyte differentiation through FoxO1 acetylation/deacetylation. *Cell Metab* **6**, 105-14 (2007).
22. Li, W. et al. Sirtuin 2, a mammalian homolog of yeast silent information regulator-2 longevity regulator, is an oligodendroglial protein that decelerates cell differentiation through deacetylating alpha-tubulin. *J Neurosci* **27**, 2606-16 (2007).
23. North, B.J. et al. SIRT2 induces the checkpoint kinase BubR1 to increase lifespan. *EMBO J* **33**, 1438-53 (2014).
24. Serrano, L. et al. The tumor suppressor SirT2 regulates cell cycle progression and genome stability by modulating the mitotic deposition of H4K20 methylation. *Genes Dev* **27**, 639-53 (2013).
25. Liu, P.Y. et al. The histone deacetylase SIRT2 stabilizes Myc oncoproteins. *Cell Death Differ* **20**, 503-14 (2013).
26. Eskandarian, H.A. et al. A role for SIRT2-dependent histone H3K18 deacetylation in bacterial infection. *Science* **341**, 1238858 (2013).
27. Das, C., Lucia, M.S., Hansen, K.C. & Tyler, J.K. CBP/p300-mediated acetylation of histone H3 on lysine 56. *Nature* **459**, 113-7 (2009).
28. Vempati, R.K. et al. p300-mediated acetylation of histone H3 lysine 56 functions in DNA damage response in mammals. *J Biol Chem* **285**, 28553-64 (2010).
29. Black, J.C., Mosley, A., Kitada, T., Washburn, M. & Carey, M. The SIRT2 deacetylase regulates autoacetylation of p300. *Mol Cell* **32**, 449-55 (2008).
30. Wang, F. et al. Deacetylation of FOXO3 by SIRT1 or SIRT2 leads to Skp2-mediated FOXO3 ubiquitination and degradation. *Oncogene* **31**, 1546-57 (2012).
31. Zhao, Y. et al. Anti-neoplastic activity of the cytosolic FoxO1 results from autophagic cell death. *Autophagy* **6**, 988-90 (2010).
32. Seo, K.S. et al. SIRT2 regulates tumour hypoxia response by promoting HIF-1alpha hydroxylation. *Oncogene* (2014).
33. Rothgiesser, K.M., Erener, S., Waibel, S., Luscher, B. & Hottiger, M.O. SIRT2 regulates NF-kappaB dependent gene expression through deacetylation of p65 Lys310. *J Cell Sci* **123**, 4251-8 (2010).
34. Krishnan, J. et al. Dietary obesity-associated Hif1alpha activation in adipocytes restricts fatty acid oxidation and energy expenditure via suppression of the Sirt2-NAD+ system. *Genes Dev* **26**, 259-70 (2012).
35. Yang, X. et al. Sirtuin 2 regulates cellular iron homeostasis via deacetylation of transcription factor NRF2. *J Clin Invest* **127**, 1505-1516 (2017).
36. Zhang, H. et al. SIRT2 directs the replication stress response through CDK9 deacetylation. *Proc Natl Acad Sci U S A* **110**, 13546-51 (2013).
37. Kim, H.S. et al. SIRT2 maintains genome integrity and suppresses tumorigenesis through regulating APC/C activity. *Cancer Cell* **20**, 487-99 (2011).
38. Zhang, H. et al. ATRIP Deacetylation by SIRT2 Drives ATR Checkpoint Activation by Promoting Binding to RPA-ssDNA. *Cell Rep* **14**, 1435-1447 (2016).
39. Zhao, D. et al. Lysine-5 acetylation negatively regulates lactate dehydrogenase A and is decreased in pancreatic cancer. *Cancer Cell* **23**, 464-76 (2013).
40. Lin, R. et al. Acetylation stabilizes ATP-citrate lyase to promote lipid biosynthesis and tumor growth. *Mol Cell* **51**, 506-18 (2013).
41. Xu, S.N., Wang, T.S., Li, X. & Wang, Y.P. SIRT2 activates G6PD to enhance NADPH production and promote leukaemia cell proliferation. *Sci Rep* **6**, 32734 (2016).
42. Ye, H. et al. HSPB1 Enhances SIRT2-Mediated G6PD Activation and Promotes

Glioma Cell Proliferation. *PLoS One* **11**, e0164285 (2016).
43. Xu, Y. et al. Oxidative stress activates SIRT2 to deacetylate and stimulate phosphoglycerate mutase. *Cancer Res* **74**, 3630-42 (2014).
44. Zhao, D. et al. NOTCH-induced aldehyde dehydrogenase 1A1 deacetylation promotes breast cancer stem cells. *J Clin Invest* **124**, 5453-65 (2014).
45. Park, J.M., Kim, T.H., Jo, S.H., Kim, M.Y. & Ahn, Y.H. Acetylation of glucokinase regulatory protein decreases glucose metabolism by suppressing glucokinase activity. *Sci Rep* **5**, 17395 (2015).
46. Park, S.H. et al. SIRT2-Mediated Deacetylation and Tetramerization of Pyruvate Kinase Directs Glycolysis and Tumor Growth. *Cancer Res* **76**, 3802-12 (2016).
47. Ma, L. et al. SIRT1 and SIRT2 inhibition impairs pediatric soft tissue sarcoma growth. *Cell Death Dis* **5**, e1483 (2014).
48. Yang, M.H. et al. HDAC6 and SIRT2 regulate the acetylation state and oncogenic activity of mutant K-RAS. *Mol Cancer Res* **11**, 1072-7 (2013).
49. Song, H.Y. et al. SIRT2 deletion enhances KRAS-induced tumorigenesis in vivo by regulating K147 acetylation status. *Oncotarget* **7**, 80336-80349 (2016).
50. Beirowski, B. et al. Sir-two-homolog 2 (Sirt2) modulates peripheral myelination through polarity protein Par-3/atypical protein kinase C (aPKC) signaling. *Proc Natl Acad Sci U S A* **108**, E952-61 (2011).
51. Saxena, M. et al. The sirtuins promote Dishevelled-1 scaffolding of TIAM1, Rac activation and cell migration. *Oncogene* **34**, 188-98 (2015).
52. Wang, J. et al. Sirtuin 2 aggravates postischemic liver injury by deacetylating mitogen-activated protein kinase phosphatase-1. *Hepatology* **65**, 225-236 (2017).
53. Snider, N.T. et al. Glucose and SIRT2 reciprocally mediate the regulation of keratin 8 by lysine acetylation. *J Cell Biol* **200**, 241-7 (2013).
54. Kaufmann, T. et al. SIRT2 regulates nuclear envelope reassembly through ANKLE2 deacetylation. *J Cell Sci* **129**, 4607-4621 (2016).
55. Kim, H.-S. et al. SIRT2 Maintains Genome Integrity and Suppresses Tumorigenesis through Regulating APC/C Activity. *Cancer Cell* **20**, 487-499 (2011).
56. Naini, S.M. et al. Cytosolic phospholipase A2alpha regulates G1 progression through modulating FOXO1 activity. *FASEB J* **30**, 1155-70 (2016).
57. Bajpe, P.K. et al. A chromatin modifier genetic screen identifies SIRT2 as a modulator of response to targeted therapies through the regulation of MEK kinase activity. *Oncogene* **34**, 531-6 (2015).
58. Yeung, F. et al. Regulation of the mitogen-activated protein kinase kinase (MEK)-1 by NAD(+)-dependent deacetylases. *Oncogene* **34**, 798-804 (2015).
59. Nguyen, P., Lee, S., Lorang-Leins, D., Trepel, J. & Smart, D.K. SIRT2 interacts with beta-catenin to inhibit Wnt signaling output in response to radiation-induced stress. *Mol Cancer Res* **12**, 1244-53 (2014).
60. Fiskus, W. et al. SIRT2 Deacetylates and Inhibits the Peroxidase Activity of Peroxiredoxin-1 to Sensitize Breast Cancer Cells to Oxidant Stress-Inducing Agents. *Cancer Res* **76**, 5467-78 (2016).
61. Hiratsuka, M. et al. Proteomics-based identification of differentially expressed genes in human gliomas: down-regulation of SIRT2 gene. *Biochem Biophys Res Commun* **309**, 558-66 (2003).
62. Ming, M., Qiang, L., Zhao, B. & He, Y.Y. Mammalian SIRT2 inhibits keratin 19 expression and is a tumor suppressor in skin. *Exp Dermatol* **23**, 207-9 (2014).
63. Du, Y., Wu, J., Zhang, H., Li, S. & Sun, H. Reduced expression of SIRT2 in serous ovarian carcinoma promotes cell proliferation through disinhibition of CDK4 expression. *Mol Med Rep* **15**, 1638-1646 (2017).

64. Zhang, L.L. et al. SIRT2 mediated antitumor effects of shikonin on metastatic colorectal cancer. *Eur J Pharmacol* **797**, 1-8 (2017).
65. Jing, E., Gesta, S. & Kahn, C.R. SIRT2 Regulates Adipocyte Differentiation through FoxO1 Acetylation/Deacetylation. *Cell metabolism* **6**, 105-114 (2007).
66. Zhao, Y. et al. Cytosolic FoxO1 is essential for the induction of autophagy and tumour suppressor activity. *Nat Cell Biol* **12**, 665-75 (2010).
67. Yang, M.H. et al. HDAC6 and SIRT2 regulate the acetylation state and oncogenic activity of mutant K-RAS. *Mol. Cancer Res.* **11**, 1072-7 (2013).
68. Ramakrishnan, G. et al. Sirt2 Deacetylase Is a Novel AKT Binding Partner Critical for AKT Activation by Insulin. *J Biol Chem* **289**, 6054-66 (2014).
69. Zhou, W. et al. The SIRT2 Deacetylase Stabilizes Slug to Control Malignancy of Basal-like Breast Cancer. *Cell Rep* **17**, 1302-1317 (2016).
70. van Leeuwen, I.M. et al. Modulation of p53 C-terminal acetylation by mdm2, p14ARF, and cytoplasmic SirT2. *Mol Cancer Ther* **12**, 471-80 (2013).
71. McCarthy, A.R. et al. Tenovin-D3, a novel small-molecule inhibitor of sirtuin SirT2, increases p21 (CDKN1A) expression in a p53-independent manner. *Mol Cancer Ther* **12**, 352-60 (2013).
72. Peck, B. et al. SIRT inhibitors induce cell death and p53 acetylation through targeting both SIRT1 and SIRT2. *Mol Cancer Ther* **9**, 844-55 (2010).
73. Soung, Y.H., Pruitt, K. & Chung, J. Epigenetic silencing of ARRDC3 expression in basal-like breast cancer cells. *Sci Rep* **4**, 3846 (2014).
74. Zhao, D. et al. Lysine-5 acetylation negatively regulates lactate dehydrogenase A and is decreased in pancreatic cancer. *Cancer cell* **23**, 464-476 (2013).
75. Deng, A., Ning, Q., Zhou, L. & Liang, Y. SIRT2 is an unfavorable prognostic biomarker in patients with acute myeloid leukemia. *Sci Rep* **6**, 27694 (2016).
76. Hou, H. et al. Cortactin is associated with tumour progression and poor prognosis in prostate cancer and SIRT2 other than HADC6 may work as facilitator in situ. *J Clin Pathol* **65**, 1088-96 (2012).
77. Grbesa, I. et al. Expression of sirtuin 1 and 2 is associated with poor prognosis in non-small cell lung cancer patients. *PLoS One* **10**, e0124670 (2015).
78. Chen, J. et al. SIRT2 overexpression in hepatocellular carcinoma mediates epithelial to mesenchymal transition by protein kinase B/glycogen synthase kinase-3beta/beta-catenin signaling. *Hepatology* **57**, 2287-98 (2013).
79. Wilking-Busch, M.J., Ndiaye, M.A., Huang, W. & Ahmad, N. Expression profile of SIRT2 in human melanoma and implications for sirtuin-based chemotherapy. *Cell Cycle* **16**, 574-577 (2017).
80. Heltweg, B. et al. Antitumor activity of a small-molecule inhibitor of human silent information regulator 2 enzymes. *Cancer Res.* **66**, 4368-4377 (2006).
81. Li, Y. et al. SIRT2 down-regulation in HeLa can induce p53 accumulation via p38 MAPK activation-dependent p300 decrease, eventually leading to apoptosis. *Genes to Cells* **16**, 34-45 (2011).
82. Zhang, Y. et al. Identification of a small molecule SIRT2 inhibitor with selective tumor cytotoxicity. *Biochem. Biophys. Res. Commun.* **386**, 729-733 (2009).
83. Liu, Y., Wang, D.-L., Chen, S., Zhao, L. & Sun, F.-L. Oncogene Ras/phosphatidylinositol 3-kinase signaling targets histone H3 acetylation at lysine 56. *J. Biol. Chem.* **287**, 41469-41480 (2012).
84. Liu, P.Y. et al. The histone deacetylase SIRT2 stabilizes Myc oncoproteins. *Cell Death Differ.* **20**, 503-514 (2013).
85. Sunami, Y. et al. Inhibition of the NAD-dependent protein deacetylase SIRT2 induces granulocytic differentiation in human leukemia cells. *PLoS ONE* **8**, e57633 (2013).

86. He, X. et al. SIRT2 activity is required for the survival of C6 glioma cells. *Biochem. Biophys. Res. Comm.* **417**, 468-472 (2012).
87. He, X. et al. SIRT2 activity is required for the survival of C6 glioma cells. *Biochem Biophys Res Commun* **417**, 468-72 (2012).
88. He, B., Du, J. & Lin, H. Thiosuccinyl peptides as Sirt5-specific inhibitors. *J Am Chem Soc* **134**, 1922-5 (2012).
89. Hu, J., He, B., Bhargava, S. & Lin, H. A fluorogenic assay for screening Sirt6 modulators. *Org Biomol Chem* **11**, 5213-6 (2013).
90. Tervo, A.J. et al. An in silico approach to discovering novel inhibitors of human sirtuin type 2. *J Med Chem* **47**, 6292-8 (2004).
91. Audrito, V. et al. Nicotinamide blocks proliferation and induces apoptosis of chronic lymphocytic leukemia cells through activation of the p53/miR-34a/SIRT1 tumor suppressor network. *Cancer Res* **71**, 4473-83 (2011).
92. Jung-Hynes, B., Nihal, M., Zhong, W. & Ahmad, N. Role of sirtuin histone deacetylase SIRT1 in prostate cancer. A target for prostate cancer management via its inhibition? *J Biol Chem* **284**, 3823-32 (2009).
93. Suzuki, T. et al. Design, synthesis, and biological activity of a novel series of human sirtuin-2-selective inhibitors. *J Med Chem* **55**, 5760-73 (2012).
94. Cui, H. et al. Discovery of potent and selective sirtuin 2 (SIRT2) inhibitors using a fragment-based approach. *J Med Chem* **57**, 8340-57 (2014).
95. Taylor, D.M. et al. A brain-permeable small molecule reduces neuronal cholesterol by inhibiting activity of sirtuin 2 deacetylase. *ACS Chem Biol* **6**, 540-6 (2011).
96. Cheon, M.G., Kim, W., Choi, M. & Kim, J.E. AK-1, a specific SIRT2 inhibitor, induces cell cycle arrest by downregulating Snail in HCT116 human colon carcinoma cells. *Cancer Lett* **356**, 637-45 (2015).
97. Lee, S.D., Kim, W., Jeong, J.W., Park, J.W. & Kim, J.E. AK-1, a SIRT2 inhibitor, destabilizes HIF-1alpha and diminishes its transcriptional activity during hypoxia. *Cancer Lett* **373**, 138-145 (2016).
98. Luthi-Carter, R. et al. SIRT2 inhibition achieves neuroprotection by decreasing sterol biosynthesis. *Proc Natl Acad Sci U S A* **107**, 7927-32 (2010).
99. Chopra, V. et al. The sirtuin 2 inhibitor AK-7 is neuroprotective in Huntington's disease mouse models. *Cell Rep* **2**, 1492-7 (2012).
100. Sakai, T. et al. Design, synthesis and structure-activity relationship studies of novel sirtuin 2 (SIRT2) inhibitors with a benzamide skeleton. *Bioorg Med Chem* **23**, 328-39 (2015).
101. Hoffmann, G., Breitenbucher, F., Schuler, M. & Ehrenhofer-Murray, A.E. A novel sirtuin 2 (SIRT2) inhibitor with p53-dependent pro-apoptotic activity in non-small cell lung cancer. *J Biol Chem* **289**, 5208-16 (2014).
102. Alhazzazi, T.Y. et al. Sirtuin-3 (SIRT3), a novel potential therapeutic target for oral cancer. *Cancer* **117**, 1670-8 (2011).
103. Khanfar, M.A. et al. Development and characterization of 3-(benzylsulfonamido)benzamides as potent and selective SIRT2 inhibitors. *Eur J Med Chem* **76**, 414-26 (2014).
104. Smith, B.C. & Denu, J.M. Mechanism-based Inhibition of Sir2 deacetylases by thioacetyl-lysine peptide. *Biochemistry* **46**, 14478-14486 (2007).
105. Hawse, W.F. et al. Structural insights into intermediate steps in the Sir2 deacetylation reaction. *Structure* **16**, 1368-77 (2008).
106. Fatkins, D.G., Monnot, A.D. & Zheng, W. Nepsilon-thioacetyl-lysine: a multi-facet functional probe for enzymatic protein lysine Nepsilon-deacetylation. *Bioorg Med Chem Lett* **16**, 3651-6 (2006).

107. Kiviranta, P.H. et al. N(epsilon)-thioacetyl-lysine-containing tri-, tetra-, and pentapeptides as SIRT1 and SIRT2 inhibitors. *J Med Chem* **52**, 2153-6 (2009).
108. Jamonnak, N., Fatkins, D.G., Wei, L. & Zheng, W. N(epsilon)-methanesulfonyl-lysine as a non-hydrolyzable functional surrogate for N(epsilon)-acetyl-lysine. *Org Biomol Chem* **5**, 892-6 (2007).
109. Huhtiniemi, T. et al. N(epsilon)-Modified lysine containing inhibitors for SIRT1 and SIRT2. *Bioorg Med Chem* **18**, 5616-25 (2010).
110. Smith, B.C. & Denu, J.M. Acetyl-lysine analog peptides as mechanistic probes of protein deacetylases. *J Biol Chem* **282**, 37256-65 (2007).
111. Smith, B.C., Settles, B., Hallows, W.C., Craven, M.W. & Denu, J.M. SIRT3 substrate specificity determined by peptide arrays and machine learning. *ACS Chem Biol* **6**, 146-57 (2011).
112. Chakrabarty, S.P., Ramapanicker, R., Mishra, R., Chandrasekaran, S. & Balaram, H. Development and characterization of lysine based tripeptide analogues as inhibitors of Sir2 activity. *Bioorg Med Chem* **17**, 8060-72 (2009).
113. Hirsch, B.M. et al. A mechanism-based potent sirtuin inhibitor containing Nepsilon-thiocarbamoyl-lysine (TuAcK). *Bioorg Med Chem Lett* **21**, 4753-7 (2011).
114. Jamonnak, N., Hirsch, B.M., Pang, Y. & Zheng, W. Substrate specificity of SIRT1-catalyzed lysine Nepsilon-deacetylation reaction probed with the side chain modified Nepsilon-acetyl-lysine analogs. *Bioorg Chem* **38**, 17-25 (2010).
115. Suzuki, T. et al. Identification of a cell-active non-peptide sirtuin inhibitor containing N-thioacetyl lysine. *Bioorg Med Chem Lett* **19**, 5670-2 (2009).
116. Huhtiniemi, T. et al. Structure-based design of pseudopeptidic inhibitors for SIRT1 and SIRT2. *J Med Chem* **54**, 6456-68 (2011).
117. Mellini, P. et al. Screen of pseudopeptidic inhibitors of human sirtuins 1-3: two lead compounds with antiproliferative effects in cancer cells. *J Med Chem* **56**, 6681-95 (2013).
118. Morimoto, J., Hayashi, Y. & Suga, H. Discovery of macrocyclic peptides armed with a mechanism-based warhead: isoform-selective inhibition of human deacetylase SIRT2. *Angew Chem Int Ed Engl* **51**, 3423-7 (2012).
119. Grozinger, C.M., Chao, E.D., Blackwell, H.E., Moazed, D. & Schreiber, S.L. Identification of a class of small molecule inhibitors of the sirtuin family of NAD-dependent deacetylases by phenotypic screening. *J Biol Chem* **276**, 38837-43 (2001).
120. Mai, A. et al. Design, synthesis, and biological evaluation of sirtinol analogues as class III histone/protein deacetylase (Sirtuin) inhibitors. *J Med Chem* **48**, 7789-95 (2005).
121. Ota, H. et al. Sirt1 inhibitor, Sirtinol, induces senescence-like growth arrest with attenuated Ras-MAPK signaling in human cancer cells. *Oncogene* **25**, 176-85 (2006).
122. Kojima, K. et al. A role for SIRT1 in cell growth and chemoresistance in prostate cancer PC3 and DU145 cells. *Biochem Biophys Res Commun* **373**, 423-8 (2008).
123. Jin, K.L. et al. The effect of combined treatment with cisplatin and histone deacetylase inhibitors on HeLa cells. *J Gynecol Oncol* **21**, 262-8 (2010).
124. Bhalla, S. & Gordon, L.I. Functional characterization of NAD dependent de-acetylases SIRT1 and SIRT2 in B-Cell Chronic Lymphocytic Leukemia (CLL). *Cancer Biol Ther* **17**, 300-9 (2016).
125. Lara, E. et al. Salermide, a Sirtuin inhibitor with a strong cancer-specific proapoptotic effect. *Oncogene* **28**, 781-91 (2009).
126. Liu, G. et al. Salermide up-regulates death receptor 5 expression through the ATF4-ATF3-CHOP axis and leads to apoptosis in human cancer cells. *J Cell Mol Med* **16**, 1618-28 (2012).

127. Rotili, D. et al. Discovery of salermide-related sirtuin inhibitors: binding mode studies and antiproliferative effects in cancer cells including cancer stem cells. *J Med Chem* **55**, 10937-47 (2012).
128. Bedalov, A., Gatbonton, T., Irvine, W.P., Gottschling, D.E. & Simon, J.A. Identification of a small molecule inhibitor of Sir2p. *Proc Natl Acad Sci U S A* **98**, 15113-8 (2001).
129. Hirao, M. et al. Identification of selective inhibitors of NAD+-dependent deacetylases using phenotypic screens in yeast. *J Biol Chem* **278**, 52773-82 (2003).
130. Neugebauer, R.C. et al. Structure-activity studies on splitomicin derivatives as sirtuin inhibitors and computational prediction of binding mode. *J Med Chem* **51**, 1203-13 (2008).
131. Pagans, S. et al. SIRT1 regulates HIV transcription via Tat deacetylation. *PLoS Biol* **3**, e41 (2005).
132. Lain, S. et al. Discovery, in vivo activity, and mechanism of action of a small-molecule p53 activator. *Cancer Cell* **13**, 454-63 (2008).
133. McCarthy, A.R. et al. Synthesis and biological characterisation of sirtuin inhibitors based on the tenovins. *Bioorg Med Chem* **20**, 1779-93 (2012).
134. Yuan, H. et al. Activation of stress response gene SIRT1 by BCR-ABL promotes leukemogenesis. *Blood* **119**, 1904-14 (2012).
135. Outeiro, T.F. et al. Sirtuin 2 inhibitors rescue alpha-synuclein-mediated toxicity in models of Parkinson's disease. *Science* **317**, 516-9 (2007).
136. Di Fruscia, P. et al. The discovery of a highly selective 5,6,7,8-tetrahydrobenzo[4,5]thieno[2,3-d]pyrimidin-4(3H)-one SIRT2 inhibitor that is neuroprotective in an in vitro Parkinson's disease model. *ChemMedChem* **10**, 69-82 (2015).
137. Garske, A.L., Smith, B.C. & Denu, J.M. Linking SIRT2 to Parkinson's disease. *ACS Chem Biol* **2**, 529-32 (2007).
138. Rumpf, T. et al. Selective Sirt2 inhibition by ligand-induced rearrangement of the active site. *Nat Commun* **6**, 6263 (2015).
139. Gutierrez, M. et al. Structural and synthetic investigations of tanikolide dimer, a SIRT2 selective inhibitor, and tanikolide seco-acid from the Madagascar marine cyanobacterium Lyngbya majuscula. *J Org Chem* **74**, 5267-75 (2009).
140. Friden-Saxin, M. et al. Synthesis and evaluation of substituted chroman-4-one and chromone derivatives as sirtuin 2-selective inhibitors. *J Med Chem* **55**, 7104-13 (2012).
141. Disch, J.S. et al. Discovery of Thieno[3,2-d]pyrimidine-6-carboxamides as Potent Inhibitors of SIRT1, SIRT2, and SIRT3. *J Med Chem* **56**, 3666-3679 (2013).
142. Michishita, E., Park, J.Y., Burneskis, J.M., Barrett, J.C. & Horikawa, I. Evolutionarily conserved and nonconserved cellular localizations and functions of human SIRT proteins. *Mol Biol Cell* **16**, 4623-4635 (2005).
143. Liszt, G., Ford, E., Kurtev, M. & Guarente, L. Mouse Sir2 homolog SIRT6 is a nuclear ADP-ribosyltransferase. *J. Biol. Chem.* **280**, 21313-21320 (2005).
144. Haigis, M.C. et al. SIRT4 Inhibits glutamate dehydrogenase and opposes the effects of calorie restriction in pancreatic β Cells. *Cell* **126**, 941-954 (2006).
145. Mao, Z. et al. SIRT6 promotes DNA repair under stress by activating PARP1. *Science* **332**, 1443-6 (2011).
146. Kowieski, T.M., Lee, S. & Denu, J.M. Acetylation-dependent ADP-ribosylation by *Trypanosoma brucei* Sir2. *J. Biol. Chem.* **283**, 5317-5326 (2008).
147. Du, J., Jiang, H. & Lin, H. Investigating the ADP-ribosyltransferase activity of sirtuins with NAD analogs and ^{32}P-NAD. *Biochemistry* **48**, 2878-2890 (2009).

148. Du, J. et al. Sirt5 is an NAD-dependent protein lysine demalonylase and desuccinylase. *Science* **334**, 806-809 (2011).
149. Jiang, H. et al. SIRT6 regulates TNF-a secretion through hydrolysis of long-chain fatty acyl lysine. *Nature* **496**, 110-113 (2013).
150. Feldman, J.L., Baeza, J. & Denu, J.M. Activation of the protein deacetylase SIRT6 by long-chain fatty acids and widespread deacylation by mammalian sirtuins. *J Biol Chem* **288**, 31350-6 (2013).
151. Teng, Y.B. et al. Efficient demyristoylase activity of SIRT2 revealed by kinetic and structural studies. *Sci Rep* **5**, 8529 (2015).
152. He, B., Hu, J., Zhang, X. & Lin, H. Thiomyristoyl peptides as cell-permeable Sirt6 inhibitors. *Org Biomol Chem* **12**, 7498-502 (2014).
153. Vaziri, H. et al. hSIR2(SIRT1) functions as an NAD-dependent p53 deacetylase. *Cell* **107**, 149-59 (2001).
154. Jin, J., He, B., Zhang, X., Lin, H. & Wang, Y. SIRT2 Reverses 4-Oxononanoyl Lysine Modification on Histones. *J Am Chem Soc* **138**, 12304-7 (2016).
155. Cui, Y., Li, X., Lin, J., Hao, Q. & Li, X.D. Histone Ketoamide Adduction by 4-Oxo-2-nonenal Is a Reversible Posttranslational Modification Regulated by Sirt2. *ACS Chem Biol* **12**, 47-51 (2017).
156. Schwer, B., North, B.J., Frye, R.A., Ott, M. & Verdin, E. The human silent information regulator (Sir)2 homologue hSIRT3 is a mitochondrial nicotinamide adenine dinucleotide-dependent deacetylase. *J Cell Biol* **158**, 647-57 (2002).
157. Mathias, R.A. et al. Sirtuin 4 is a lipoamidase regulating pyruvate dehydrogenase complex activity. *Cell* **159**, 1615-25 (2014).
158. Anderson, K.A. et al. SIRT4 Is a Lysine Deacylase that Controls Leucine Metabolism and Insulin Secretion. *Cell Metab* **25**, 838-855 e15 (2017).
159. Schuetz, A. et al. Structural basis of inhibition of the human NAD+-dependent deacetylase SIRT5 by suramin. *Structure* **15**, 377-89 (2007).
160. Du, J. et al. Sirt5 is a NAD-dependent protein lysine demalonylase and desuccinylase. *Science* **334**, 806-9 (2011).
161. Tan, M. et al. Lysine glutarylation is a protein posttranslational modification regulated by SIRT5. *Cell Metab* **19**, 605-17 (2014).
162. Michishita, E. et al. SIRT6 is a histone H3 lysine 9 deacetylase that modulates telomeric chromatin. *Nature* **452**, 492-6 (2008).
163. Yang, B., Zwaans, B.M., Eckersdorff, M. & Lombard, D.B. The sirtuin SIRT6 deacetylates H3 K56Ac in vivo to promote genomic stability. *Cell Cycle* **8**, 2662-3 (2009).
164. Michishita, E. et al. Cell cycle-dependent deacetylation of telomeric histone H3 lysine K56 by human SIRT6. *Cell Cycle* **8**, 2664-6 (2009).
165. Jiang, H. et al. SIRT6 regulates TNF-alpha secretion through hydrolysis of long-chain fatty acyl lysine. *Nature* **496**, 110-3 (2013).
166. Tong, Z. et al. SIRT7 Is Activated by DNA and Deacetylates Histone H3 in the Chromatin Context. *ACS Chem Biol* **11**, 742-7 (2016).
167. Tong, Z. et al. SIRT7 Is an RNA-Activated Protein Lysine Deacylase. *ACS Chem Biol* **12**, 300-310 (2017).
168. He, B., Du, J. & Lin, H. Thiosuccinyl peptides as Sirt5-specific inhibitors. *J. Am. Chem. Soc.* **134**, 1922-1925 (2012).

CHAPTER 2

A SIRT2-SELECTIVE INHIBITOR PROMOTES C-MYC ONCOPROTEIN DEGRADATION AND EXHIBITS BROAD ANTICANCER ACTIVITY [b]

Abstract

Targeting sirtuins for cancer treatment has been a topic of debate due to conflicting reports and lack of potent and specific inhibitors. We have developed a thiomyristoyl lysine compound, TM, as a potent SIRT2-specific inhibitor with broad anticancer effect in various human cancer cells and mouse models of breast cancer. Mechanistically, SIRT2 inhibition promotes c-Myc ubiquitination and degradation. The anticancer effect of TM correlates with its ability to decrease c-Myc level. TM had limited effects on non-cancerous cells and tumor-free mice, suggesting that cancer cells have an increased dependency on SIRT2 that can be exploited for therapeutic benefit. Our studies demonstrate that SIRT2-selective inhibitors are promising anticancer agents and may represent a general strategy to target certain c-Myc-driven cancers.

[b] This is a revised version of our published paper: Jing, H., Hu, J., He, B., Negrón Abril, Y.L., Stupinski, J., Weiser, K., Carbonaro, M., Chiang, Y.L., Southard, T., Giannakakou, P., Weiss, R.S., Lin, H.. A SIRT2-Selective Inhibitor Promotes c-Myc Oncoprotein Degradation and Exhibits Broad Anticancer Activity. *Cancer Cell* **29**, 297-310 (2016).
For this paper, I (HJ) designed and performed all the biochemical studies except those noted below. I would like to acknowledge the great contribution made by all the authors below. BH and HL designed the sirtuin inhibitors. JH, BH and YLC synthesized the inhibitors and biotin-conjugated compounds. HJ, JH, and BH purified the sirtuin enzymes, performed *in vitro* inhibitor assay and determined the mechanism of SIRT2 inhibition. YLNA and JS performed the animal studies. KW, MC and PG carried out the Biotin-TM pull-down assay and immunofluorescence of acetyl-α-tubulin. PG suggested the NCI60 screening, which helped making the c-Myc connection. TS performed pathologic review. RSW directed the animal studies. HL directed the inhibitor development and biochemical studies, and wrote the manuscript with help from HJ, RSW, PG, JH and YLNA.

1. Introduction

Oncogenes that drive tumorigenesis have attracted extensive interest as therapeutic targets for treating cancers. *MYC*, and *c-Myc* in particular, is one such oncogene. *MYC* was discovered in studies of fulminant chicken tumors caused by oncogenic retroviruses, which co-opted cellular c-Myc to generate the oncogenic v-Myc [1]. Subsequently, mouse plasmacytomas and human Burkitt lymphomas were found to be caused by *c-Myc* activation due to chromosomal translocations that fused *c-Myc* to the immunoglobin (Ig) gene loci [1]. Recent genomic sequencing efforts identified *c-Myc* as one of the most highly amplified oncogenes in many different human cancers, further highlighting the oncogenic role of c-Myc activation [2]. The identification of effective therapeutic strategies targeting Myc has been challenging. Recently it was demonstrated that bromodomain inhibitors that target BRD4 could suppress *c-Myc* transcription and lead to tumor inhibition *in vivo* [3]. This finding underscores the therapeutic value of targeting Myc.

The sirtuin family of NAD-dependent protein lysine deacylases has been shown to play important roles in many physiological processes, including the regulation of transcription, metabolism, and DNA repair [4-6]. Many of these functions are achieved by their ability to deacylate various substrate proteins, including histones, transcription factors, and metabolic enzymes [4-11]. Because the functionally related but structurally distinct zinc-dependent histone deacetylases (HDACs) are established cancer targets [12,13], there is interest in exploring whether sirtuins can also be important targets for cancers [14-16]. However, there is evidence suggesting both tumor suppressor and oncogenic roles of sirtuins [14-16]. In the case of SIRT2, genetic studies indicated that aged *Sirt2* knockout (KO) mice show increased tumor incidence as compared to wild-type (WT) [17] controls. In contrast, SIRT2 was also observed to have tumor promoting activity in several studies [18-24]. Moreover, several SIRT2 inhibitors have also been reported to

have anticancer effects [25-34]. However, the moderate potency and specificity of the existing sirtuin inhibitors are insufficient to draw conclusions about the anticancer potential of sirtuin inhibition. Thus, whether sirtuin inhibitors are useful anticancer agents is still an open question. Here we set out to develop sirtuin inhibitors with improved potency and selectivity to explore the potential of targeting sirtuins for treating human cancers, especially c-Myc driven cancers.

2. Results

2.1 Development of a highly selective and potent SIRT2 inhibitor

Most existing sirtuin inhibitors are either not very potent (e.g. with IC_{50} values in the high micromolar range) or not very selective (i.e. they inhibit several different sirtuins). More potent and more selective sirtuin inhibitors would greatly aid in evaluating the therapeutic potential of targeting sirtuins. To develop potent inhibitors specific for a particular sirtuin, we used mechanism-based thioacyl lysine compounds. Thioacyl lysine peptides can react with NAD in the sirtuin active site, forming a relatively stable intermediate that inhibits sirtuin (Fig. 2.1A) [35-37]. Recent studies suggested that different sirtuins may have different acyl group specificity [7,9,10,38], which can be utilized to design inhibitors specific for different sirtuins [25,39,40]. To target the sirtuins that can recognize aliphatic acyl groups, we synthesized four thioacyl lysine compounds, TA (thioacetyl) [41], TB (thiobutyryl), TH (thioheptanoyl), and TM (thiomyristoyl) (Fig. 2.1B), and then analyzed their ability to inhibit different sirtuins.

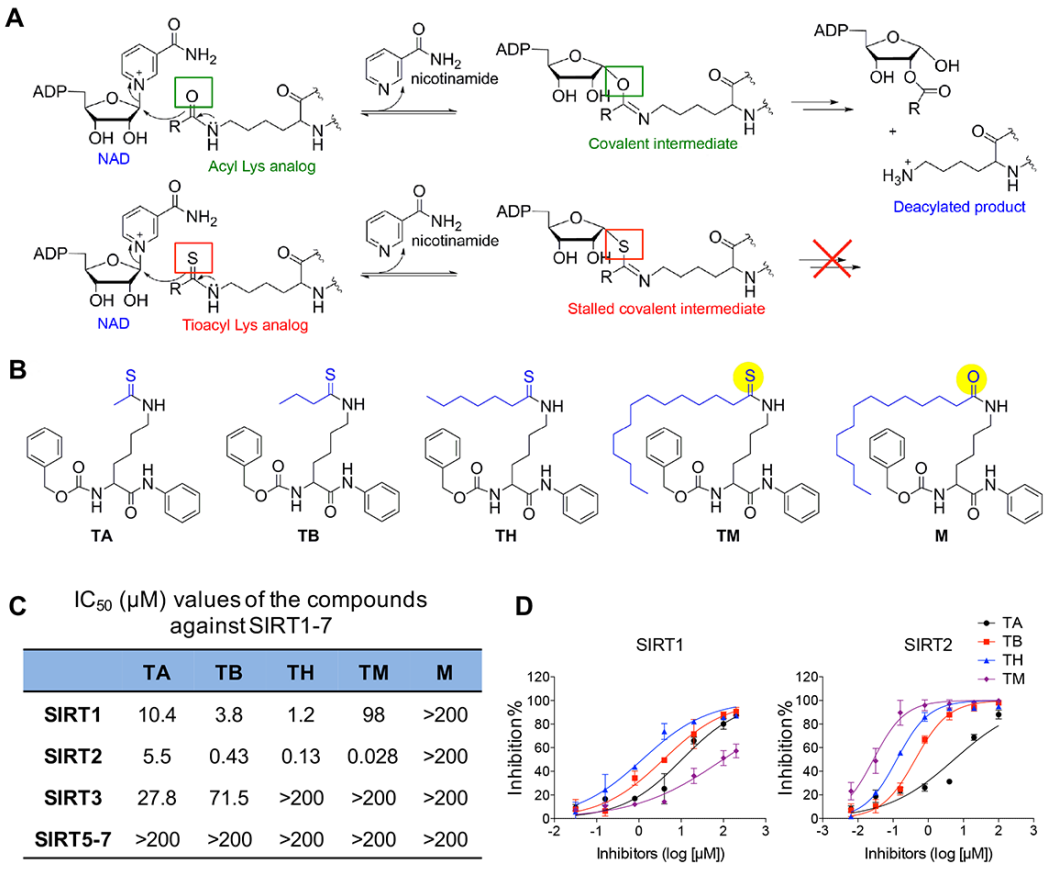

C IC_{50} (μM) values of the compounds against SIRT1-7

	TA	TB	TH	TM	M
SIRT1	10.4	3.8	1.2	98	>200
SIRT2	5.5	0.43	0.13	0.028	>200
SIRT3	27.8	71.5	>200	>200	>200
SIRT5-7	>200	>200	>200	>200	>200

Figure 2.1 Development of mechanism-based inhibitor of sirtuins. (**A**) The enzymatic reaction mechanism of sirtuin-catalyzed NAD-dependent deacylation (upper panel). Thioacyl lysine compounds act as suicide substrates to inhibit sirtuins (lower panel). (**B**) Structures of four different thioacyl lysine sirtuin inhibitors, TA, TB, TH, and TM. M, which differs from TM by just one atom (highlighted by yellow color), is an inactive control of TM. (**C**) IC_{50} (μM) values of the TA, TB, TH, TM and M against SIRT1-7. IC_{50} values derived from Graphpad Prism are presented as mean values from three independent experiments. (**D**) Dose-responsive curve for TA, TB, TH, TM and M against SIRT1 and SIRT2. Error bars represent mean ± sd.

Remarkable differences in the potency and selectivity of these compounds were observed by sirtuin activity assays *in vitro* (Fig. 2.1C & D). TA could inhibit SIRT1, SIRT2 and SIRT3, but not very potently. TB was a better SIRT1/SIRT2 inhibitor than TA. The IC_{50} of TB for SIRT1 (3.8 μM) and SIRT2 (0.43 μM) were about 3 fold and >10-fold, respectively, better than those of TA (Fig. 2.1C). Further increasing the size of the thioacyl group by three methylene groups lead to TH, which had even lower IC_{50} values for SIRT1 (1.2 μM) and SIRT2 (0.13 μM). Remarkably, TM, with a 14-carbon thioacyl group, could inhibit SIRT2 with an IC_{50} value of

0.028 μM, but inhibited SIRT1 with an IC_{50} value of 98 μM and did not inhibit SIRT3 even at 200 μM (Fig. 2.1C). None of these compounds can efficiently inhibit SIRT5, SIRT6, or SIRT7. Thus, TM is a SIRT2-speific inhibitor *in vitro*. To facilitate later investigations of TM, we also synthesized the corresponding myristoyl lysine compound (M, Fig. 2.1B) as an inactive control for TM. M differs from TM by only one atom (the S atom in TM is changed to an O atom in M). As expected, M did not show sirtuin inhibition even at 200 μM (Fig. 2.1C).

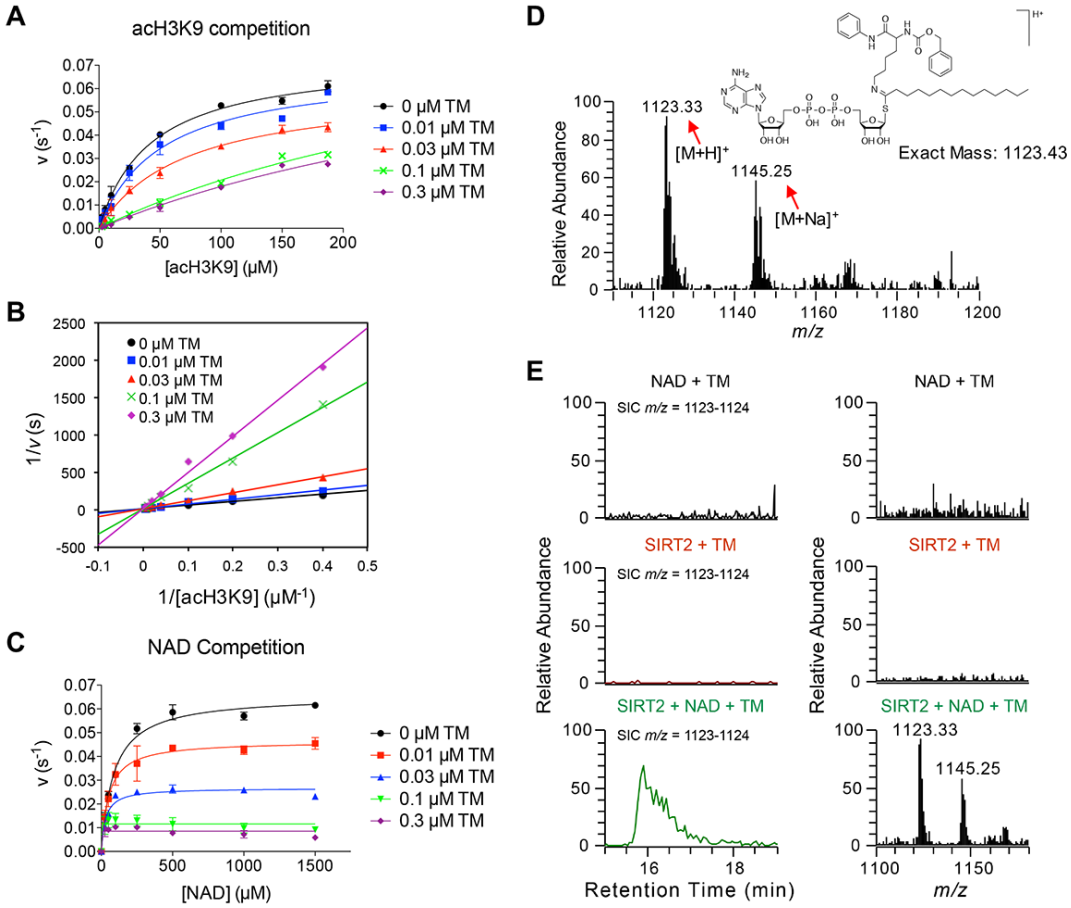

Figure 2.2 TM is a mechanism-based SIRT2 inhibitor. (**A**) Henri-Michaelie-Menten plots showing acH3K9 competition analyses of TM-mediated SIRT2 inhibition. (**B**) Double reciprocal plot with varied TM and acH3K9 concentrations. Data was fit to competitive inhibition using Graphpad Prism. (**C**) Henri-Michaelie-Menten plots showing NAD competition analyses of TM-mediated SIRT2 inhibition. (**D, E**) Mass spectrometry detection of the stable covalent intermediate formed by TM and NAD. (**D**) The selected ion chromatogram (SIC) (*m/z* = 1123-1124) for the reaction containg SIRT2, NAD and TM. (**E**) The selected ion chromatogram (SIC) (*m/z* = 1123-1124) was shown on the left, the mass spectrum was shown on the right. The data from the reaction mixture containing NAD and TM or the mixture containing SIRT2 and TM were shown as negative controls. Error bars represent mean ± sd.

To further confirm that TM is a mechanism-based inhibitor of SIRT2, we performed substrate competition analyses for TM-mediated SIRT2 inhibition. At saturating NAD concentration, the apparent K_m value for acetyl-H3K9 peptide (acH3K9) increased with increasing TM concentrations, whereas the v_{max} remained relatively constant (Fig. 2.2A). The double-reciprocal plot of $1/v$ versus 1/[acH3K9] revealed a series of lines that intersect at the $1/v$ axis (Fig. 2.2B), suggesting that TM is competitive with acH3K9. This is consistent with our recent finding that SIRT2 possesses a large hydrophobic pocket that can accommodate the myristoyl group [42]. At saturating acH3K9 concentration, both the apparent K_m value for NAD and v_{max} decreased with increasing TM concentrations (Fig. 2.2C), suggesting that TM is uncompetitive with NAD, which is consistent with the fact that formation of the inhibitory covalent intermediate requires NAD. We then used liquid chromatography-mass spectrometry (LC-MS) to examine the formation of the stalled covalent intermediate. Ions with *m/z* of 1123.33 (the protonated intermediate) and 1145.25 (the sodium adduct of the intermediate) were detected only when TM was incubated with both SIRT2 and NAD (Fig. 2.2D), but not without SIRT2 or NAD (Fig. 2.2E). Overall, these results indicate that TM acts as a mechanism-based inhibitor of SIRT2.

2.2 TM exhibited potent anticancer activity

Sirtuin inhibitors have been reported to have anticancer properties. However, most of the inhibitors used are not very selective and thus, inhibiting which sirtuins can provide beneficial effects remains unclear. Having a potent and very selective SIRT2 inhibitor provided a unique opportunity to investigate whether inhibiting SIRT2 can be useful as an anticancer strategy. We initially explored this in several breast cancer cell lines because of the substantial tumor-promoting role of SIRT2 in breast cancer [22-24] and the previous studies showing that SIRT2 inhibitors exert anti-proliferative effect against breast cancer cell lines [27,30,43-45]. We assayed the ability of TA, TB, TH, and TM to inhibit three different human breast cancer cell lines, MCF-

7, MDA-MB-468 and MDA-MB-231. The cytotoxicity effects of these compounds correlated with their *in vitro* SIRT2 inhibitory effects (Fig. 2.3A). TA, which showed modest SIRT1, SIRT2 and SIRT3 inhibition *in vitro*, did not inhibit cell viability at 50 μM. TB had greater inhibitory effect on cell viability than TA, but only showed inhibition at 50 μM. TH and TM were more potent than TA and TB. Compared with TH, the SIRT2-selective inhibitor TM showed greater inhibition of cell viability. The inactive inhibitor mimic M did not affect cell viability at 50 μM. Next we treated eight different human normal and breast cancer cell lines with TM. As shown in Fig. 2.3B, different malignant cells showed differential susceptibility to TM. And the two non-cancerous cell lines, MCF-10A and HME1, were much less sensitive to TM, suggesting that the cytotoxicity of TM is relatively selective toward cancer cells. We further evaluated the anticancer activity of TM using soft agar colony formation assay. TM significantly inhibited anchorage-independent growth of various cancer cells tested (Fig. 2.3C, D & E), while the control compound M did not (Fig. 2.3C).

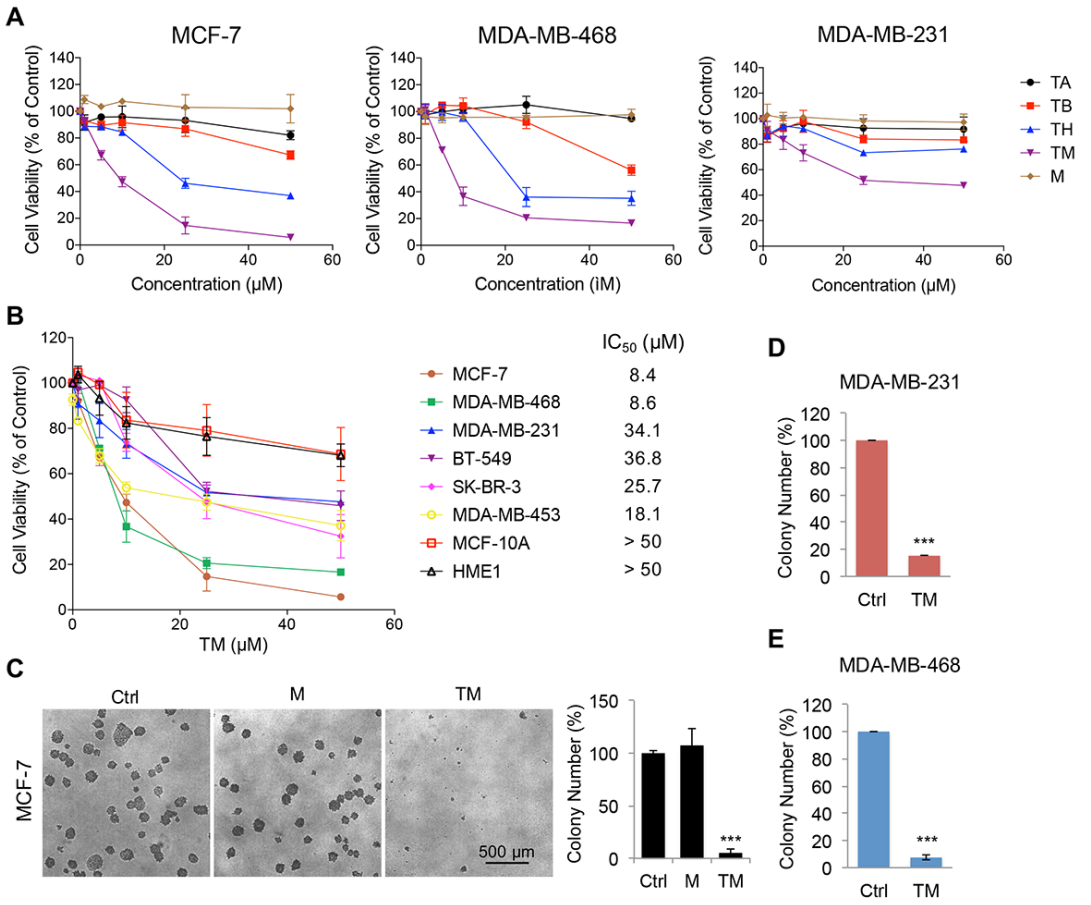

Figure 2.3 TM inhibits human cancer cells. (**A**) Cell viability of MCF-7, MDA-MB-468 and MDA-MB-231 cells treated with the indicated inhibitors for 72 hr. (**B**) Cell viability of the indicated human normal and breast cancer cells treated with TM for 72 hr. IC_{50} values were means from 3 independent experiments. (**C**) Soft agar colony formation of MCF-7 cells treated with ethanol, TM (25 μM in ethanol) or M (25 μM in ethanol). Representative images of colonies were shown on the left panel. (**D, E**) Soft agar colony formation of MDA-MB-468 (**D**) and MDA-MB-231 (**E**) cells treated with ethanol or TM (25 μM). Quantification of the colony numbers was shown on the right panel. The y axis represents percent colony number relative to ethanol-treated cells. Statistics, two-tailed Student's t-test. Error bars represent mean ± sd. ***$p < 0.001$.

The correlation between the cytotoxic effects of TA, TB, TH, TM and M and their *in vitro* SIRT2 inhibitory activities suggests that SIRT2 inhibition could have anticancer effects. To further confirm this, we knocked down all seven sirtuins individually (Fig. 2.4A) in MCF-7, MDA-MB-468 cells, which were relatively sensitive to TM. *SIRT2* knockdown (KD) produced the strongest cytotoxicity in both cell lines (Fig. 2.4B), which further supported SIRT2 inhibition as a promising anticancer strategy.

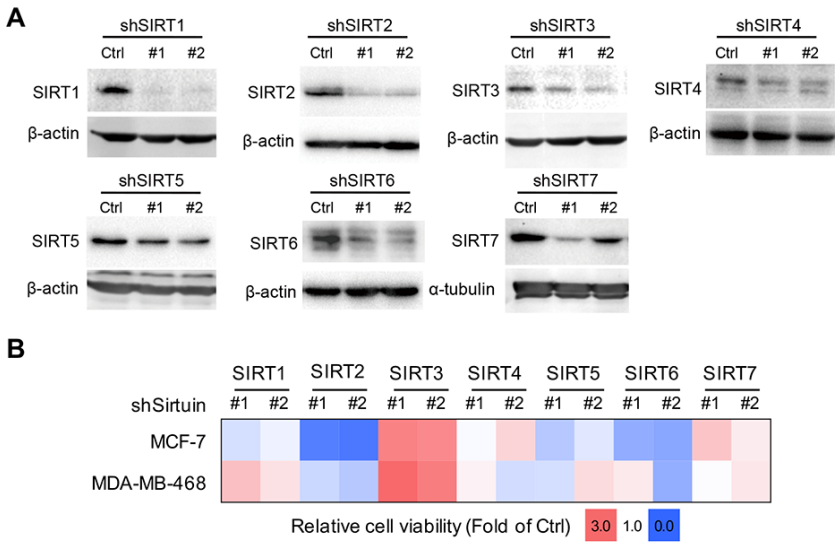

Figure 2.4 SIRT2 KD exerts the best cytotoxic effect compared to other sirtuin KDs. (**A**) Representative results showing the knockdown efficiency of SIRT1-7 in HeLa cells. Cells were infected with lentivirus carrying Luciferase shRNA and shRNAs against SIRT1-7 for 72 hr before analyzed by Western blot for sirtuin levels. (**B**) Cell viability of MCF-7 and MDA-MB-468 cells infected with lentivirus carrying luciferase shRNA (Ctrl) or SIRT1-7 shRNAs for 72 hr. The heat map presents average relative cell viability compared to Ctrl shRNA-infected cells from three independent experiments.

We then further examined the effect of SIRT2 KD in the same set of human breast cancer and non-tumorigenic mammary cell lines in which the cytotoxic effect of TM was tested. SIRT2 KD (Fig. 2.5A) significantly decreased cell viability in a time-dependent manner in MCF-7, MDA-MB-468, and MDA-MB-231 cells, but did not show much cytotoxicity in BT-549, SK-BR-3, and MDA-MB-453 cells or the non-transformed MCF-10A and HME1 cells (Fig. 2.5B). In MCF-7 and MDA-MB-468 cells, SIRT2 KD resulted in less than 1% cell viability after 10 days of lentiviral infection (Fig. 2.5C). Moreover, colony formation in soft agar by MCF-7 cells was dramatically diminished by SIRT2 KD (Fig. 2.5E). The knockdown data are thus consistent with the small molecule data, indicating that SIRT2 inhibition can effectively suppress cancer cell proliferation and that the anticancer effect of TM is likely through SIRT2 inhibition.

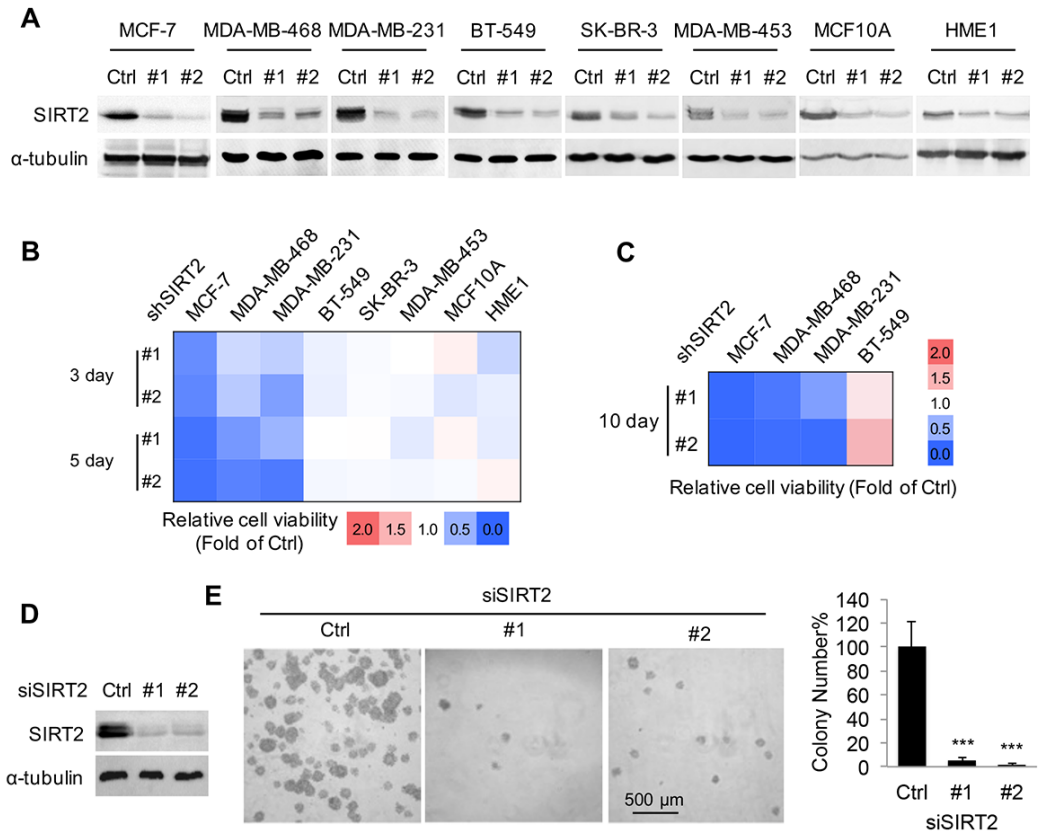

Figure 2.5 SIRT2 KD decreases the viability of various cancer cell lines. (**A**) SIRT2 knockdown efficiency in various human normal and breast cancer cells was confirmed by Western blot (the first row) 3 days after lentiviral infection. The α-tubulin level was used as internal standard of total protein amount. (**B**) Cell viability of various human normal and breast cancer cells infected with lentivirus carrying luciferase (Ctrl) or SIRT2 shRNAs for 3 or 5 days. (**C**) Cytotoxicity effects of SIRT2 knockdown in MCF-7, MDA-MB-468, MDA-MB-231 and BT-549 cells at day 10 after the infection. (**D**) Representative Western blots showing the knockdown efficiency of SIRT2 by siRNAs in MCF-7 cells. (**E**) Soft agar colony formation of MCF-7 cells transfected with scrambled siRNA or SIRT2 siRNA. Quantification of the colony numbers is shown in the right panel. The y axis represents percent colony number relative to scrambled siRNA-transfected cells. Statistics, two-tailed Student's *t*-test. Error bars represent mean ± sd. ***$p < 0.001$.

2.3 TM inhibits SIRT2 in cells

We next wanted to determine whether TM inhibits cancer cells by targeting SIRT2. We first carried out a number of experiments to validate that SIRT2 is the target of TM in cells. We conjugated biotin to TM and M to generate Biotin-TM and Biotin-M compounds (Fig. 2.6A). We then added these compounds to either total protein extract (Fig. 2.6B) or live cells (Fig. 2.6C) to pull down sirtuins. Biotin-TM was able to pull down SIRT2 but not SIRT1 from the

HEK293T cell extract. In contrast, Biotin-M, the inactive control compound, did not pull out SIRT2 (Fig. 2.6B). When assayed using SIRT2 KD cells, the amount of SIRT2 pulled down by Biotin-TM was also decreased (Fig. 2.6C). These data suggest that TM targets SIRT2 but not SIRT1 in cells.

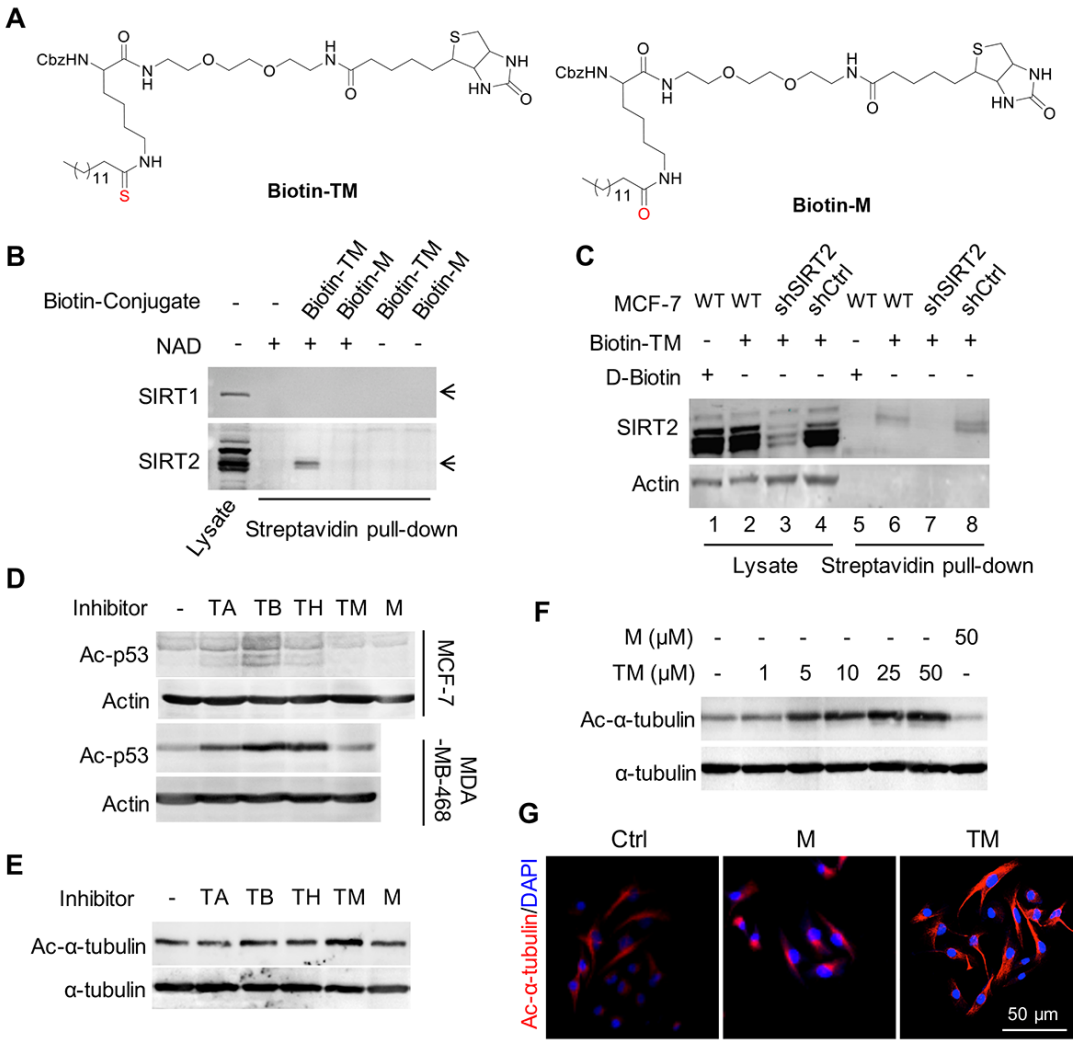

Figure 2.6 TM specifically inhibits SIRT2 in cells. (**A**) Structures of Biotin-TM and Biotin-M. (**B**) Pull-down assay to detect the binding of Biotin-M (10 μM) and Biotin-TM (10 μM) to SIRT1 and SIRT2 in HEK293T total cell lysate. (**C**) Pull-down assay to detect the binding of Biotin-TM (50 μM) to SIRT2 in MCF-7 cells. D-Biotin (50 μM) was used as a negative control. (**D**) Immunoblot for the acetylation of p53 (K382) in In MCF-7 or MDA-MB-468 cells treated with TSA (200 nM) and the indicated inhibitors (25 μM) for 6 hr. (**E**) Immunoblot for the acetyl-α-tubulin (K40) levels in SIRT2-overexpressing MCF-7 cells treated with indicated inhibitors (25 μM) for 6 hr. (**F**) Immunoblot for acetyl-α-tubulin (K40) levels in MCF-7 cells treated with TM or M for 6 hr. (**G**) Immunofluorescence detection of the acetyl-α-tubulin (K40) level in MDA-MB-231 cells treated with ethanol, M or TM (25 μM in ethanol) for 6 hr.

Second, we confirmed that TM inhibits SIRT2 in cells by detecting the acetylation level of known SIRT2 as well as SIRT1 targets. In MCF-7 and MDA-MB-468 cells, TA, TB, and TH, inhibited SIRT1, based on the acetylation level of a known SIRT1 deacetylation target, p53. In contrast, TM showed almost no inhibition of p53 deacetylation (Fig. 2.6D). By detecting the acetylation of α-tubulin, a known SIRT2 target, we monitored SIRT2 inhibition. TA or M, which did not inhibit SIRT2 well, did not affect the acetylation of α-tubulin. TB and TH, which have intermediate SIRT2 inhibition potency, slightly increased the acetylation of α-tubulin. TM, the best SIRT2 inhibitor, led to the greatest increase in α-tubulin acetylation (Fig. 2.6E). The effect of TM on α-tubulin acetylation was dose-dependent, whereas M did not affect acetyl-α-tubulin level at 50 μM (Fig. 2.6F). Similarly, TM, but not M, increased the level of α-tubulin acetylation in MDA-MB-231 cells based on immunofluorescence imaging (Fig. 2.6G). SIRT2 has been reported to be not only a deacetylase, but also a defatty-acylase (He et al., 2014; Liu et al., 2014), so we further examined the effect of TM on the defatty-acylase activity of SIRT2 in cells. Metabolic labeling of fatty-acylated proteins revealed that SIRT2 KD (Fig. 2.7A) but not TM (Fig. 2.7B) was able to elevate the fatty acylation levels of many proteins, suggesting that in cells TM is a potent inhibitor of SIRT2 deacetylase but not defatty-acylase.

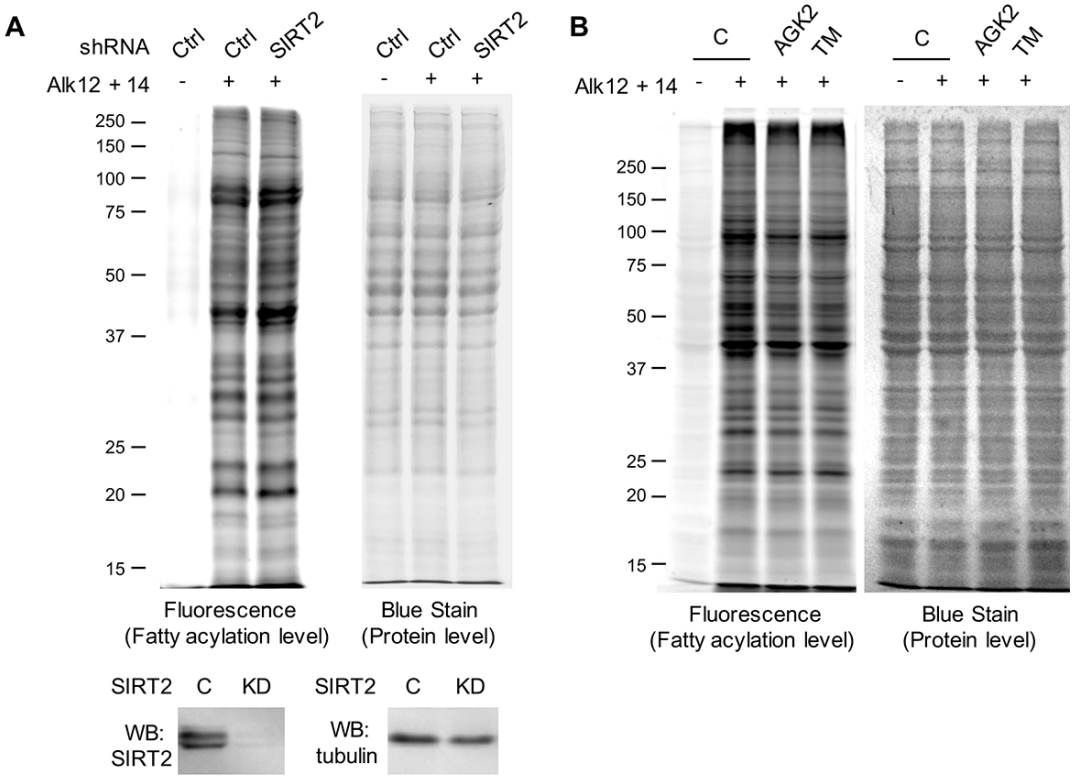

Figure 2.7 TM does not inhibit SIRT2 defatty-acylase activity. (**A**) Global protein fatty acylation in HEK293T cells with Ctrl and SIRT2 knockdown. Protein fatty acylation was detected by a metabolic labeling method using alkyne-tagged fatty acid analogs Alk12 (50 μM) and Alk14 (50 μM). SIRT2 KD efficiency by western blot analyses is shown in the bottom panel. (**B**) Global protein fatty acylation in HEK293T cells treated with the ethanol, AGK2 (25 μM) or TM (25 μM) for 6 hr in the presence of Alk12 (50 μM) and Alk14 (50 μM).

Finally, to confirm that the anticancer effect of TM is due to SIRT2 inhibition, we tested the sensitivity of cells to TM under SIRT2 overexpression or knockdown conditions. If TM inhibits cancer cells by targeting SIRT2, overexpression of SIRT2 would decrease the sensitivity of cells to TM (the increased SIRT2 level would require more TM for inhibition), while partial and transient knockdown of SIRT2 would increase the sensitivity. Indeed, overexpression of SIRT2 (Fig. 2.8A) significantly decreased the cytotoxicity of TM (Fig. 2.8B), while transient and partial knockdown of SIRT2 (Fig. 2.8C) sensitized cells to TM (Fig. 2.8D). These results support the conclusion that the anticancer effect of TM is through SIRT2 inhibition instead of other off-target effects.

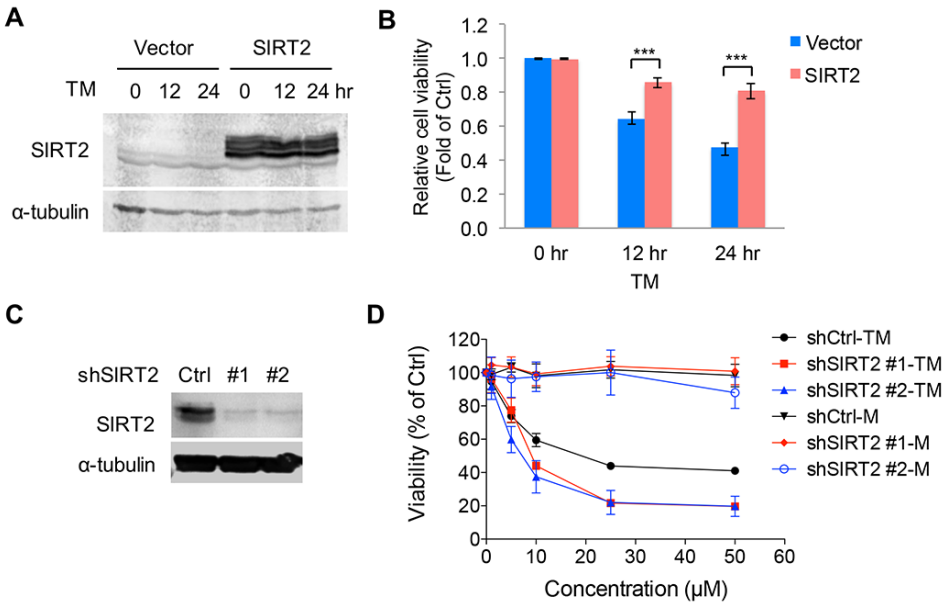

Figure 2.8 TM targets SIRT2 in exert anticancer effect. (**A**) Confirmation of SIRT2 overexpression in MCF-7 cells transfected with pCMV vector or pCMV-*SIRT2* for 12 hr. (**B**) Effect of SIRT2 overexpression on the cytotoxicity effect of TM. MCF-7 cells were transfected with pCMV vector or pCMV-*SIRT2* for 12 hr before being treated with 25 μM of TM for 12 or 24 hr. The y axis represents relative cell viability compared to ethanol-treated controls. (**C**) Confirmation of SIRT2 KD in MDA-MB-231 cells infected with lentiviral Luciferase shRNA and SIRT2 shRNAs. (**D**) Effect of SIRT2 knockdown on the sensitivity of MDA-MB-231 cells to TM. MDA-MB-231 cells were infected with lentiviral Luciferase shRNA and SIRT2 shRNAs, respectively, for 24 hr before being treated with different concentrations of TM for another 72 hr. Cell viability was measured by CellTiter-Blue® assay. Stat lentiviral Luciferase shRNA and SIRT2 shRNAs istics, two-tailed Student's *t*-test. Error bars represent mean ± sd. ***p < 0.001.

2.4 TM inhibits tumor growth in mouse models of breast cancer

To further demonstrate that SIRT2 inhibition can be useful for treating cancers, we tested TM in two mouse models of cancer. The first was a xenograft model in which the triple-negative breast cancer cell line, MDA-MB-231, was injected subcutaneously into immunocompromised mice. When tumor size reached ~200 mm^3, the mice were divided into two groups and treated by either direct intratumor (IT) (Fig. 2.9) or intraperitoneal (IP) (Fig. 2.10) injection of the control vehicle solvent (DMSO) or TM (1.5 mg TM in 50 μL DMSO; n = 5) daily. Tumors were collected after 30-days of treatment and analyzed. TM treatment significantly inhibited tumor growth as compared to the control (Fig. 2.9A, 2.9B, & 2.10A). Histopathological examination

revealed central areas of necrosis in tumors from both DMSO and TM treated mice, but the necrosis was more extensive and the overall tumor size was smaller in the TM treated mice (Fig. 2.9D and 2.10C). IT TM injection showed a stronger effect in reducing tumor volume and increasing areas of necrosis as compared to IP TM injection. Analysis of TM content in tissue samples from TM-treated mice showed that IP-administered TM reached the tumors, even though the serum concentration of TM was low and a significant amount of TM accumulated in abdominal fat (Fig. 2.10D). TM did not cause significant toxicity in mice (one mouse from each treatment group died, likely due to infection caused by repeated IP injection but not due to TM toxicity) and no significant weight loss was observed in TM-treated mice (Fig. 2.9C & 2.10B). Immunohistochemistry staining of Ki-67 was performed to assess the effect of TM on the proliferation of tumor cells *in vivo*. As shown in Fig. 2.9F (upper panel) and 2.9G, as well as Fig. 2.10E (upper panel) and 2.10F, a significant decrease in Ki-67^{+} cells was observed with TM treatment relative to vehicle treatment. To determine whether TM inhibits SIRT2 *in vivo*, we performed immunofluorescence staining of acetyl-α-tubulin in the xenograft tumors. As shown in Fig. 2.9F (lower panel) and 2.9H and Fig. 2.10E (lower panel) and 2.10G, the acetyl-α-tubulin level was moderately but statistically significantly increased in tumors from TM treated mice compared with those from vehicle-treated mice, suggesting that TM indeed inhibits SIRT2 *in vivo*.

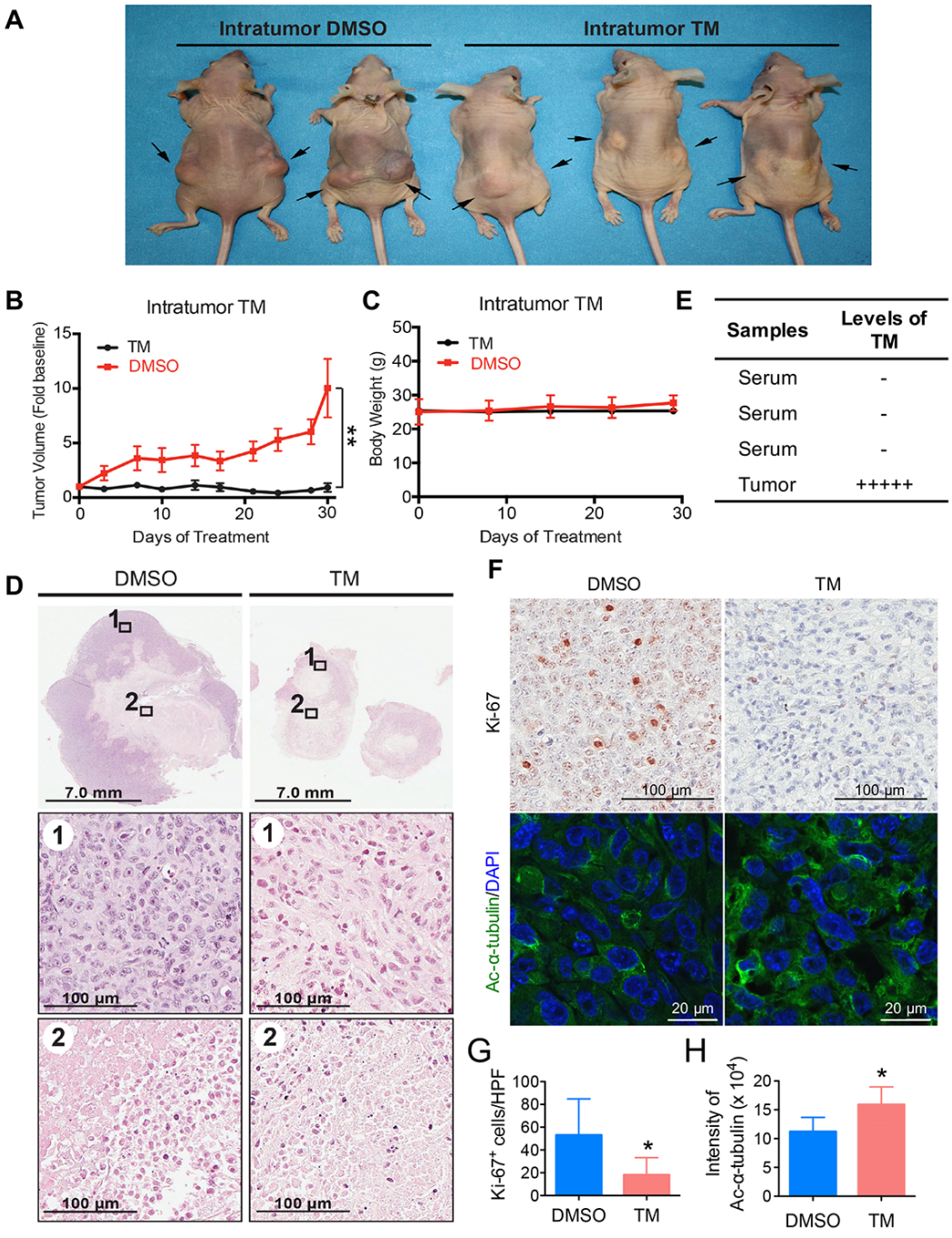

Figure 2.9 Analysis of tumor growth and histopathological findings of xenografted mice treated by intratumor TM injection. Mice bearing MDA-MB-231 human breast cancer xenograft were divided into two groups and treated by direct intratumor injection with either the control vehicle solvent (DMSO) or TM (0.75 mg TM in 50 uL DMSO; n = 5) three times per week. Tumors were collected after 30-day treatment. (**A**) Gross findings at necropsy after 30 days of intratumor treatment with either DMSO or TM. (**B**) Tumor growth chart. Statistics, paired Student's *t*-test. (**C**) Mouse body weight chart. (**D**) Hematoxylin and eosin staining of tumor tissues after 30 days of treatment with either DMSO or TM. (**E**) Detection of TM in mouse serum and tumor tissues by mass spectrometry. (**F**) Representative images of Ki-67 immunohistochemistry staining and acetyl-α-tubulin (K40) immunofluorescence staining of tumor

tissues after 30 days of treatment with either DMSO or TM. (**G**) Quantification of Ki-67$^+$ cells in (**F**). The y axis represents Ki-67$^+$ cells per high power field (10 HPFs/tumor for all the tumors analyzed, n = 4 for DMSO, n = 6 for TM). Statistics, unpaired Student's *t*-test. (**H**) Quantification of acetyl-α-tubulin fluorescence intensity in (**F**). The y axis represents integrated intensity per cell. (10 HPFs/tumor for all the tumors analyzed, n = 4 for DMSO, n = 6 for TM). Statistics, unpaired Student's *t*-test. Error bars represent mean ± sd. *p < 0.05, **p < 0.01.

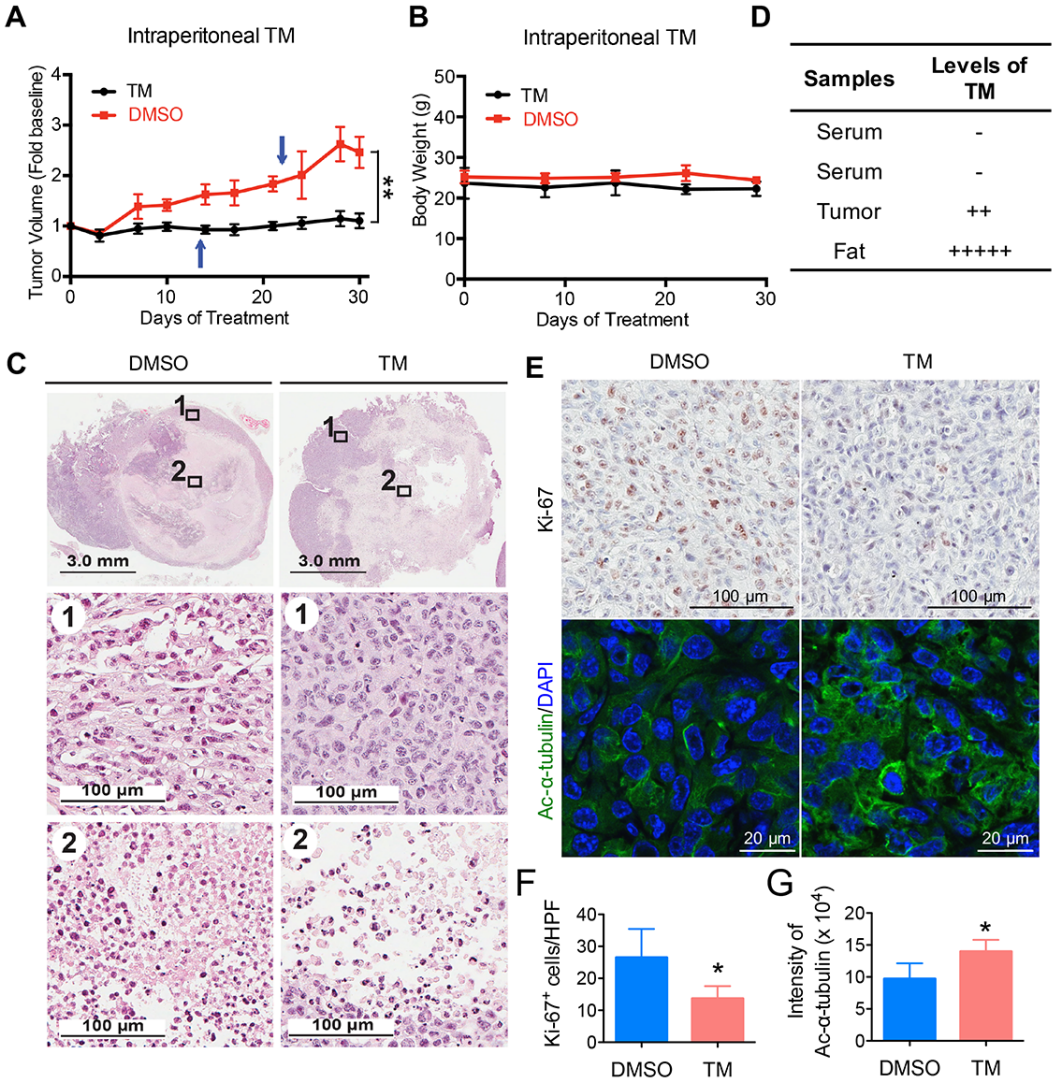

Figure 2.10 Analysis of tumor growth and histopathological findings of xenografted mice treated by intraperitoneal TM injection. Mice bearing MDA-MB-231 human breast cancer xenograft were divided into two groups and treated by IP injection with either the vehicle (DMSO) or TM (1.5 mg TM in 50 μL DMSO; n = 5) daily. Tumors were collected after 30-day treatment. (**A**) Tumor growth chart. Arrows indicate time point when an animal was found dead (1 untreated, 1 treated). Statistics, paired Student's *t*-test. (**B**) Mouse body weight chart. (**C**) Hematoxylin and eosin staining of tumor tissues after 30 days of treatment with DMSO or TM. (**D**) Detection of TM in mouse serum, fat and tumor tissues by mass spectrometry. (**E**) Representative images of Ki-67 immunohistochemistry staining and acetyl-α-tubulin (K40) immunofluorescence staining of tumor tissues after 30 days of treatment with DMSO or TM. (**F**) Quantification of Ki-67$^+$ cells in (**E**). The y axis represents Ki-67$^+$ cells per high power field (10

HPFs/tumor for all the tumors analyzed, n = 3 for DMSO, n = 4 for TM). Statistics, unpaired Student's *t*-test. (**F**) Quantification of acetyl-α-tubulin fluorescence intensity in (**E**) by ImageJ. The y axis represents integrated intensity per cell. (10 HPFs/tumor for all the tumors analyzed, n = 3 for DMSO, n = 4 for TM). Statistics, unpaired Student's *t*-test. Error bars represent mean ± sd. *p < 0.05, **p < 0.01.

The second mouse model was the mammary tumor model driven by mammary gland-specific expression of polyoma middle T antigen under the control of mouse mammary tumor virus promoter/enhancer (MMTV-PyMT model) [46]. The MMTV-PyMT mice received daily IP injections with either the control vehicle solvent (DMSO) or TM (1.5 mg TM in 50 μL DMSO; n = 10). The Kaplan-Meier tumor-free survival curve showed that TM treatment significantly prolonged the tumor-free survival of mice compared with vehicle-treated mice (Fig. 2.11A). While the average time to tumor onset in the control group was 48 days, the mean latency for TM-treated mice was 54 days. Histopathological examination revealed more extensive areas of necrosis in the neoplasms from TM-treated mice as compared to the control group (Fig. 2.11B). A significant decrease in proliferation of tumor cells was observed with TM treatment relative to vehicle treatment as measured by Ki-67 staining (Fig. 2.11C, upper panel, and 2.11D). A modest but statistically significant increase in the acetyl-α-tubulin level was observed in tumors from TM-treated mice compared to those from vehicle-treated mice (Fig. 2.11C, lower panel, and 2.11E), indicating that SIRT2 was inhibited by TM *in vivo*. The data demonstrate that SIRT2 inhibition with TM delays tumor onset in the MMTV-PyMT model and reduces tumor growth *in vivo*.

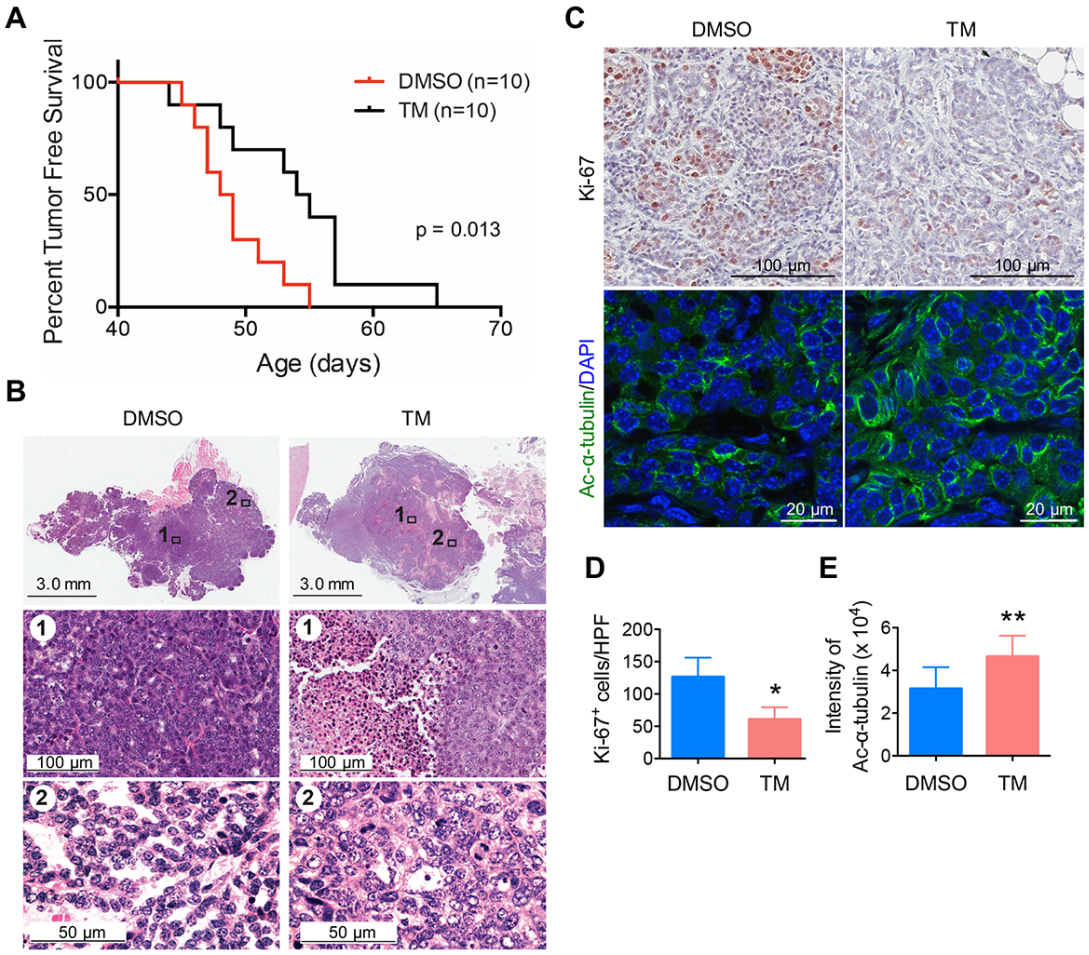

Figure 2.11 Mammary tumorigenesis in MMTV-*PyMT* female mice following intraperitoneal TM injection. (**A**) Kaplan-Meier tumor-free survival curve of MMTV-*PyMT* mice treated by IP injection with either the vehicle (DMSO) or TM (1.5 mg TM in 50 µL DMSO; n = 10) daily. The x-axis shows mice age; the y-axis shows proportion of mice remaining tumor-free. Statistics, log-rank test. (**B**) Hematoxylin and eosin staining of mammary tumors after 30 days of treatment with either DMSO or TM. (**C**) Representative images of Ki-67 immunohistochemistry staining and acetyl-α-tubulin (K40) immunofluorescence staining of tumor tissues after 30 days of treatment with either DMSO or TM. (**D**) Quantification of Ki-67$^+$ cells in (**C**). The y axis shows Ki-67$^+$ cells per high power field (10 HPFs/tumor for all the tumors analyzed, n = 4 for DMSO, n = 4 for TM). Statistics, unpaired Student's *t*-test. (**E**) Quantification of acetyl-α-tubulin fluorescence intensity in (**C**) by ImageJ. The y axis shows integrated intensity per cell. (10 HPFs/tumor for all the tumors analyzed, n = 8 for DMSO, n = 8 for TM). Statistics, unpaired Student's *t*-test. Error bars represent mean ± sd. *p < 0.05, **p < 0.01.

2.5 COMPARE analysis with the NCI-60 cancer cell panel points to possible mechanism of action for the SIRT2 inhibitor TM

To further investigate the anticancer effects of TM, we first examined whether the level of SIRT2 in different cell lines could be used to predict which cell lines would be more sensitive

to SIRT2 inhibitors. We checked the SIRT2 protein level in all the eight human normal and breast cancer cell lines above (Fig. 2.3B & 2.5B) to see if the sensitivity to TM correlated with SIRT2 level in these cell lines. Compared to MCF-10A and HME1 cells, the cancer cell lines showed relatively high SIRT2 expression. However, we did not see an obvious correlation between SIRT2 level and TM sensitivity (Fig. 2.12A & B) among the cancer cell lines, suggesting that other factors account for the SIRT2 inhibitor sensitivity.

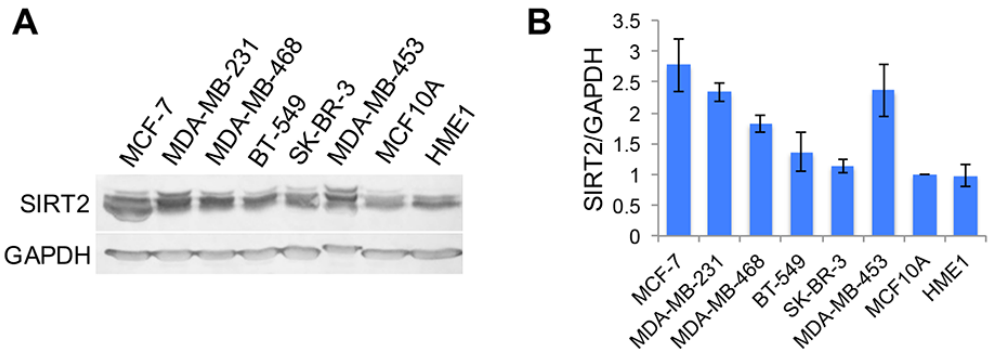

Figure 2.12 SIRT2 levels in different human normal and breast cancer cell lines. Western blot analysis of SIRT2 level (**A**) and semi-quantification of SIRT2 level relative to GAPDH level (**B**).

To examine the anticancer activity of TM against other malignancies and the molecular mechanisms underlying its activity, we submitted the TM compound to the Developmental Therapeutics Program of the National Cancer Institute (NCI) at the National Institutes of Health for screening against the NCI-60 panel of human cancer cell lines [47]. The screening result showed that TM inhibited 36/56 of the NCI-60 cell lines by >50% at 10 μM (Fig. 2.13A). In particular, all the leukemia cell lines were very sensitive to TM and most of colon cancer cell lines were sensitive to TM. In contrast, melanoma and ovarian cancer cells were less sensitive to TM. Consistent with our earlier findings (Fig. 2.3), MCF-7 and MDA-MB-468 cells were very sensitive to TM.

A

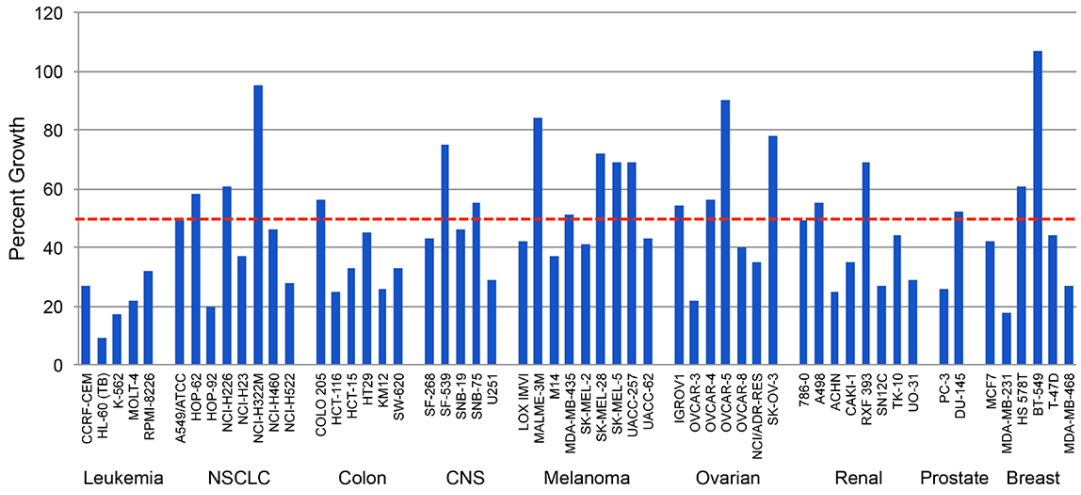

B

Top four correlated genes from molecular target Compare analysis of the NCI-60 assay data of TM

Rank	Target ID	Gene	Correlation value	Target pattern description
1	MT18283	Myc	0.503	c-Myc phosphorylation level at T58 and S62
2	MT18332	Myc	0.493	c-Myc protein level
3	MT11065	FGFR2	0.477	Fraction of DNA methylation at FGFR2 5' UTR
4	MT1125	CDC25A	0.465	Relative mRNA levels of CDC25A

Figure 2.13 COMPARE analysis with the NCI-60 cancer cell panel suggests possible mechanism of action for TM (**A**) NCI-60 cell line screening of TM. NCI-60 cell lines were cultured with and without 10 μM TM for 24 hr. The percent growth of TM-treated cells compared to the controls is shown. The horizontal dotted red line shows 50% growth. (**B**) Top four correlated genes from molecular target Compare analysis of the NCI-60 assay data of TM. The data set used is the MT series.

To investigate how SIRT2 inhibition halts cancer cell proliferation, we took advantage of NCI molecular target COMPARE analysis [48]. NCI has accumulated many data sets regarding the properties of the NCI-60 cell lines, including gene expression, DNA methylation, protein expression, and post-translational modifications. The molecular target COMPARE analysis serves to correlate the response of the NCI-60 panel to a small molecule (TM in this case) to known molecular patterns. From this analysis, we found that the sensitivity of NCI-60 cell lines to TM correlated best with c-Myc phosphorylation/protein levels. In other words, cell lines with higher c-Myc phosphorylation/protein levels were more sensitive to TM (Fig. 2.13B). The

correlation between TM sensitivity and c-Myc is intriguing as c-Myc is an oncoprotein that is up-regulated in many cancers.

2.6 TM decreases c-Myc oncoprotein level in cancer cells

The correlation between TM efficacy and c-Myc was informative, but the small correlation value (~0.5) was not sufficient to establish a mechanistic relationship. To further understand the connection, we measured c-Myc levels in the cells treated with and without TM or M. TM decreased c-Myc protein levels in a time-dependent manner in MCF-7 cells, whereas M treatment had no effect on the c-Myc protein level (Fig. 2.14A). Similar effects of TM on c-Myc were also observed in K562 (Fig. 2.18C) and MDA-MB-468 cells (Fig. 2.18D). Consistent with the effect of TM, c-Myc abundance was also reduced by SIRT2 KD (Fig. 2.14C), suggesting that TM works through SIRT2 inhibition to decrease c-Myc. To further establish that the reduction in c-Myc protein is important for the anticancer effect of TM, we examined whether the sensitivity of cancer cell lines to TM correlated with the decrease in c-Myc level induced by TM treatment. Among the six breast cancer cell lines in the NCI-60 panel, BT-549 did not respond to treatment with 10 μM TM (Fig. 2.13A). This result was in line with our own findings (Fig. 2.3B). Although higher concentrations of TM did decrease the viability of BT-549, the sensitivity was much lower than that of MCF-7 cells. Consistent with the reduced sensitivity to TM, SIRT2 KD in BT-549 cells did not decrease cell viability (Fig. 2.3B & 2.5B). We therefore examined whether TM could affect c-Myc protein levels in BT-549 cells. Consistent with the decreased TM sensitivity, TM treatment did not have a significant effect on c-Myc protein abundance in BT-549 cells (Fig. 2.14B). SIRT2 KD also failed to decrease c-Myc levels in BT-549 cells (Fig. 2.14C). These data collectively suggest that the sensitivity of cancer cell lines to TM correlates with the ability of TM to decrease c-Myc levels *via* SIRT2 inhibition in these cell lines. We further measured the IC_{50} values of TM in six different cancer cell lines and the corresponding decrease in c-Mycs level in these cell lines upon TM treatment.

Plotting the IC_{50} values against the decreases in c-Myc levels indicates that there was an excellent correlation between them (Fig. 2.14D), supporting that the ability of TM to decrease c-Myc is important for its anticancer effect in the cell lines that are very sensitive to TM.

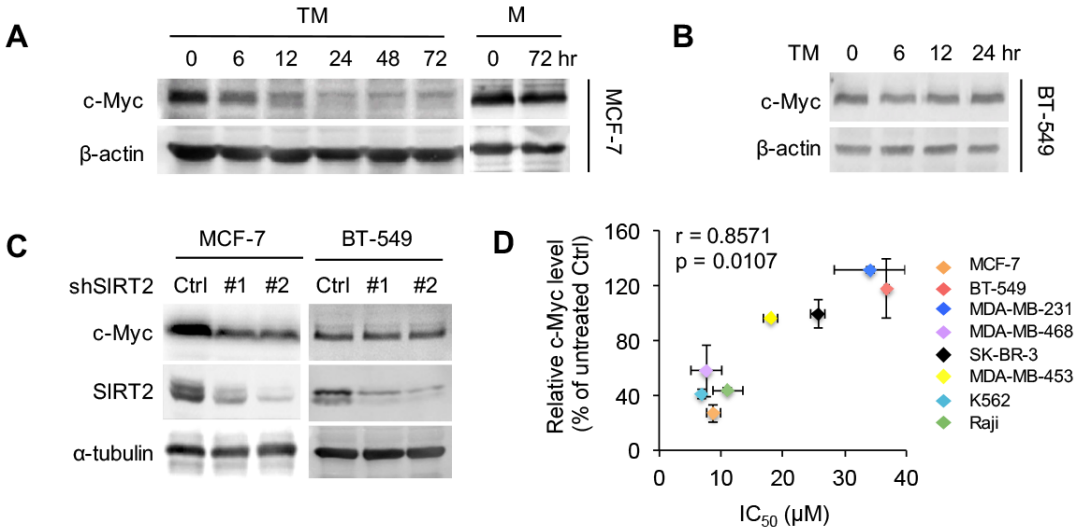

Figure 2.14 TM decreases c-Myc protein level. (**A**) c-Myc protein levels in MCF-7 cells treated with TM (25 μM) or M (25 μM). (**B**) c-Myc protein levels in BT-549 cells treated with TM (25 μM). (**C**) The levels of c-Myc, SIRT2 and α−tubulin in MCF-7 or BT-549 cells infected with luciferase or SIRT2 shRNAs for 72 hr. (**D**) The correlation between the ability of TM to inhibit cancer cell lines and its ability to decrease c-Myc level. The x axis shows IC_{50} values of TM in different cell lines. The y axis shows the TM-induced decreases in c-Myc level. Relative c-Myc level was obtained by comparing the c-Myc protein level in cells treated with TM for 24 hr to that in vehicle-treated control cells. Error bars represent mean ± sd.

Then to test the effect of TM or SIRT2 KD on c-Myc transcriptional activity, we did RNA-sequencing to compare gene expression in vehicle-treated versus TM-treated, or Ctrl KD versus SIRT2 KD MCF-7 cells. We then used Geneset enrichment analysis (GSEA)[49] to test whether a previously defined set of c-Myc target genes was affected by TM or SIRT2 KD. The analysis result showed that c-Myc target gene sets were enriched in both TM- and SIRT2 KD-decreased genes (Fig. 2.15), indicating that both TM and SIRT2 KD downregulate c-Myc transcriptional activity.

A

NAME	TM 12h		SIRT2 KD	
	NES	FDR q	NES	FDR q
HALLMARK_MYC_TARGETS_V1	-3.15	0.0000	-2.33	0.0000
HALLMARK_MYC_TARGETS_V2	-2.94	0.0000	-2.33	0.0000
DANG_REGULATED_BY_MYC_UP	-1.73	0.0348	-2.10	0.0004
MENSSEN_MYC_TARGETS	-2.09	0.0029	-1.88	0.0062
DANG_MYC_TARGETS_UP	-2.39	0.0000	-1.86	0.0075
SCHUHMACHER_MYC_TARGETS_UP	-1.99	0.0062	-1.84	0.0089

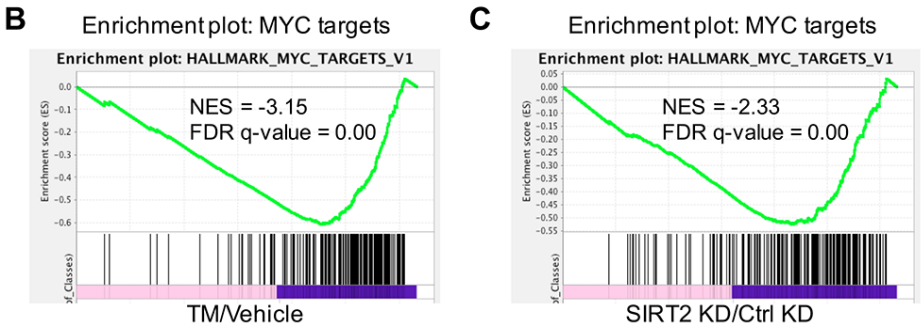

Figure 2.15 TM and SIRT2 KD inhibit c-Myc transcriptional activity. (**A**) Table of c-Myc target gene sets enriched among genes downregulated by TM (25 μM, 12 hr) or SIRT2 KD (72 hr) in MCF-7 cells. The normalized enrichment score (NES), and test of statistical significance (FDR q value) are shown. (**B, C**) Enrichment of a representative set of c-Myc target genes in TM-treated (B) and SIRT2 KD (C) MCF-7 cells.

MCF-7 cells were then further analyzed for Myc-specific biological effects. Flow cytometry of TM-treated cells revealed a pronounced increase in cells arrested in G0/G1 phase, with a concomitant decrease of cells in S phase (Fig. 2.16A). Treatment of TM resulted in significant cellular senescence by β-galactosidase staining (Fig. 2.16B). Similar effects of TM on cell cycle progression and cellular senescence were also observed in K562 cells (Fig. 2.16C & D), suggesting that the effect of TM-induced c-Myc decrease is not restricted to breast cancer cells. Overall, the phenotypes of G0/G1 cell cycle arrest and cellular senescence are consistent with the anticipated effects of inhibiting cellular c-Myc function [50].

To further establish that decreasing c-Myc is important for the anticancer effect of TM, we examined whether forced overexpression of c-Myc in MCF-7 cells is able to reduce TM-mediated cytotoxicity. Cells were transfected with c-Myc for 12 hr before being treated with

TM. Overexpression of c-Myc significantly reduced the cytotoxicity effect of TM (Fig. 2.16E, F & G). Together, these results demonstrate TM decreases c-Myc, which is important for the cytotoxicity of TM in tumor cell, although it is likely not the only mechanism that underlies the cytotoxicity.

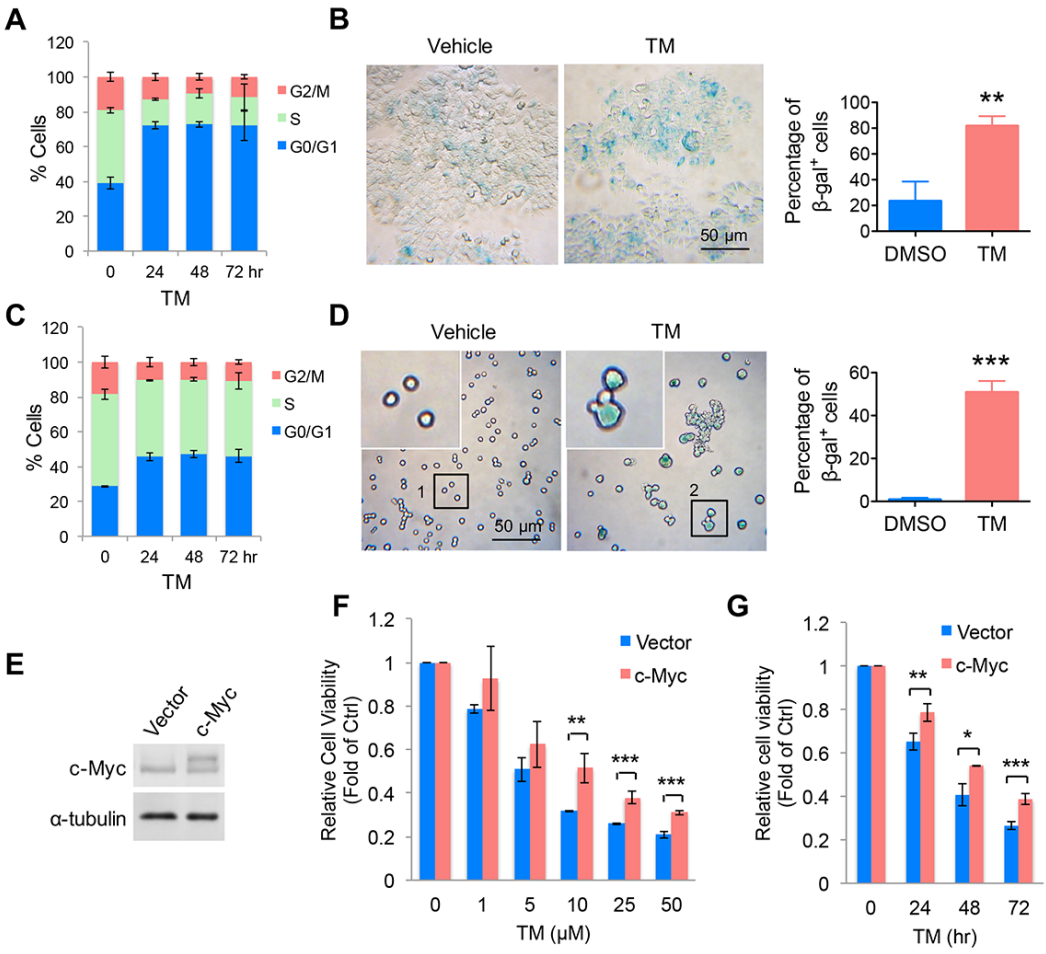

Figure 2.16 Decreasing c-Myc protein abundance contributes to the anticancer effect of TM. (**A, C**) Cell cycle distribution (assessed by propidium iodide staining-coupled flow cytometry) of MCF-7 (**B**) and K562 (**C**) cells treated with TM (25 μM) for 0, 24, 48 or 72 hr. (**B, D**) Acidic β-gal (β-gal) staining in MCF-7 (**B**) and K562 (**D**) cells treated with TM (25 μM) for 5 days. Representative images were shown in the upper panel, quantification was shown as percentage of β-gal$^+$ cells in the lower panel. (**E, F, G**) Effect of c-Myc overexpression (**E**) on the cytotoxicity effect of TM. MCF-7 cells were transfected with pCDH vector or pCDH-c-Myc for 12 hr before being treated with TM at indicated concentrations for 72 hr (**F**) or with TM (25 μM) for another 0, 24, 48 or 72 hr (**G**). Cell viability was assessed by CellTiter-Blue® assay. Statistics, two-tailed Student's *t*-test. Error bars represent mean ± sd. **p < 0.01, ***p < 0.001.

The *c-Myc* mRNA level was not affected by TM treatment, suggesting that TM does not affect *c-Myc* transcription (Fig. 2.17A & 2.17E). Therefore, the effect of TM on c-Myc protein turnover was tested. The half-life of c-Myc was shortened by TM treatment, suggesting that TM promoted c-Myc degradation (Fig. 2.17B). Treatment with a proteasome inhibitor, MG132, prevented the TM-induced down-regulation of c-Myc, suggesting that TM promoted the proteasomal degradation of c-Myc (Fig. 2.17C). Increased proteasomal degradation was associated with increased c-Myc ubiquitination (Fig. 2.17D).

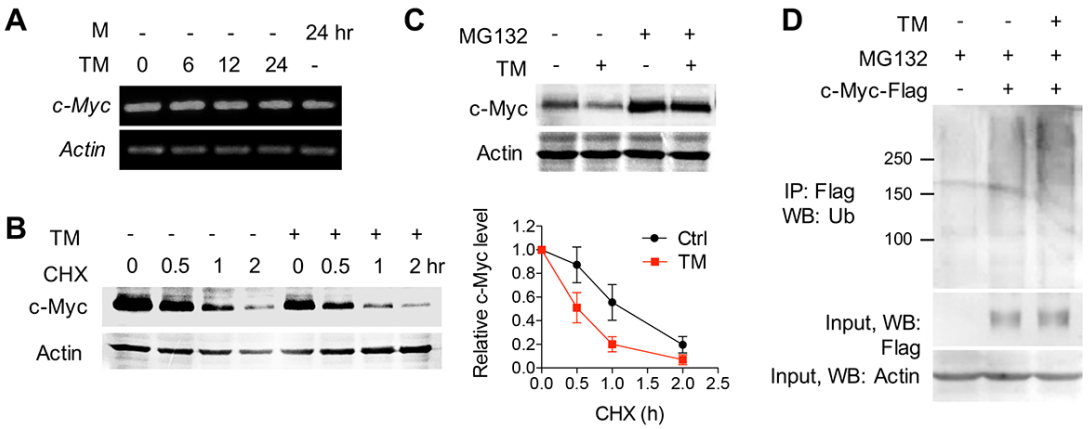

Figure 2.17 TM promotes ubiquitin-proteosomal degradation of c-Myc. (**A**) The mRNA levels of *c-Myc* in MCF-7 cells treated with TM (25 μM) or M (25 μM) analyzed by RT-PCR. (**B**) Effect of TM on c-Myc degradation in MCF-7 cells. Cells were incubated ethanol or TM (25 μM in ethanol) for 4 hr and then with CHX (10 μg/mL) for 0, 0.5, 1, or 2 hr. Loading was normalized based on the level of the internal control, actin. The relative c-Myc protein levels at different time point of CHX treatment were calculated by normalizing to the corresponding level without CHX treatment. The relative c-Myc levels were plotted against the time of treatment with CHX. (**C**) Effect of MG132 on TM-mediated decrease in c-Myc protein level in MCF-7 cells. Cells were treated with ethanol or TM (25 μM in ethanol) for 4 hr and then MG132 (10 μM) for 2 hr. (**D**) Effect of TM (25 μM) on the polyubiquitination of c-Myc in MCF-7. Error bars represent mean ± sd.

It was previously reported that SIRT2 can suppress the expression of NEDD4, an E3 ubiquitin ligase for c-Myc [18], which could explain why SIRT2 inhibition promotes c-Myc degradation. Indeed, NEDD4 was up-regulated by TM at the transcriptional level (Fig. 2.18A & E) and also modestly at the protein level (Fig. 2.18B & C) in both MCF-7 and K562 cells. However, this is not a universal mechanism as alteration of NEDD4 level was not detected in TM-treated MDA-MB-468 cells despite the observed reduction in c-Myc protein abundance

(Fig. 2.18D & E). As TM regulates the protein stability of c-Myc in all three cell lines, we checked the effect of TM on the transcription levels of several additional known E3 ligases that destabilize c-Myc [18,51-54]. As shown in Fig. 2.18E, *NEDD4* and *TRPC4AP* were increased in MCF-7 and K562 cells, but not in MDA-MB-468 cells; *FBXW7* and *STUB1* were up-regulated in only in MDA-MB-468 cells; *FBXO32* was increased in all the three cell lines. However, none of the E3 ligase genes was obviously up-regulated by TM in BT-549 cells in which neither cell viability nor c-Myc level was affected by TM. These results suggested that SIRT2 inhibition led to up-regulation of several c-Myc E3 enzymes, which may result in the destabilization of c-Myc by TM.

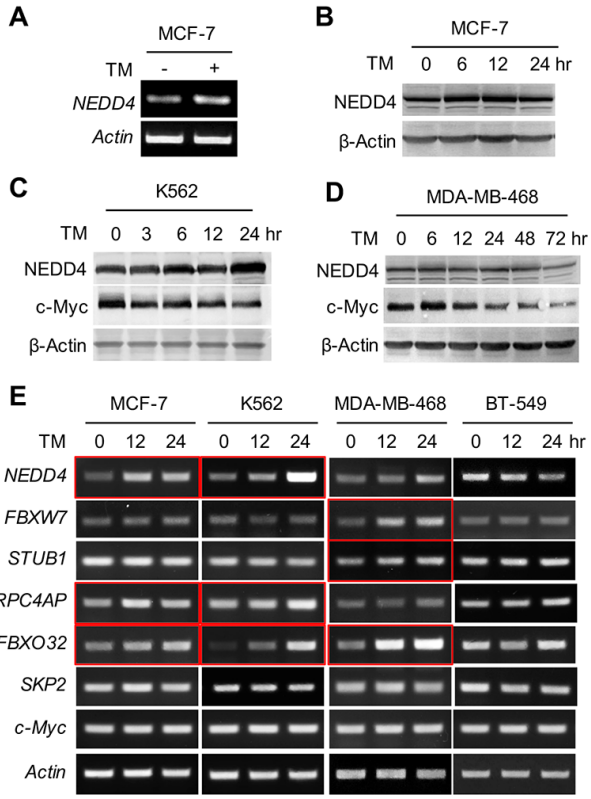

Figure 2.18 TM upregulates transcriptional levels of c-Myc E3 ubiquitin ligases. (**A**) The mRNA level of *NEDD4* in MCF-7 cells treated with TM (25 μM) for 12 hr. (**B**) Western blot analysis of NEDD4 protein level in MCF-7 cells treated with TM (25 μM). (**C, D**) Effects of TM on c-Myc and NEDD4 protein levels in K562 (**C**) and MDA-MB-468 (**D**) cells. Cells were treated as indicated. (**E**) Effect of TM on the transcript levels of various E3 ligases of c-Myc. MCF-7, K562, MDA-MB-468 or BT-549 cells were treated with TM (25 μM) for the indicated time. PCR was performed for the assessment of transcript levels of E3 ligases (*NEDD4, FBXW7, STUB1, TRPC4AP, FBXO32, SKP2*), *c-Myc* and *Actin*.

3. Discussion

Previous reports have suggested that SIRT1 or SIRT2 inhibitors can have anticancer activity. However, the potency of most of these inhibitors is modest, with IC_{50} values in the micromolar range at inhibiting purified sirtuins. Most of the sirtuin inhibitors tested for anticancer activity are also not very selective and can inhibit several sirtuins. The modest potency and selectivity make it hard to rule out off-target effects and pinpoint which sirtuin should be targeted for treating cancers. Our SIRT2 inhibitor TM described here has an excellent combination of potency and selectivity that allowed us to conclude that inhibiting SIRT2 produces anticancer effects in a variety of human cancer cell lines. Knocking down of all seven sirtuins also confirmed that SIRT2 is important for the viability of various cancer cell lines while knocking down other sirtuins either had no significant effect or much less effect on cancer cell viability.

C-Myc is an important oncoprotein and is up-regulated in many human tumors. Thus, it has been considered as a promising cancer target. So far, no small molecules can directly target c-Myc *in vivo*. Recent studies showed that bromodomain inhibitors targeting BRD4 can suppress *c-Myc* transcription and inhibit tumorigenesis [3]. Our studies demonstrate that inhibiting SIRT2 offers a different way to target c-Myc. We show here that our SIRT2 inhibitor TM can effectively decrease the level of c-Myc in various cancer cell lines. Our data suggest that the ability of TM to decrease c-Myc abundance in different cell lines correlates with the sensitivity of the cell lines to TM. We further demonstrate here that decreasing c-Myc protein level is an important mechanism that accounts for hypersensitivity of certain cancer cell lines to TM. However, it should be pointed out that effects on other SIRT2-regulated pathways may also contribute to the activity of TM in cancer cells. This is especially true given that even cells without TM-induced c-Myc decrease (e.g. MDA-MB-231 and BT-549 cells) can still be inhibited by TM at higher concentrations. This also likely explains why c-Myc overexpression

confers some but not complete resistance to TM (Fig. 2.16 F & G). We found that TM promotes the proteolytic degradation of c-Myc without affecting its transcription, which serves as an important but perhaps not the only mechanism by which TM destabilizes c-Myc. Aberrant translational control of the Myc oncoprotein has been implicated in many cancers [55,56] and might also be involved in TM-induced reduction in c-Myc level. Our work establishes SIRT2 inhibition as a strategy to target the oncoprotein c-Myc, which is effective in many human cancer cell lines. Future detailed mechanistic investigations of the SIRT2/c-Myc regulatory pathway could potentially lead to the identification of additional therapeutic targets.

The roles of sirtuins in cancer have been a topic of debate. Both tumor-promoting and tumor-suppressing roles of SIRT1 have been reported. For SIRT2, Kim et al. reported that *SIRT2* is a tumor suppressor because *Sirt2* KO mice develop tumors earlier than WT mice [17]. Serrano and co-workers did not find a cancer-prone phenotype in unchallenged *Sirt2* KO mice that they generated, although they did observe that *Sirt2* KO mice had increased tumorigenesis when challenged with carcinogens (Serrano et al., 2013).[57]. Contradictory to these genetic studies that pointed to a weak tumor suppressor role of SIRT2, we found that inhibiting SIRT2 with TM has broad anticancer activity in many cancer cell lines.

Different outcomes for mouse genetic studies and pharmacological studies in cancer cells are not without precedent. Similar cases have been well documented in the literature [58]. There are several possible explanations. First, there are several examples of factors that have tumor suppressor activity in normal cells but nevertheless are required for the growth and survival of transformed cells. For example, loss of function for the DNA damage checkpoint kinase ATR causes modest tumor predisposition, but greatly impairs the growth of established tumors [59]. SIRT2 has been identified as a regulator of mitotic chromosome segregation [17], a function that could account for the weak tumor predisposition phenotype in *Sirt2*-deficient mice given the oncogenic consequences of genomic instability. Nevertheless, a greater dependency of

transformed cells on SIRT2 due to increased mitotic and other stresses, or because of the regulation of other targets such as c-Myc by SIRT2, result in heightened sensitivity to SIRT2 inhibition in cancer cells. It also should be noted that small molecules may have off target effects, which could contribute to observed pharmacological effects. While it is difficult to completely rule out this possibility for the anticancer effect of TM, our studies using the inactive control compound (M) and the SIRT2 KD studies suggest that the anticancer effect is largely through SIRT2 inhibition.

An alternative explanation relates to the fact that in a genetic knockout, the protein is gone and thus all the enzymatic activities and protein-protein interactions involving the enzyme also are gone. In contrast, when using a small molecule to inhibit the enzyme, the protein is intact and so are the protein-protein interactions that involve the protein. In the case of SIRT2, another layer of complexity is that SIRT2 has multiple enzymatic functions. We and others recently found that sirtuins are not only deacetylases. Some sirtuins, such as SIRT5 [7] and SIRT6 [11], prefer to hydrolyze other acyl lysine modifications. Perhaps more surprising is the fact that even the well-studied deacetylases (SIRT1, SIRT2, and SIRT3) can remove long chain fatty acyl groups efficiently [25,60]. Although the exact substrate proteins for the defatty-acylase activity of SIRT2 remain to be identified, our preliminary studies showed that the fatty acylation levels of many proteins were elevated when SIRT2 was knocked down (Fig. 2.7A), but not when SIRT2 inhibitor TM was used (Fig. 2.7 B). Thus, the small molecule inhibitor may selectively target one of the enzymatic functions of SIRT2, thus contributing to the fact that small molecule inhibitors may produce beneficial pharmacological effects that are different from genetic knockout.

4. Methods

Reagents, antibodies and plasmids. All chemicals were obtained in the highest purity available. MG132 was from Cayman Chemical Co. (Ann Arbor, MI). Cycloheximide was purchased from Amresco (Euclid, OH). Trichostatin A (TSA) and AGK2 (2-Cyano-3-[5-(2,5-dichlorophenyl)-2-furanyl]-N-5-quinolinyl-2-propenamide) were obtained from Sigma-Aldrich (St. Louis, MO).

The anti-human SIRT1 antibody (3H10.2) was from EMD Chemicals Inc. (San Diego, CA). The anti-human SIRT2 (EPR1667), SIRT6 antibodies were from Abcam (Cambridge, MA). The anti-human SIRT3 (C73E3), acetyl-p53 (Lys382) antibodies were obtained from Cell Signaling Technology (Danvers, MA). The anti-SIRT7 (C-3), c-Myc (9E10), NEDD4 (H-135), ubiquitin (P4D1), β-actin (C4) and the goat anti-mouse/rabbit IgG-horseradish peroxidase-conjugated antibodies were purchased from Santa Cruz Biotechnology (Santa Cruz, CA). The anti-SIRT4 (LS-C100490) antibody was purchased from LSBio, Inc. (Seattle, WA). The anti-SIRT5 antibody (Center) was from Abgent (San Diego, CA). The anti-acetyl-α-tubulin (6-11B-1), α-tubulin (B-5-1-2) antibodies, the anti-Flag M2 antibody conjugated with horseradish peroxidase and the anti-Flag M2 affinity gel were from Sigma-Aldrich.

The pLKO.1-puro lentiviral shRNAs constructs toward Luciferase and SIRT1-7 were purchased from Sigma-Aldrich. Luciferase shRNA (SHC007), SIRT1 shRNA1 (TRCN0000018980), SIRT1 shRNA2 (TRCN0000018981), SIRT2 shRNA1 (TRCN0000040221), SIRT2 shRNA2 (TRCN0000310335), SIRT3 shRNA1 (TRCN0000038890), SIRT3 shRNA2 (TRCN0000038893), SIRT4 shRNA1 (TRCN0000018948), SIRT4 shRNA2 (TRCN0000232894), SIRT5 shRNA1 (TRCN0000018544), SIRT5 shRNA2 (TRCN0000018545), SIRT6 shRNA 1 (TRCN0000378253) and shRNA 2 (TRCN0000232528), SIRT7 shRNA1 (TRCN0000359663), and SIRT7 shRNA2 (TRCN0000020254) were used. The scrambled siRNA and Stealth Select RNAi™ siRNA targeting SIRT2 (HSS117928 and HSS177042) were purchased from

Invitrogen (Carlsbad, CA). To generate human SIRT2 with C-terminal Flag-tag expression vector, full-length human SIRT2 cDNA was amplified by PCR and inserted into pCMV-tag-4a vector between BamHI and XhoI sites. A human c-Myc expression vector with N-terminal Flag-tag was obtained by PCR amplification of Flag-c-Myc and subcloning via BamHI and XhoI sites into pCMV-tag-4a vector.

Cloning, expression and purification of human sirtuins. Human SIRT1, SIRT3, SIRT5 and SIRT6 were expressed as previously described [11,61]. Human SIRT2 (aa38-356) was cloned and inserted into pET28a vector for the expression of N-terminal His6-SUMO fusion protein. Then SIRT2 expression vector was introduced into an *E. coli* BL21. Successful transformation were selected by plating the cells on kanamycin (50 μg mL^{-1}) and chloramphenicol (20 μg mL^{-1}) luria broth (LB) plates. Single colonies were selected and grown in LB with kanamycin (50 μg mL^{-1}) and chloramphenicol (20 μg mL^{-1}) overnight at 37 °C. On the following day the cells were subcultured (1:1000 dilution) into 2 L of LB with kanamycin (50 μg mL^{-1}) and chloramphenicol (20 μg mL^{-1}). The cells were induced with 20 μM of isopropyl β-D-1-thiogalactopyranoside (IPTG) at an OD_{600} of 0.6 and grown overnight at 15 °C, 200 rpm. The cells were harvested by centrifugation at 8000 rpm for 5 min at 4 °C (Beckman Coulter refrigerated floor centrifuge) and passed through an EmulsiFlex-C3 cell disruptor (AVESTIN, Inc.) 3 times. Cellular debris was removed by centrifuging at 20,000 rpm for 30 min at 4 °C (Beckman Coulter). The supernatant was loaded onto a nickel column (Histrap, Ge Healthcare) pre-equilibrated with 20 mM Tris-HCl pH 8.0 with 500 mM NaCl. The protein was eluted with a linear gradient of imidazole (0-500 mM). The desired fractions were pooled, concentrated and buffer exchanged. The His6-SUMO tag was removed by overnight incubation at 4 °C with ULP1, followed by Ni-affinity column purification to remove any undigested SIRT2. The tag-free SIRT2 was further purified on a Superdex 75 column (Bio-Rad, Hercules, CA). The protein

was eluted with 20 mM Tris-HCl, pH 8.0, 500 mM NaCl. After concentration, the target protein was frozen at -80 °C.

Inhibition assay for SIRT1, SIRT2, SIRT3, SIRT5. Different concentrations (0.0064, 0.032, 0.16, 0.8, 4.0, 20, 100 and 200 μM) of TA~TM, and M were pre-incubated with 0.1 μM of SIRT1, 0.2 μM of SIRT2, 1 μM of SIRT3 or 1 μM of SIRT5, respectively, and 1 mM NAD in 20 mM Tris-HCl buffer (pH 8.0) with 1 mM dithiothreitol (DTT) at 37 °C for 15 min. Then 10 μM of acyl peptide (acetyl-H3K9 for SIRT1, SIRT2 and SIRT3; succinyl-H3K9 for SIRT5) was added to initiate the reactions. Then reactions were incubated at 37°C in a total volume of 60 μL (5 min for SIRT1, 5 min for SIRT2, 20 min for SIRT3, and 10 min for SIRT5). The reactions were stopped by adding 60 μL of an aqueous solution of 50% methanol containing 200 mM HCl and 320 mM acetic acid.

After quenching the sirtuin reactions, centrifugation was used to remove precipitated proteins and the supernatant was analyzed by HPLC with a reverse phase C18 column (Kinetex XB-C18 100A, 100 mm × 4.60 mm, 2.6 μm, Phenomenex) with a gradient of 0 % in 2 min, 0% to 20% in 2min, 20% to 40% B in 13 min and then 40% to 100% for 2 min at 0.5 mL/min. Product quantification was based on the area of absorbance monitored at 280 nm. The peak areas were integrated and the conversion rate was calculated from the peak areas as the fraction of the free H3K9 peptide from the total peptide. All reactions were done in duplicate.

Determination of kinetic parameters for TM. For SIRT2 inhibition kinetics of TM, a mixture of acetyl-H3K9 (acH3K9) peptide substrate (2.5, 5, 10, 25, 50, 100, 187.5 μM), NAD (25, 50, 100, 250, 500, 1000, 1500 μM), TM (0, 0.01, 0.03, 0.1, and 0.3 μM), 20 mM Tris-HCl (pH 8.0) and 1 mM DTT was incubated at 37 °C. 1 mM NAD was used for determining the kinetic parameters for acH3K9 peptide, 100 μM of acH3K9 peptide was used for the determination of kinetic parameters for NAD. The reaction was started by adding 0.2 μM of

SIRT2, and stopped after 5 min by adding 60 μL of an aqueous solution of 50% methanol containing 200 mM HCl and 320 mM acetic acid. The samples were analyzed by HPLC as described above and the initial velocity was calculated. The K_m and v_{max} were obtained from Michaelie-Menten plots using Graphpad Prism software.

Mass spectrometry detection of the stalled intermediate formed by TM and NAD. Reactions containing 50 μM SIRT2, 100 μM NAD, 100 μM TM, 1 mM DTT, and 20 mM pyridinium formate (pH 7.0) was reacted for 5 min at 37 °C. Controls were run in which NAD or SIRT2 was removed from the reaction mixture. Reactions were quenched with 1 volume of acetonitrile and the mixture was centrifuged to remove the precipitated protein. The supernatant was then analyzed by LC-MS using water and acetonitrile as solvents.

Inhibition assay for SIRT6. Different concentrations (0.0125, 0.05, 0.2, 0.8, 3.2, 12.8, 51.2, 204.8 μM) of TA~TM were pre-incubated with 1 μM of SIRT6 and 1 mM NAD in 20 mM Tris-HCl buffer (pH 8.0) with 1 mM DTT at 37°C for 20 min. Then 50 μM of myristoyl-H3K9 peptide (myrH3K9) was added to initiate the reactions. The reactions were incubated at 37 °C in a total volume of 60 μL for 1 hr. The reactions were stopped by adding 60 μL of an aqueous solution of 50% methanol containing 200 mM HCl and 320 mM acetic acid.

Inhibition assay for SIRT7. Different concentrations (0.0125, 0.05, 0.2, 0.8, 3.2, 12.8, 51.2, 204.8 μM) of TA~TM were pre-incubated with 1 μM of SIRT7 and 1 mM NAD in 150mM NaCl and 50 mM KH_2PO_4 buffer (pH 8.0) with 1 mM DTT at 37°C for 20 min. Then 10 μM myrH3K9 peptide and 0.083mg/mL tRNA were added to initiate the reactions. Then reactions were incubated at 37 °C in a total volume of 60 μL for 110 min. The reactions were stopped by adding 60 μL of an aqueous solution of 50% methanol containing 200 mM HCl and 320 mM acetic acid.

Cell viability assay. Cells were seeded into 96-well plates at 3000-4000 cells per well. After 24 hr, test compounds were added to cells to final concentrations ranging from 1–50 μM. Cells were then incubated for 72 hr and cell viability was measured using the CellTiter-Blue viability assay (Promega) following the manufacturer's instruction. Relative cell viability in the presence of test compounds was normalized to the vehicle-treated controls after background subtraction. Graphpad Prism software was used to determine the IC_{50} values.

Knockdown of SIRT1-7 in various cell lines was achieved by lentiviral infection. Lentiviral supernatants were generated as described previously (Jiang et al., 2013). Cell viability was assessed after 3, 5 or 10 days of infection by using CellTiter-Blue.

Cell culture and transfection. All cell culture media contained 10% (vol/vol) heat-inactivated fetal bovine serum (FBS; Invitrogen, Carlsbad, CA) and 1% penicillin-streptomycin (Invitrogen) unless otherwise specified. Human MCF-7, MDA-MB-231, MDA-MB-468, HeLa, HME1 cells were grown in DMEM media (Invitrogen). Human BT-549, SK-BR-3, MDA-MB-453 and K562 cells were grown in RPMI-1640 media (Invitrogen). The MCF-10A cells were cultured in mammary epithelial cell growth medium (MEGM; Lonza, Walkersville, MD) with supplements according to manufacturer's instruction.

To overexpress SIRT2 or c-Myc in cells, the pCMV-tag-4a vector containing *SIRT2* or *c-Myc,* or pCDH vector containing *c-Myc* were transfected into cells using FuGene 6 (Promega, Madison, WI) according to manufacturer's protocol. Empty vector was transfected as negative control.

Soft agar colony formation assay. For colony formation in semisolid medium, 1.0×10^4 cells were plated in 0.3% low-melting point agarose (LMP, Invitrogen) onto 6-well plate coated with 1.2% LMP mixed with 2 × complete medium. For treatments, 2 × inhibitor was added to cells at the time of plating. The medium and inhibitor were replaced with fresh ones every 3

days. For colony formation of the SIRT2 KD cells, cells were transfected with the scrambled siRNA or SIRT2 siRNAs for 48 hr before plating in 6-well plate. Similarly, cell media was replaced every 3 days. After 14 days of incubation, colonies were photographed and counted with ImageJ.

Western blot analysis. Western blot analysis was performed as described previously (Jiang et al., 2013). The proteins of interest were detected using enzyme-linked chemiluminescence (ECL; Pierce Biotechnology Inc.) and visualized using the Storm Imager (GE Healthcare, Piscataway, NJ). Quantification of Western blots was done using the Quantity One software (Bio-Rad).

Biotin-TM/M pull-down assay. HEK293T cells were collected and lysed in lysis buffer containing 25 mM Tris, pH 7.4, 150 mM NaCl, 10% glycerol, 1% Nonidet P-40 and 1 × protease inhibitor cocktail (Sigma-Aldrich). The cell extract supernatant was collected after centrifugation at 14,000 g for 20 min at 4 °C. Cell lysates were incubated with 10 μM Biotin-TM or Biotin-M in the absence or presence of 1 mM NAD at 4 °C for 1 hr. The high capacity streptavidin resin (Pierce Biotechnology, Rockford, IL) was added to the mixture and incubated at 4 °C for another 1 hr. After centrifugation at 500 g for 2 min at 4 °C, the streptavidin resin was washed 3 times with 1 mL washing buffer (25 mM Tris, pH 7.4, 150 mM NaCl, 10% glycerol, 0.2% Nonidet P-40). The resin-bound proteins were then separated with SDS-PAGE and immunoblotted with anti-SIRT1 or anti-SIRT2 antibodies.

To assess the binding of TM to SIRT2 in cells, MCF-7 parental cells, Luciferase KD and SIRT2 KD cells were treated with 50 μM D-Biotin or Biotin-TM as indicated for 6 hr and then lysed in lysis buffer containing 1 mM NAD. Cell extract was collected, streptavidin pull-down and western blot analysis was performed as described above.

SIRT1 inhibition in cells. MCF-7 or MDA-MB-468 cells were treated with indicated test compounds in the presence of 200 nM TSA for 6 hr. The acetylation level of p53 protein was determined by western blot using anti-acetyl-p53 ($_{K382}$) antibody. β-actin served as a loading control.

SIRT2 inhibition in cells. MCF-7 cells were treated with indicated inhibitors at for 6 hr after being transfected with pCMV-tag-4a-SIRT2 for 18 hr. Cells were collected and lysed in lysis buffer containing 25 mM Tris, pH 7.4, 150 mM NaCl, 10% glycerol, 4 mM $MgCl_2$, 0.2 mM DTT, 100 mM NAD, 1% Nonidet P-40 and 1 × protease inhibitor cocktail. And the cell lysates were subjected to western blot for the analysis of acetyl-α-tubulin (K40) and α-tubulin levels.

TM treatment of mice bearing human breast cancer xenotransplants. Two million MDA-MB-231 cells suspended in 100 μL 1 × PBS and 100 μL Matrigel were injected subcutaneously on the flanks of female Ncr Nu/Nu mice. Following the injections, mice were permitted to recover and monitored biweekly, including tumor measurement using calipers. Once the majority of tumors reached a threshold size of 200 mm^3, mice with intraperitoneal (IP) or intra-tumor (IT) injections of vehicle alone (DMSO) or inhibitor (TM in DMSO) over one month. IP injections of 1.5 mg TM in 50 μL DMSO were given daily. IT injections of 0.75 mg TM in 50 μL DMSO per tumor were given 3 days per week. After one month of treatment or if mice met humane endpoint criteria, mice were euthanized by CO_2 asphyxiation. Tissues were collected, fixed with 10% neutral-buffered formalin, embedded in paraffin, sectioned, and stained with hematoxylin and eosin (H&E). H&E-stained sections were scanned using an Aperio ScanScope and analyzed by a veterinarian certified in anatomic pathology by the American College of Veterinary Pathologists blinded to treatment group. Serum, tumor tissues and organs were snap frozen in liquid N_2 and stored at -80 °C for subsequent analyses.

TM treatment of MMTV-PyMT mice. MMTV-PyMT transgenic female mice on a pure FVB/N background were obtained from the Jackson Laboratory and treated beginning at 6 weeks of age with daily IP injections of vehicle (DMSO) or 1.5 mg TM in 50 μL DMSO over one month. Mice were monitored daily for tumor development and health status, and tumor size was measured twice per week. After one month of treatment or if mice met humane endpoint criteria, mice were euthanized by CO_2 asphyxiation and necropsied. Tissues were collected and analyzed as described above.

Ubiquitination assay. MCF-7 cells were transfected with pCMV-tag-4a or pCMV-tag-4a-c-Myc, respectively. 18 hours after transfection, cells were treated with 25 μM TM for 6 hr in the presence of proteasome inhibitor MG132 (10 μM). Immunoprecipitation was performed with the cell lysates by anti-Flag M2 affinity gel as described previously [25]. The gel-bound proteins were resolved on SDS-PAGE and detected with anti-ubiquitin antibody. The c-Myc level in total cell lysates was used as input control.

Reverse transcription (RT)-PCR analysis of mRNA levels. Total RNA was extracted from vehicle-, TM- or M-treated cells using RNeasy Mini Kit (Qiagen, CA, USA) according to the manufacturer's instructions. The concentration and purity of total RNA were determined by using the NanoDrop (Thermo Fisher Scientific Inc, Wilmington, DE). cDNA was synthesized using SuperScript III reverse transcriptase (Invitrogen). Amplification of genes of interest was performed using Herculase II Fusion DNA Polymerase (Agilent Technologies, Santa Clara, CA) with the gene-specific primers shown below. 10 μl of each PCR product were analyzed by gel electrophoresis on a 2% agarose gel.

Primer target	Direction	Sequence
c-Myc	Forward	GGCTCCTGGCAAAAGGTCAGAGT
c-Myc	Reverse	CTGCGTAGTTGTGCTGATGTGT
NEDD4	Forward	TCAGGACAACCTAACAGATGCT

NEDD4	Reverse	TTCTGCAAGATGAGTTGGAACAT
Actin	Forward	CATGTACGTTGCTATCCAGGC
Actin	Reverse	CTCCTTAATGTCACGCACGAT
STUB1	Forward	AGCAGGGCAATCGTCTGTTC
STUB1	Reverse	CAAGGCCCGGTTGGTGTAATA
SKP2	Forward	ATGCCCCAATCTTGTCCATCT
SKP2	Reverse	CACCGACTGAGTGATAGGTGT
TRPC4AP	Forward	ACAAGCACACGCTTCTTGC
TRPC4AP	Reverse	CTGACACCTTTCGAGTCGCC
FBXW7	Forward	CGACGCCGAATTACATCTGTC
FBXW7	Reverse	CGTTGAAACTGGGGTTCTATCA
FBXO32	Forward	GCCTTTGTGCCTACAACTG
FBXO32	Reverse	CTGCCCTTTGTCTGACAGAAT

Immunofluorescence of cultured cells. MDA-MB-231 cells were treated with ethanol, M (25 μM) or TM (25 μM) for 6 hr. Immunostaining was performed and images were acquired by confocal microscopy as previously described [62].

Flow cytometry. For cell cycle analyses, MCF-7 or K562 cells were treated with 25 μM for 0, 24, 48 and 72 hr. Cells were spun down, washed with PBS, fixed with 70% ethanol overnight, and then washed with PBS. RNA was degraded with RNAse A and DNA was stained with propidium iodide (Invitrogen). Samples were analyzed on a BD LSR-II. Cell cycle analysis was performed with FlowJo flow cytometry analysis software (Tree Star, Inc., Ashland, OR).

Cellular senescence staining. MCF-7 or K562 cells were treated with ethanol or 25 μM TM. After 5 days of treatment, cells were stained for senescence as previously described [63].

Immunofluorescence and Immunohistochemistry of tumor sections. Formalin-fixed, paraffin-embedded (FFPE) tumors were sectioned, dewaxed and submitted to heat mediated antigen retrieval in 0.01 M citrate buffer for 50 min. For immunofluorescence, sections were

incubated with anti-acetyl-α-tubulin, followed by Alexa Fluro-488 conjugated secondary antibodies from Invitrogen and cell nuclei counterstaining with DAPI Fluoromount-G® from SouthernBiotech. Fluorescent images were taken using Zeiss LSM880 inverted confocal microscopy (Carl Zeiss Inc., Thornwood, NY). For immunohistochemistry, sections were incubated with anti-Ki67 Clone MM1 (Vector Laboratories) antibody followed by biotinylated polyclonal rabbit anti-mouse (DAKO). Color was developed using 3,3'-Diaminobenzidine tetrahydrochloride substrate from Invitrogen and counterstained with hematoxilin. Images were scanned using an Aperio ScanScope.

Whole-Transcriptome Sequencing (RNA-seq) and Gene Set Enrichment Analysis (GSEA). MCF-7 cells were treated with ethanol or TM (25 μM) for 12 hr, or infected by shCtrl- or shSIRT2-carring lentivirus for 72 hr. Total RNA was isolated using the RNeasy Kit (Qiagen) and digested with DNase (Qiagen). mRNA was then purified with oligo-dT DynaBeads, the cDNA and sequencing library was constructed as described previously [64]. Sequencing, reads mapping and transcription quantification were then performed as described previously [65]. The read numbers of the transcripts in each sample were used for GSEA (Broad Institute). And the analysis parameters were selected following the instruction at the GSEA website (http://software.broadinstitute.org/gsea/index.jsp).

Statistical analysis. Quantitative data were expressed as mean ± sd (standard deviation, shown as error bar) from at least three independent experiments. Differences between two groups were examined statistically as indicated (*$p < 0.05$, **$p < 0.01$, and ***$p < 0.001$).

Synthesis of compounds used in the study

General methods. Reagents were obtained from Aldrich or Acros in the highest purity available and used as supplied. ^{1}HNMR was performed on INOVA 400/500 spectrometer. LCMS was carried out on a SHIMADZU LC and Thermo LCQ FLEET MS with a Sprite TARGA C18 column (40 × 2.1 mm, 5 μm, Higgins Analytical, Inc.) monitoring at 215 and 260

nm. Solvents used in LCMS were water with 0.1% acetic acid and acetonitrile with 0.1% acetic acid.

1. Synthetic Route for TA

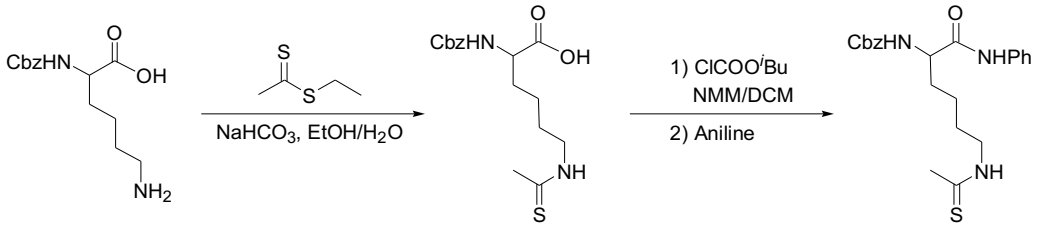

1 **2** **TA**

Synthesis of compound 2. To a solution of Z-Lys-OH (2.8 g, 10 mmol) in ethanol (100 mL) was added 20 mL of 10% (w/v) Na_2CO_3 aqueous solution at 0°C. The reaction mixture was allowed to warm to room temperature (rt) while stirred extensively. Ethyl dithioacetate (1.32 g, 11 mmol) was added and the reaction mixture was stirred overnight at rt. Solvent was evaporated and then the crude product was acidified to pH＝2 with 3 M HCl on ice and extracted with DCM (3 x 100 mL). The organic phase was washed with brine (2 x 30 mL), dried with Na_2SO_4, and evaporated to obtain compound **2,** which was directly used in the next step without further purification.

Synthesis of compound TA. To a solution of compound **2** (3.38 g, 10 mmol) and N-methylmorpholine (1.1 ml, 10 mmol) in dry dichloromethane (100 mL) at 0°C was added dropwisely iso-butylchloroformate (1.3 ml, 10 mmol). The reaction mixture was stirred for 30 min at 0°C. Aniline (1.09 ml, 12 mmol) was added at 0°C and the reaction mixture was stirred overnight at room temperature. The solvent was removed under reduced pressure and the resulting residue was purified by flash chromatography on silica gel (Hexane/ethyl acetate = 2/1) to afford the expected compound **3** (3.95 g, 95.5% yield). ^{1}H NMR (400 MHz, CD_3OD): δ 7.53-7.51 (m, 2H), 7.34-7.22 (m, 7H), 7.08-7.04(t, *J* =7.2Hz, 1H), 5.06 (q, *J*=8.0Hz, 2H), 4.26-4.22 (m, 1H), 3.54 (t, *J*=7.1Hz, 2H), 2.39 (s, 3H), 1.89-1.76(m, 1H), 1.78-1.70 (m, 1H), 1.66-1.58 (m, 2H), 1.55-1.35 (m, 2H). ^{13}C NMR (126 MHz, $CDCl_3$): δ 200.88, 170.34, 156.79,

137.34, 135.87, 129.01, 128.62, 128.35, 127.93, 124.78, 120.23, 120.13, 67.34, 55.19, 45.74, 33.97, 32.04, 27.00, 22.70.LCMS (ESI) calcd. for $C_{22}H_{28}N_3O_3S$ $[M+H]^+$ 414.2, obsd. 414.3.

2. Synthetic Route for TB, TH, and TM

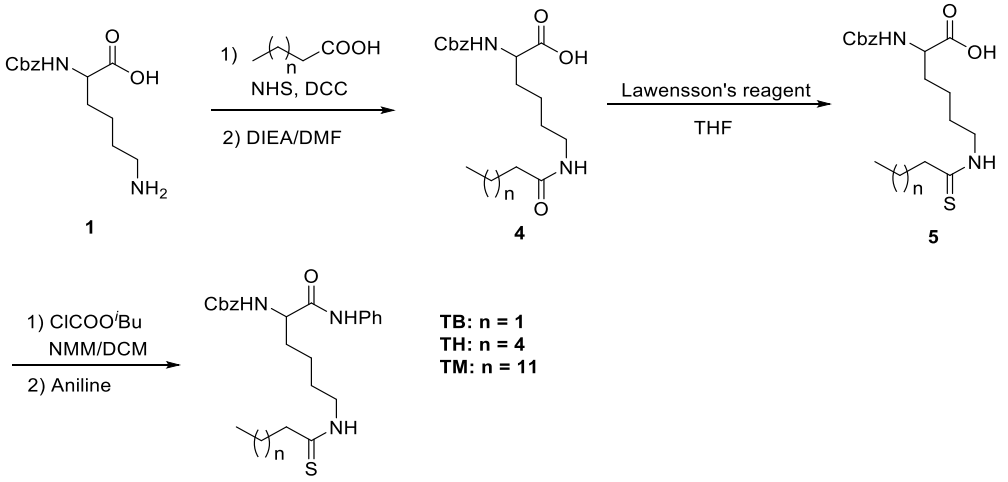

Synthesis of compound 4. To the solution of acid (30 mmol) in anhydrous *N, N'*-dimethylformamide (DMF, 20 mL) was added *N*-hydroxysuccinimide (NHS, 3.45 g, 30 mmol) with stirring at rt. Then *N, N'*-dicyclohexylcarbodiimide (DCC, 6.19 g, 30 mmol) in anhydrous DMF (20 mL) was added to the reaction. After stirring for 2 hr, the reaction mixture was filtered. The filtrate was added to a solution of Z-Lys-OH (8.4 g, 30 mmol) with *N, N*-diisopropylethylamine (DIEA, 5.2 mL, 30 mmol) in anhydrous DMF (50.0 mL) at room temperature. The resulting reaction mixture was stirred overnight. Then 44 mL water and 26 mL 1 M HCl was added to the reaction mixture to adjust pH to 2~3. The mixture was extracted ethyl acetate (3 x 200 mL) and washed brine (2 x 100 mL). The organic layer was dried over anhydrous sodium sulfate. After removal of the solvents in vacuum, the residue was purified by flash chromatography on silica gel (DCM/MeOH = 20:1) to afford the expected compound **4** (85% yield).

Synthesis of compound 5. To a solution of compound **4** (20 mmol) in THF (100 mL) was added Lawesson's reagent (8.0 g, 20 mmol) at room temperature. The reaction mixture was

stirred overnight under nitrogen (monitored by LCMS). After removal of THF using a rotary evaporator, the residue was purified by silica gel column (DCM/MeOH = 20:1) to give the product as a white solid (76% yield).

Synthesis of compound TB, TH and TM. To a solution of compound **5** (10 mmol) and N-methylmorpholine (1.1 ml, 10 mmol) in dry dichloromethane (100 mL) at 0°C was added dropwisely iso-butylchloroformate (1.3ml, 10 mmol). The reaction mixture was stirred for 30 min at 0°C. Aniline (1.09 ml, 12 mmol) was then added at 0°C and the reaction mixture was stirred overnight at room temperature. The solvent was removed under reduced pressure and the resulting residue was purified by flash chromatography on silica gel (Hexane/ethyl acetate= 2/1) to afford the expected compound **TB, TH, and TM**.

TB (91% yield) ^{1}H NMR (400 MHz, CD_3OD): δ 7.57-7.45 (m, 2H), 7.39-7.12 (m, 7H), 7.12-6.99 (m, 1H), 5.05 (q, *J* = 12.5 Hz, 2H), 4.27-4.23 (m, 1H), 3.55 (q, *J* = 12.5 Hz, 2H), 2.51 (t, *J* = 7.2Hz, 2H), 1.91-1.78 (m, 1H), 1.78-1.57 (m, 5H), 1.55-1.33 (m, 2H), 0.86 (t, *J* = 7.2 Hz, 3H).. ^{13}C NMR (126 MHz, $CDCl_3$): δ 205.60, 170.19, 156.74, 137.36, 135.88, 128.99, 128.60, 128.33, 127.96, 124.72, 120.16, 120.06, 119.98, 67.34, 55.19, 48.93, 45.30, 31.89, 27.07, 22.78, 22.63, 13.36. LCMS (ESI) calcd. for C24H32N3O3S $[M+H]^+$ 442.2, obsd. 442.3;

TH (89% yield) ^{1}H NMR (500 MHz, $CDCl_3$): δ 8.54 (s, 1H), 7.73 (s, 1H), 7.49 (d, *J* = 7.5 Hz, 2H), 7.41-7.20 (m, 7H), 7.11 (t, *J* = 7.4 Hz, 1H), 5.79 (d, *J* = 7.5 Hz, 1H), 5.19 -5.03 (m, 2H), 4.45-4.31 (m, 1H), 3.70-3.62 (m, 2H), 2.60(t, *J* = 7.5 Hz, 2H), 1.98-1.91 (m, 1H), 1.81-1.60 (m, 5H), 1.54-1.41 (m, 2H), 1.36-1.18 (m, 6H), 0.87 (t, *J* = 7.0 Hz, 3H). ^{13}C NMR (126 MHz, $CDCl_3$): δ 205.84, 170.21, 156.75, 137.38, 135.88, 128.99, 128.60, 128.33, 127.95, 124.71, 120.16, 67.34, 55.19, 47.16, 45.34, 31.91, 31.52, 29.47, 28.66, 27.07, 22.65, 22.53, 14.06. LCMS (ESI) calcd. for C27H38N3O3S $[M+H]^+$ 484.3, obsd. 484.3;

TM (91% yield) ^{1}H NMR (400 MHz, CD_3OD): δ 7.53 (d, *J* = 8.0 Hz, 2H), 7.41-7.12 (m, 7H), 7.08 (t, *J* = 7.4 Hz, 1H), 5.22-4.97 (m, 2H), 4.22 (dd, *J* = 8.8, 5.4 Hz, 1H), 3.57 (t, *J* = 7.1

Hz, 2H), 2.54 (t, *J* = 7.6 Hz, 2H), 1.90-1.79(m, 1H), 1.79-1.61 (m, 5H), 1.55-1.37 (m, 2H), 1.26 (s, 20H), 0.87 (t, *J* = 6.7 Hz, 3H). ^{13}C NMR (126 MHz, $CDCl_3$): δ 205.84, 170.18, 156.75, 137.37, 135.88, 128.99, 128.60, 128.33, 127.95, 124.71, 120.16, 67.35, 55.19, 47.21, 45.35, 31.93, 29.70, 29.67, 29.65, 29.55, 29.40, 29.37, 29.06, 27.08, 22.70, 22.65, 14.15.

LCMS (ESI) calcd. for C34H52N3O3S $[M+H]^+$ 582.4, obsd. 582.4;

3. Synthesis of compound M

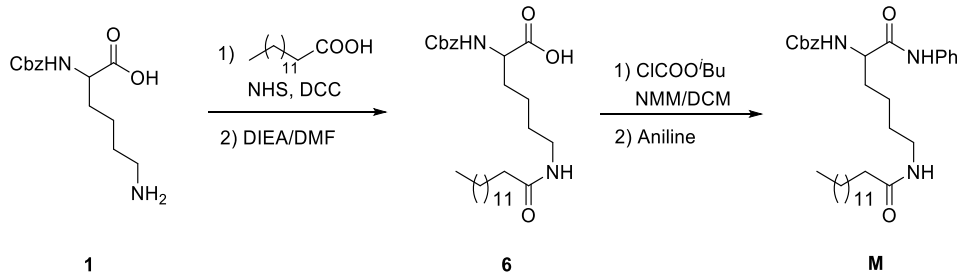

1 **6** **M**

The synthesis of compound **6** followed the method using in the synthesis of compound **4.** To a solution of compound **6** (4.9 g, 10 mmol) and *N*-methylmorpholine (1.1ml, 10 mmol) in dry dichloromethane (100 mL) at 0°C was added dropwisely iso-butylchloroformate (1.3 ml, 10 mmol). The reaction mixture was stirred 30 min at 0°C. Aniline (1.09 ml, 12 mmol) was added at 0°C and the reaction mixture was stirred overnight at rt. The solvent was removed under reduced pressure and the resulting residue was purified by silica gel chromatography (DCM/MeOH = 50:1) to afford the expected compound **M** (5.14 g, 91% yield). ^{1}H NMR (400 MHz, CD_3OD): δ 7.53 (d, *J* = 7.9 Hz, 2H), 7.40-7.13 (m, 7H), 7.08 (t, *J* = 7.4 Hz, 1H), 5.13-5.02 (m, 2H), 4.20 (dd, *J* = 8.5, 5.5 Hz, 1H), 3.15 (t, *J* = 6.7 Hz, 2H), 2.11 (t, *J* = 7.6 Hz, 2H), 1.88-1.64 (m, 2H), 1.62-1.34 (m, 6H), 1.32-1.21 (s, 20H), 0.87 (t, *J* = 7.0 Hz, 3H). ^{13}C NMR (126 MHz, DMSO-d6): δ 172.35, 171.54, 156.53, 139.43, 137.46, 129.11, 128.77, 128.22, 128.14, 123.67, 119.66, 65.87, 55.85, 38.61, 35.92, 31.98, 31.76, 29.53, 29.50, 29.48, 29.41, 29.35, 29.24, 29.18, 29.15, 25.77, 23.48, 22.56, 14.41.LCMS (ESI) calcd. for C34H52N3O4 $[M+H]^+$ 566.4, obsd. 566.5;

4. Synthetic Route for Biotin-TM and Biotin-M

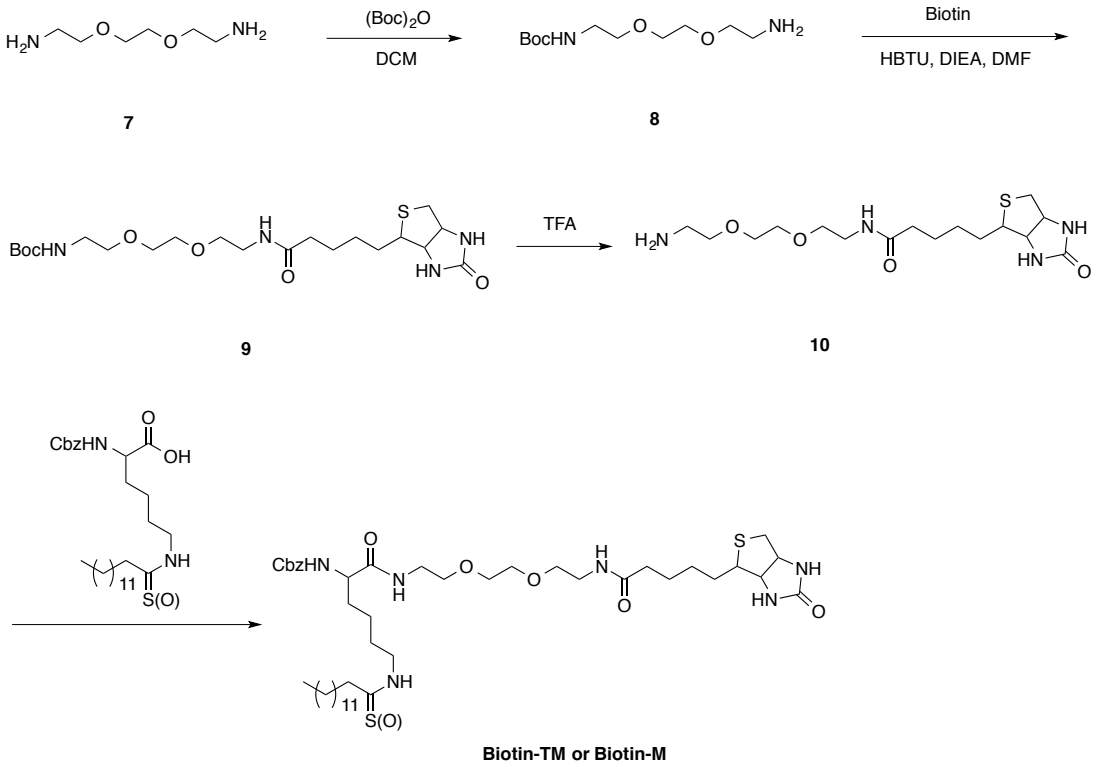

Synthesis of Compound 8. To a solution of compound **7** (14.8 g, 100 mmol) in DCM (200 mL) was added 100 mL of di-tert-butyl dicarbonate (2.18 g, 10mmol) in DCM at 0°C. The reaction mixture was allowed to warm to rt and stirred extensively overnight. The organic phase was washed with water, until all the unreacted compound **7** was extracted. After drying over Na_2SO_4 and concentration under vacuum the Boc-protected compound **8** was quantitatively obtained.

Synthesis of Compound 9. To a solution of Biotin (2.2 g, 9 mmol) and HBTU (3.41 g, 9 mmol) in DMF (30 mL) was added DIEA (3.6 mL, 20 mmol) at room temperature with stirring for 30 min. Then compound **8** was added to the resulting mixture. The reaction mixture was stirred extensively overnight. After removal of the solvents under reduced pressure, the residue was purified by flash chromatography on silica gel (DCM/MeOH = 20:1 then 10:1) to afford the expected compound **9** (3.5 g, 81% yield).

Synthesis of Compound 10. To 20 mL of TFA was added the compound **9** (2 g, 4.2 mmol) and the resulting mixture was stirred for 30 min at room temperature. After removing the solvent under vacuum the deprotected compound **10** was quantitatively obtained and used in the next step without further purification.

Synthesis of Compound Biotin-TM and Biotin-M. The synthesis followed the method using in the synthesis of **TM**. The solvent used to dissolve the compound **10** is DMF instead of DCM.

Biotin-TM (81% yield) ^{1}H NMR (500 MHz, CD_3OD): δ 7.41-7.29 (m, 5H), 5.18-5.05 (m, 2H), 4.49 (dd, *J* = 7.8, 4.8 Hz, 1H), 4.30 (dd, *J* = 7.9, 4.5 Hz, 1H), 4.10 (dd, *J* = 8.7, 5.4 Hz, 1H), 3.66-3.52 (m, 10H), 3.44 -3.34 (m, 4H), 3.21 (dt, *J* = 9.9, 5.6 Hz, 1H), 2.93 (dd, *J* = 12.7, 5.0 Hz, 1H), 2.71 (d, *J* = 12.7 Hz, 1H), 2.59 (t, *J* = 7.4 Hz, 2H), 2.22 (t, *J* = 7.4 Hz, 2H), 1.86-1.55 (m, 10H), 1.48-1.38 (m, 4H), 1.35-1.25(m, 20H), 0.91 (t, *J* = 6.9 Hz, 3H). ^{13}C NMR (126 MHz, CD_3OD): δ 205.01, 174.72, 173.54, 164.68, 156.99, 136.77, 128.10, 127.64, 127.42, 69.92, 69.21, 69.09, 66.29, 61.95, 60.21, 55.61, 55.06, 45.68, 45.16, 39.66, 38.91, 35.35, 31.68, 29.44, 29.41, 29.37, 29.33, 29.24, 29.08, 28.57, 28.37, 28.10, 26.92, 25.45, 22.95, 22.34, 13.06. LCMS (ESI) calcd. for $C_{44}H_{75}N_6O_7S_2$ $[M+H]^+$ 863.5, obsd. 863.6.

Biotin-M (83% yield)^{1}H NMR (400 MHz, CD_3OD): δ 7.39-7.22 (m, 5H), 5.10-5.04 (m, 2H), 4.46 (dd, *J* = 7.9, 4.9 Hz, 1H), 4.27 (dd, *J* = 7.8, 4.5 Hz, 1H), 4.05 (dd, *J* = 8.8, 5.3 Hz, 1H), 3.58 (s, 4H), 3.52 (q, *J* = 5.2 Hz, 4H), 3.37-3.32 (m, 4H), 3.19-3.11 (m, 3H), 2.89 (dd, *J* = 12.7, 5.0 Hz, 1H), 2.68 (d, *J* = 12.7 Hz, 1H), 2.19 (t, *J* = 7.5 Hz, 2H), 2.13(t, *J* = 7.5 Hz, 2H), 1.80-1.34 (m, 14H), 1.26 (s, 20H), 0.88 (t, *J* = 6.8 Hz, 3H). ^{13}C NMR (126 MHz, DMSO): δ 172.58, 172.50, 172.35, 163.15, 156.36, 137.49, 128.77, 128.21, 128.10, 69.98, 69.62, 69.42, 65.79, 61.48, 59.64, 55.88, 55.06, 38.97, 38.88, 38.65, 35.90, 35.55, 32.14, 31.76, 29.53, 29.49, 29.41, 29.31, 29.25, 29.18, 29.15, 28.66, 28.49, 25.78, 25.72, 23.36, 22.56, 14.43. LCMS (ESI) calcd. for $C_{44}H_{75}N_6O_8S$ $[M+H]^+$ 847.5, obsd. 847.8.

5. References

1. Meyer, N. & Penn, L.Z. Reflecting on 25 years with MYC. *Nat Rev Cancer* **8**, 976-990 (2008).
2. Beroukhim, R. et al. The landscape of somatic copy-number alteration across human cancers. *Nature* **463**, 899-905 (2010).
3. Delmore, J.E. et al. BET bromodomain inhibition as a therapeutic strategy to target c-Myc. *Cell* **146**, 904-17 (2011).
4. Imai, S.-i., Armstrong, C.M., Kaeberlein, M. & Guarente, L. Transcriptional silencing and longevity protein Sir2 is an NAD-dependent histone deacetylase. *Nature* **403**, 795-800 (2000).
5. Imai, S.-i. & Guarente, L. Ten years of NAD-dependent SIR2 family deacetylases: implications for metabolic diseases. *Trends Pharmacol. Sci.* **31**, 212-220 (2010).
6. Haigis, M.C. & Sinclair, D.A. Mammalian Sirtuins: Biological Insights and Disease Relevance. *Annu. Rev. Pathol.* **5**, 253-295 (2010).
7. Du, J. et al. Sirt5 is an NAD-dependent protein lysine demalonylase and desuccinylase. *Science* **334**, 806-809 (2011).
8. Peng, C. et al. The first identification of lysine malonylation substrates and its regulatory enzyme. *Mol. Cell. Proteomics* **10**, 10.1074/mcp.M111.012658 (2011).
9. Jiang, H. et al. SIRT6 regulates TNF-a secretion through hydrolysis of long-chain fatty acyl lysine. *Nature* **496**, 110-113 (2013).
10. Zhu, A.Y. et al. *Plasmodium falciparum* Sir2A preferentially hydrolyzes medium and long chain fatty acyl lysine. *ACS Chem. Biol.* **7**, 155-159 (2012).
11. Jiang, H. et al. SIRT6 regulates TNF-alpha secretion through hydrolysis of long-chain fatty acyl lysine. *Nature* **496**, 110-3 (2013).
12. Marks, P.A. & Breslow, R. Dimethyl sulfoxide to vorinostat: development of this histone deacetylase inhibitor as an anticancer drug. *Nat. Biotechnol.* **25**, 84-90 (2007).
13. Lee, J.-H., Choy, M.L. & Marks, P.A. Chapter Two - Mechanisms of Resistance to Histone Deacetylase Inhibitors. in *Adv. Cancer Res.*, Vol. Volume 116 (ed. Steven, G.) 39-86 (Academic Press, 2012).
14. Stünkel, W. & Campbell, R.M. Sirtuin 1 (SIRT1): the misunderstood HDAC. *J. Biomol. Screen.* **16**, 1153-1169 (2011).
15. Fang, Y. & Nicholl, M.B. Sirtuin 1 in malignant transformation: Friend or foe? *Cancer lett.* **306**, 10-14 (2011).
16. Herranz, D. & Serrano, M. SIRT1: recent lessons from mouse models. *Nat. Rev. Cancer* **10**, 819-823 (2010).
17. Kim, H.S. et al. SIRT2 maintains genome integrity and suppresses tumorigenesis through regulating APC/C activity. *Cancer Cell* **20**, 487-99 (2011).
18. Liu, P.Y. et al. The histone deacetylase SIRT2 stabilizes Myc oncoproteins. *Cell Death Differ.* **20**, 503-514 (2013).
19. Yang, M.H. et al. HDAC6 and SIRT2 regulate the acetylation state and oncogenic activity of mutant K-RAS. *Mol Cancer Res* **11**, 1072-7 (2013).
20. Zhao, D. et al. Lysine-5 acetylation negatively regulates lactate dehydrogenase A and is decreased in pancreatic cancer. *Cancer cell* **23**, 464-476 (2013).
21. Chen, J. et al. SIRT2 overexpression in hepatocellular carcinoma mediates epithelial to mesenchymal transition by protein kinase B/glycogen synthase kinase-3beta/beta-catenin signaling. *Hepatology* **57**, 2287-98 (2013).
22. Zhao, D. et al. NOTCH-induced aldehyde dehydrogenase 1A1 deacetylation promotes breast cancer stem cells. *J Clin Invest* **124**, 5453-65 (2014).

23. Soung, Y.H., Pruitt, K. & Chung, J. Epigenetic silencing of ARRDC3 expression in basal-like breast cancer cells. *Sci Rep* **4**, 3846 (2014).
24. McGlynn, L.M. et al. SIRT2: tumour suppressor or tumour promoter in operable breast cancer? *Eur J Cancer* **50**, 290-301 (2014).
25. He, B., Hu, J., Zhang, X. & Lin, H. Thiomyristoyl peptides as cell-permeable Sirt6 inhibitors. *Org Biomol Chem* **12**, 7498-502 (2014).
26. Heltweg, B. et al. Antitumor activity of a small-molecule inhibitor of human silent information regulator 2 enzymes. *Cancer Res* **66**, 4368-77 (2006).
27. Neugebauer, R.C. et al. Structure-activity studies on splitomicin derivatives as sirtuin inhibitors and computational prediction of binding mode. *J Med Chem* **51**, 1203-13 (2008).
28. Zhang, Y. et al. Identification of a small molecule SIRT2 inhibitor with selective tumor cytotoxicity. *Biochem Biophys Res Commun* **386**, 729-33 (2009).
29. Kim, W.J. et al. Nicotinamide inhibits growth of carcinogen induced mouse bladder tumor and human bladder tumor xenograft through up-regulation of RUNX3 and p300. *J Urol* **185**, 2366-75 (2011).
30. Rotili, D. et al. Discovery of salermide-related sirtuin inhibitors: binding mode studies and antiproliferative effects in cancer cells including cancer stem cells. *J Med Chem* **55**, 10937-47 (2012).
31. McCarthy, A.R. et al. Tenovin-D3, a novel small-molecule inhibitor of sirtuin SirT2, increases p21 (CDKN1A) expression in a p53-independent manner. *Mol Cancer Ther* **12**, 352-60 (2013).
32. Hoffmann, G., Breitenbucher, F., Schuler, M. & Ehrenhofer-Murray, A.E. A novel sirtuin 2 (SIRT2) inhibitor with p53-dependent pro-apoptotic activity in non-small cell lung cancer. *J Biol Chem* **289**, 5208-16 (2014).
33. Mahajan, S.S. et al. Development of pyrazolone and isoxazol-5-one cambinol analogues as sirtuin inhibitors. *J Med Chem* **57**, 3283-94 (2014).
34. Cheon, M.G., Kim, W., Choi, M. & Kim, J.E. AK-1, a specific SIRT2 inhibitor, induces cell cycle arrest by downregulating Snail in HCT116 human colon carcinoma cells. *Cancer Lett* **356**, 637-45 (2015).
35. Fatkins, D.G., Monnot, A.D. & Zheng, W. Ne-Thioacetyl-lysine: A multi-facet functional probe for enzymatic protein lysine Ne-deacetylation. *Bioorg. Med. Chem. Lett.* **16**, 3651-3656 (2006).
36. Smith, B.C. & Denu, J.M. Mechanism-based Inhibition of Sir2 deacetylases by thioacetyl-lysine peptide. *Biochemistry* **46**, 14478-14486 (2007).
37. Hawse, W.F. et al. Structural insights into intermediate steps in the Sir2 deacetylation reaction. *Structure* **16**, 1368-1377 (2008).
38. Feldman, J.L., Baeza, J. & Denu, J.M. Activation of the protein deacetylase SIRT6 by long-chain fatty acids and widespread deacylation by mammalian sirtuins. *J. Biol. Chem.* **288**, 31350-6 (2013).
39. He, B., Du, J. & Lin, H. Thiosuccinyl peptides as Sirt5-specific inhibitors. *J. Am. Chem. Soc.* **134**, 1922-1925 (2012).
40. He, B., Hu, J., Zhang, X. & Lin, H. Thiomyristoyl peptides as cell-permeable Sirt6 inhibitors. *Org. Biomol. Chem.* **DOI: 10.1039/c4ob00860j.**(2014).
41. Suzuki, T. et al. Identification of a cell-active non-peptide sirtuin inhibitor containing N-thioacetyl lysine. *Bioorg. Med. Chem. Lett.* **19**, 5670-5672 (2009).
42. Teng, Y.B. et al. Efficient demyristoylase activity of SIRT2 revealed by kinetic and structural studies. *Sci Rep* **5**, 8529 (2015).
43. Di Fruscia, P. et al. The Discovery of Novel 10,11-Dihydro-5H-dibenz[b,f]azepine SIRT2 Inhibitors. *Medchemcomm* (2012).

44. Seifert, T. et al. Chroman-4-one- and chromone-based sirtuin 2 inhibitors with antiproliferative properties in cancer cells. *J Med Chem* **57**, 9870-88 (2014).
45. Yoon, Y.K. et al. Benzimidazoles as new scaffold of sirtuin inhibitors: green synthesis, in vitro studies, molecular docking analysis and evaluation of their anti-cancer properties. *Eur J Med Chem* **83**, 448-54 (2014).
46. Guy, C.T., Cardiff, R.D. & Muller, W.J. Induction of mammary tumors by expression of polyomavirus middle T oncogene: a transgenic mouse model for metastatic disease. *Mol Cell Biol* **12**, 954-61 (1992).
47. Shoemaker, R.H. The NCI60 human tumour cell line anticancer drug screen. *Nat Rev Cancer* **6**, 813-823 (2006).
48. Zaharevitz, D.W., Holbeck, S.L., Bowerman, C. & Svetlik, P.A. COMPARE: a web accessible tool for investigating mechanisms of cell growth inhibition. *J Mol Graph Model* **20**, 297-303 (2002).
49. Subramanian, A. et al. Gene set enrichment analysis: a knowledge-based approach for interpreting genome-wide expression profiles. *Proc Natl Acad Sci U S A* **102**, 15545-50 (2005).
50. Wu, C.H. et al. Cellular senescence is an important mechanism of tumor regression upon c-Myc inactivation. *Proc Natl Acad Sci U S A* **104**, 13028-33 (2007).
51. Paul, I., Ahmed, S.F., Bhowmik, A., Deb, S. & Ghosh, M.K. The ubiquitin ligase CHIP regulates c-Myc stability and transcriptional activity. *Oncogene* **32**, 1284-95 (2013).
52. Welcker, M. et al. The Fbw7 tumor suppressor regulates glycogen synthase kinase 3 phosphorylation-dependent c-Myc protein degradation. *Proc Natl Acad Sci U S A* **101**, 9085-90 (2004).
53. Choi, S.H., Wright, J.B., Gerber, S.A. & Cole, M.D. Myc protein is stabilized by suppression of a novel E3 ligase complex in cancer cells. *Genes Dev* **24**, 1236-41 (2010).
54. Kim, S.Y., Herbst, A., Tworkowski, K.A., Salghetti, S.E. & Tansey, W.P. Skp2 regulates Myc protein stability and activity. *Mol Cell* **11**, 1177-88 (2003).
55. Chappell, S.A. et al. A mutation in the c-myc-IRES leads to enhanced internal ribosome entry in multiple myeloma: a novel mechanism of oncogene de-regulation. *Oncogene* **19**, 4437-40 (2000).
56. Wolfe, A.L. et al. RNA G-quadruplexes cause eIF4A-dependent oncogene translation in cancer. *Nature* **513**, 65-70 (2014).
57. Serrano, L. et al. The tumor suppressor SirT2 regulates cell cycle progression and genome stability by modulating the mitotic deposition of H4K20 methylation. *Genes Dev* **27**, 639-53 (2013).
58. Weiss, W.A., Taylor, S.S. & Shokat, K.M. Recognizing and exploiting differences between RNAi and small-molecule inhibitors. *Nat Chem Biol* **3**, 739-744 (2007).
59. Bartek, J., Mistrik, M. & Bartkova, J. Thresholds of replication stress signaling in cancer development and treatment. *Nat Struct Mol Biol* **19**, 5-7 (2012).
60. Liu, Z. et al. Integrative Chemical Biology Approaches for Identification and Characterization of "Erasers" for Fatty-Acid-Acylated Lysine Residues within Proteins. *Angew Chem Int Ed Engl* (2014).
61. Du, J., Jiang, H. & Lin, H. Investigating the ADP-ribosyltransferase activity of sirtuins with NAD analogues and 32P-NAD. *Biochemistry* **48**, 2878-90 (2009).
62. Mabjeesh, N.J. et al. 2ME2 inhibits tumor growth and angiogenesis by disrupting microtubules and dysregulating HIF. *Cancer Cell* **3**, 363-75 (2003).
63. Debacq-Chainiaux, F., Erusalimsky, J.D., Campisi, J. & Toussaint, O. Protocols to detect senescence-associated beta-galactosidase (SA-betagal) activity, a biomarker of

senescent cells in culture and in vivo. *Nat Protoc* **4**, 1798-806 (2009).
64. Zhong, S. et al. High-throughput illumina strand-specific RNA sequencing library preparation. *Cold Spring Harb Protoc* **2011**, 940-9 (2011).
65. Wang, Z. et al. Evolution of gene regulation during transcription and translation. *Genome Biol Evol* **7**, 1155-67 (2015).

CHAPTER 3

SIRT2 AND LYSINE FATTY ACYLATION REGULATE THE ONCOGENIC ACTIVITY OF K-RAS4A [c]

Abstract

Ras proteins play vital roles in numerous biological processes and Ras mutations are found in many human tumors. Understanding how Ras proteins are regulated is important for elucidating cell signaling pathways and identifying new targets for treating human diseases. Here we report that one of the K-Ras splice variants, K-Ras4a, is subject to lysine fatty acylation, a previously under-studied protein post-translational modification. Sirtuin 2 (SIRT2), one of the mammalian nicotinamide adenine dinucleotide (NAD)-dependent lysine deacylases, catalyzes the removal of fatty acylation from K-Ras4a. We further demonstrate that SIRT2-mediated lysine defatty-acylation promotes endomembrane localization of K-Ras4a, enhances its interaction with A-Raf, and thus promotes cellular transformation. Our study identifies lysine fatty acylation as a previously unknown regulatory mechanism for the Ras family of GTPases

[c] This is a revised version of our submitted paper: Jing, H., Zhang, X., Wisner, S.A., Chen, X., Spiegelman, N.A., Linder, M.E., Lin, H.. SIRT2 and lysine fatty acylation regulate the oncogenic activity of K-Ras4a.
For this paper, I (HJ) designed and performed all the biochemical and cellular studies except those noted below. I would like to acknowledge the great contribution made by all the authors below. XZ synthesized K-Ras4a-C180myr peptide, carried out mass spectrometry analyses of H-Ras and K-Ras4a lysine fatty acylation, *in vitro* cysteine depalmitoylation assay, ^{32}P-NAD assay, and K-Ras4a intereactome study. SAW purified SIRT2 protein and performed the Alk14 labeling experiment for the K-Ras4a single KR mutants, C186S and C180S mutants. XC validated HJ's results on cell proliferation and soft agar colony formation. NAS synthesized the Alk14 probe. MEL provided pCMV5-*HRAS*, pCMV5-*NRAS*, pCMV5-*K-RAS4B* and pCMV5-*RalA* plasmids and consultation on Ras GTPases. HL directed and supervised all the studies. HJ, XZ and HL wrote the manuscript and all authors reviewed and approved the manuscript.

that is distinct from cysteine fatty acylation. These findings highlight the biological significance of lysine fatty acylation and sirtuin-catalyzed protein lysine defatty-acylation.

1. Introduction

Protein fatty acylation facilitates direct association of proteins with particular membranes in cells and plays a vital role in protein trafficking, cell signaling, protein-protein interactions, and protein activity[1-3]. Dysregulation of protein fatty acylation is implicated in human cancer and neurodegenerative diseases[3]. While early studies have focused on N-terminal glycine myristoylation and cysteine palmitoylation, little is known about lysine fatty acylation[2,3]. Although first reported over two decades ago, the biological function of protein lysine fatty acylation is not clear and to date only a few proteins, such as tumor necrosis factor α (TNF-α) and interleukin 1-α, are known to be regulated by lysine fatty acylation[4-8]. The enzymes that catalyze the addition or removal of lysine fatty acylation were not known until recently when we and others found that several sirtuins, the nicotinamide adenine dinucleotide (NAD)-dependent protein lysine deacylase, could act as lysine defatty-acylase. We have previously reported that the TNF-α cytokine secretion[9,10] and exosome secretion[11] are regulated by sirtuin 6 (SIRT6)-catalyzed removal of lysine fatty acylation, demonstrating that lysine fatty acylation is reversible and physiologically important. Other sirtuin family proteins, SIRT1-3[12-15] and SIRT7[16], have also been found to efficiently remove fatty acyl groups from lysine residues *in vitro*, suggesting that lysine fatty acylation may be more prevalent. Therefore, we sought to identify other proteins that may be regulated by lysine fatty acylation.

Ras proteins are small GTPases that play important roles in numerous tumor-driving processes, including proliferation, differentiation, survival, cell cycle entry and cytoskeletal dynamics [17]. They act as binary switches: they are active when GTP- bound, turning on specific signaling pathways by recruiting effector proteins, and inactive in the GDP- bound state [17,18].

Guanine nucleotide exchange factors (GEFs) activate Ras by promoting GDP-GTP exchange, whereas GTPase-activating proteins (GAPs) inactivate Ras by promoting intrinsic GTP hydrolysis[17]. In mammals, *HRAS*, *NRAS*, and *KRAS* proto-oncogenes encode four proteins: H-Ras, N-Ras, K-Ras4a, and K-Ras4b. K-Ras4a and K-Ras4b are the two splice variants encoded by the *KRAS* gene. K-Ras4b has attracted most of the attention because it was assumed to be the more abundant and thus the more important K-Ras isoform mutated in human cancers. However, recent studies have revealed that K-Ras4a is widely expressed in many cancer cell lines and its level is similar to that of K-Ras4b in human colorectal tumors [19,20]. A requirement for oncogenic K-Ras4a in lung carcinogenesis has also been demonstrated in mice [21]. Thus, there is increasing interest in evaluating K-Ras4a as a therapeutic target and in investigating the regulation of K-Ras4a.

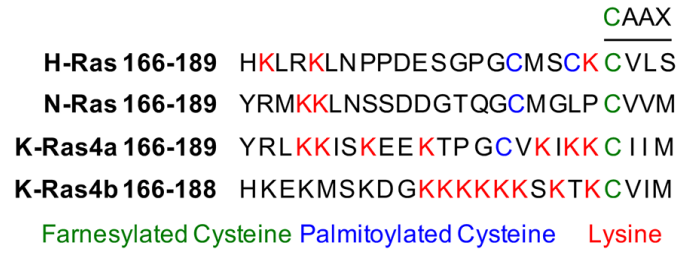

Figure 3.1 Amino acid sequences of the HVRs of Ras proteins.

Ras proteins exert their functions at cellular membranes, where they interact with distinct effectors and activate downstream signaling [18]. Ras proteins typically have two membrane-targeting signals at the C-terminal hypervariable regions (HVRs). All four Ras proteins are modified by cysteine farnesylation on their CaaX motif. H-Ras and N-Ras contain cysteine palmitoylation as the second membrane targeting signal, whereas K-Ras4b uses a polybasic region (PBR) (Fig. 3.1). K-Ras4a possesses a hybrid membrane targeting motif: multiple lysine residues at the C-terminus (similar to K-Ras4b) as well as cysteine palmitoylation (Fig. 3.1)[19,20]. As we set out to identify lysine fatty acylated proteins, the presence of multiple lysine residues

in the Ras HVRs caught our attention. If the lysine residues function simply to promote membrane binding by electrostatics, why are there almost invariably lysine but not arginine residues on the HVRs? The prevalence of lysines in Ras HVRs suggests the possibility that lysine residues are post-translationally modified by fatty acids. Thus, in this study, we set out to investigate whether Ras proteins are regulated by reversible lysine fatty acylation.

2. Results

2.1 H-Ras and K-Ras4a contain lysine fatty acylation

To examine whether the lysine residues in the Ras proteins could be fatty acylated, an alkyne-tagged fatty acid analog, Alk14, was used to metabolically label Ras proteins[9]. As shown in Fig. 3.2A, HEK293T cells transiently expressing FLAG-tagged H-Ras, N-Ras, K-Ras4a, or K-Ras4b were treated with Alk14 (50 μM). We ensured that the overexpression levels of different Ras proteins were similar (Fig. 3.2B). FLAG-tagged Ras proteins were immunoprecipitated and conjugated to rhodamine-azide (Rh-N_3) using click chemistry to allow visualization of fatty acylation by in-gel fluorescence. Hydroxylamine (NH_2OH) was then used to remove cysteine palmitoylation. Ras-related protein Ral-A (RalA)[22] and Syntaxin-6 (STX6)[23] were included as controls for the efficiency of NH_2OH in removing cysteine palmitoylation. Quantification of the fluorescent signal revealed that NH_2OH treatment removed over 95% of the fatty acylation from RalA or STX6. However, H-Ras, N-Ras and K-Ras4a retained 20%, 13% and 47% relative NH_2OH-resistant fatty acylation over total fatty acylation, respectively, whereas K-Ras4b did not show Alk14 labeling either before or after NH_2OH treatment (Fig. 3.2C). These data suggest that H-Ras, N-Ras, and K-Ras4a might possess non-cysteine fatty acylation.

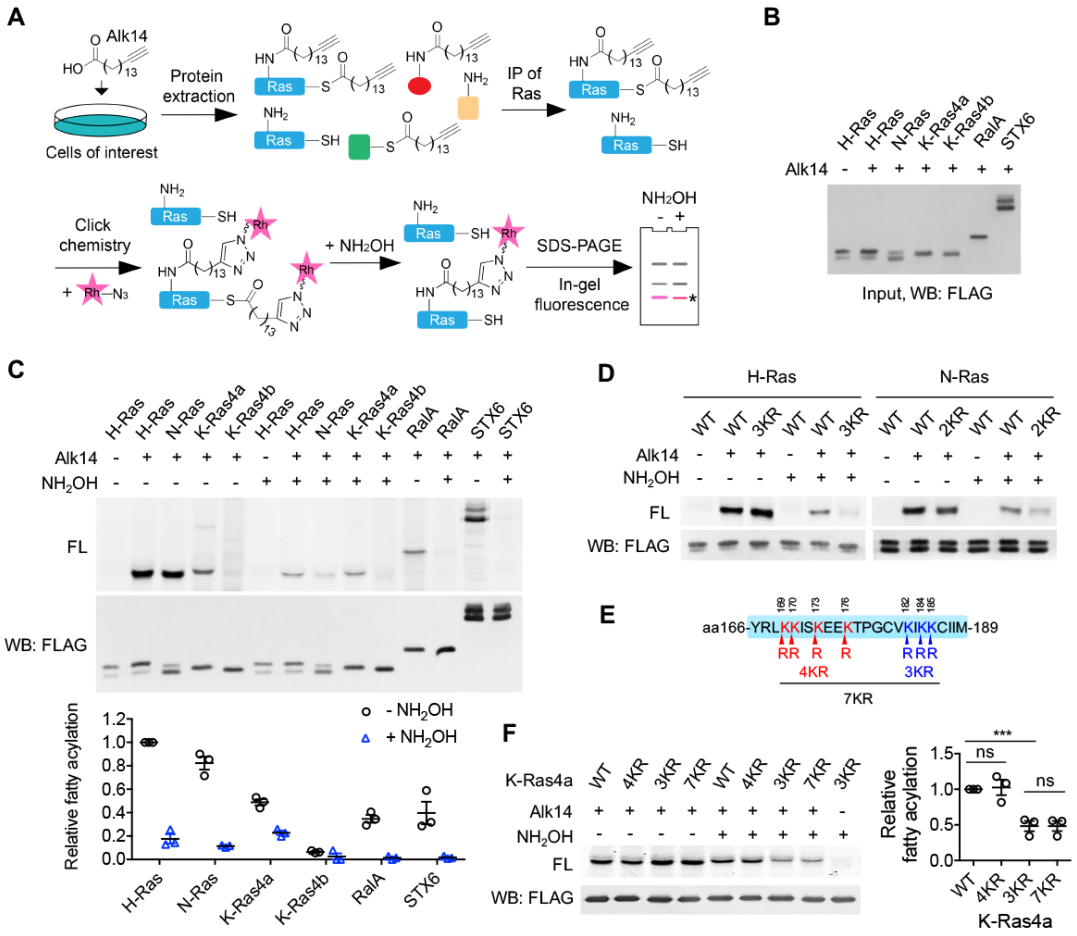

Figure 3.2 Ras proteins may be lysine fatty acylated. (**A**) Scheme showing the Alk14 metabolic labeling method to study lysine fatty acylation. (**B**) Representative western blot analyses of FLAG-tagged Ras protein, RalA and STX6 in whole cell extracts. (**C**) In-gel fluorescence detection of the fatty acylation levels of Ras proteins, RalA and STX6 in HEK293T cells (top panel) and quantification of the relative fatty acylation levels (bottom panel). The fatty acylation level of H-Ras without NH_2OH treatment was set to 1. (**D**) In-gel fluorescence showing the fatty acylation levels of H-Ras WT and 3KR mutant, N-Ras WT and 2KR mutant without or with NH_2OH treatment. (**E**) Scheme showing the lysine to arginine mutants (4KR, 3KR, and 7KR) used to identify potential fatty acylation sites. (**F**) In-gel fluorescence showing the fatty acylation levels of K-Ras4a WT and KR mutants without or with NH_2OH treatment (left panel) and quantification of fatty acylation levels with NH_2OH treatment relative to that of K-Ras4a WT (right panel). FL, fluorescence; WB, western blot. Statistical evaluation was by unpaired two-tailed Student's t test. Error bars represent SEM in three biological replicates. ***$P < 0.001$; ns, not significant. Representative images from three independent experiments are shown.

To determine whether the NH_2OH-resistant fatty acylation could be attributed to the lysine residues in the HVRs of H-Ras, N-Ras, and K-Ras4a, we mutated these lysine (K) residues to arginine (R) and examined the fatty acylation of the WT and KR mutants. The H-Ras 3KR (K167/170/185R), N-Ras 2KR (K169/170) mutant (Fig. 3.2D), and the K-Ras4a 3KR

(K182/184/185R) mutant but not K-Ras4a 4KR (K169/170/173/176) mutant (Fig. 3.2E & F) all displayed greatly reduced NH_2OH-resistant fatty acylation, implying that H-Ras, N-Ras and K-Ras might be fatty acylated on the lysine residues in their HVRs. Moreover, K-Ras4a-7KR (4KR & 3KR) showed comparable NH_2OH-resistant fatty acylation level to the 3KR mutant, suggesting that K182/184/185 of K-Ras4a might be fatty acylated. We then utilized mass spectrometry (MS) to directly identify the lysine fatty acylation of FLAG-H-Ras, -N-Ras or -K-Ras4a extracted from Alk14-treated HEK293T cells with tryptic digestion. This allowed us to identify H-Ras K170 (Fig. 3.3A) and K-Ras4a K182 (Fig. 3.3B) as being modified, confirming the lysine fatty acylation of H-Ras and K-Ras4a. Our attempt to identify N-Ras lysine fatty acylation by MS was not successful possibly because the tryptic peptide with lysine fatty acylation was less abundant (Fig. 1c), too short ($MK_{acyl}K$) or too hydrophobic ($K_{acyl}LNSSDDGTQGC_{cam}MGLPC_{prenyl,\ oMe}$)[1,2,24].

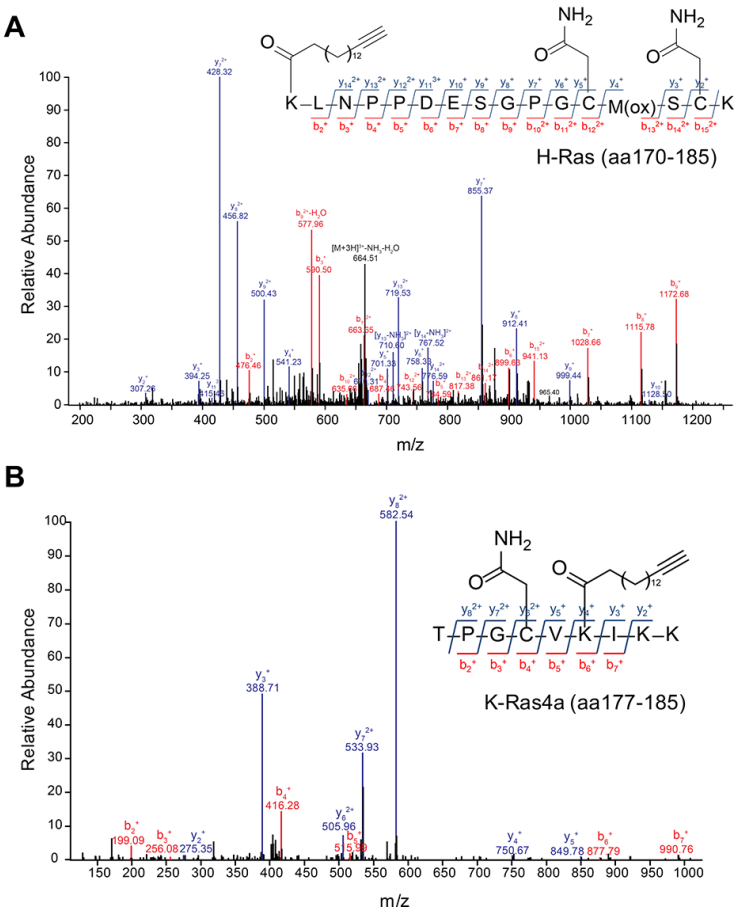

Figure 3.3 H-Ras and K-Ras4a contain lysine fatty acylation. Tandem mass (MS/MS) spectrum of triply charged H-Ras (**A**) and K-Ras4a (**B**) peptides with Alk14-modification on K170 and K182, respectively. The b- and y-ions are shown along with the peptide sequence. The cysteine residues were carbamidomethylated due to iodoacetamide alkylation during sample preparation and methionine was oxidized.

2.2 SIRT2 catalyzes the removal of lysine fatty acylation from K-Ras4a

Several mammalian sirtuins, including SIRT1, SIRT2, SIRT3, and SIRT6, can efficiently remove fatty acyl groups from protein lysine residues *in vitro* (SIRT1, SIRT2, and SIRT3)[25] or *in vivo* (SIRT6)[9,12-14,25]. So we next investigated whether any of these sirtuins could remove lysine fatty acylation from H-Ras or K-Ras4a and therefore regulate their function. We incubated H-Ras or K-Ras4a isolated from Alk14-treated HEK293T cells with purified recombinant sirtuins without or with NAD *in vitro* and examined the H-Ras or K-Ras4a fatty acylation level by in-gel fluorescence after click chemistry. Incubation of H-Ras or K-Ras4a

with *Plasmodium falciparum* Sir2A (PfSir2A), a sirtuin family member with robust lysine defatty-acylase activity[26], resulted in the removal of most of the NH_2OH-resistant fatty acylation from H-Ras and K-Ras4a in the presence of NAD (Fig. 3.4A). This result further confirmed that the NH_2OH-resistant fatty acylation is mainly from lysine residues and indicated that lysine fatty acylation of H-Ras and K-Ras4a is reversible. Furthermore, SIRT2, but not SIRT1, 3, or 6, slightly decreased the lysine fatty acylation signal of H-Ras (Fig. 3.4B); SIRT1 and SIRT2, but not SIRT3 and SIRT6, removed lysine fatty acylation from K-Ras4a. Notably, SIRT2 showed better activity than SIRT1 on K-Ras4a lysine fatty acylation (Fig. 3.4C). In contrast, SIRT1 and SIRT2 showed little effect on the fatty acylation of K-Ras4a-3KR (Fig. 3.4D), which exhibited significantly lower lysine fatty acylation than K-Ras4a-WT (Fig. 1f), suggesting that SIRT1 and SIRT2 do not possess cysteine defatty-acylase activity. An HPLC-based *in vitro* activity assay also revealed that SIRT2 was unable to remove the cysteine myristoyl group from a K-Ras4a-C180myr peptide (Fig. 3.4E).

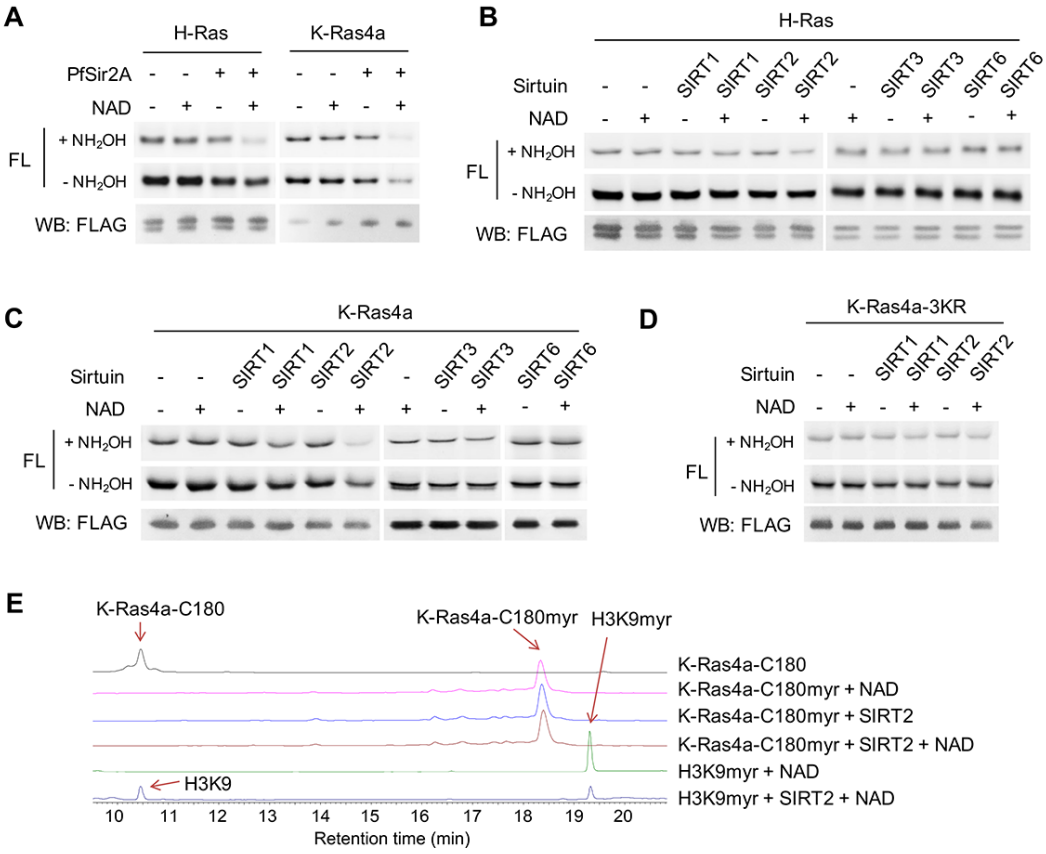

Figure 3.4 SIRT1 removes lysine fatty acylation from K-Ras4a, SIRT2 removes lysine fatty acylation from H-Ras and K-Ras4a in vitro. (**A**) In-gel fluorescence detection of fatty acylation on H-Ras and K-Ras4a treated without or with 10 μM PfSir2A and 1 mM NAD *in vitro*. (**B, C**) In-gel fluorescence detection of fatty acylation of H-Ras (B) and K-Ras4a (C) treated with 5 μM of SIRT1, 2, 3 and 6 without or with 1 mM of NAD *in vitro*. (**D**) Fatty acylation of K-Ras4a-3KR treated without or with 5 μM SIRT2 and 1 mM NAD *in vitro*. (**E**) High-performance liquid chromatography (HPLC) traces showing SIRT2 hydrolyzing myristoyl group from H3K9myr peptide but not K-Ras4a-C180myr peptide. The reaction with H3K9myr, SIRT2 and NAD serves as a control to show that SIRT2 was active.

Furthermore, knockdown (KD) of SIRT2 in HEK293T cells did not affect lysine fatty acylation of H-Ras (Fig. 3.5A & E), whereas KD of SIRT2 but not SIRT1 significantly increased lysine fatty acylation of K-Ras4a compared with control (Ctrl) KD (Fig. 3.5B, C & E). We also noted that SIRT2 KD did not affect fatty acylation of N-Ras (Fig. 3.5D & E). Taken together, these results illustrate that K-Ras4a is a lysine defatty-acylation substrate for SIRT2 in cells, but H-Ras and N-Ras are not.

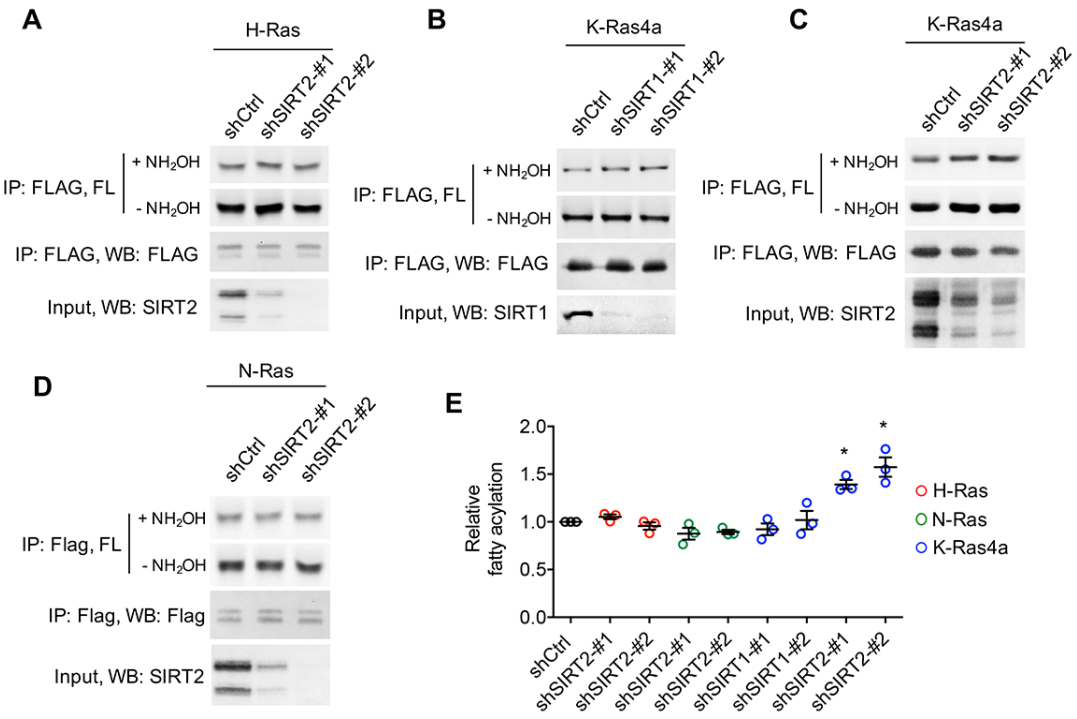

Figure 3.5 SIRT2 KD increases lysine fatty acylation of K-Ras in cells. (**A**) Effect of SIRT2 KD on the fatty acylation level of H-Ras in HEK293T cells. (**B, C**) Effect of SIRT1 KD (B) and SIRT2 KD (C) on the fatty acylation level of K-Ras4a in HEK293T cells. (**D**) Effect of SIRT2 KD on the fatty acylation level of N-Ras in HEK293T cells. (**E**) Quantification of the fatty acylation levels with NH_2OH treatment in (A-D). The fatty acylation level in the corresponding Ctrl KD was set to 1. Statistical evaluation was by unpaired two-tailed Student's t test. Error bars represent SEM in three biological replicates. $*P < 0.05$; ns, not significant. Representative images from three independent experiments are shown.

We next further validated that K-Ras4a is regulated by SIRT2-mediated defatty-acylation. We utilized the SIRT2-H187Y (HY) mutant, which has previously been shown to be catalytically dead in lysine deacetylation[27], as a negative control. An HPLC-based *in vitro* assay demonstrated that the H187Y mutation dramatically decreased SIRT2 defatty-acylation activity, while it completely abolished its deacetylation activity (Fig. 3.6B). Co-expression of SIRT2 with K-Ras4a in HEK293T cells substantially decreased K-Ras4a lysine fatty acylation, whereas co-expression of SIRT2-HY had much less effect (Fig. 3.6A), suggesting that K-Ras4a defatty-acylation requires SIRT2 catalytic activity. Interestingly, our finding that mutation of the catalytic histidine residue did not completely abolish sirtuin enzymatic activity is not without

precedent. For example, mutating the catalytic histidine of bacterial Sir2Tm deacetylase[28], yeast HST2 deacetylase[29], and human SIRT6 defatty-acylase[11] also retained some catalytic activity.

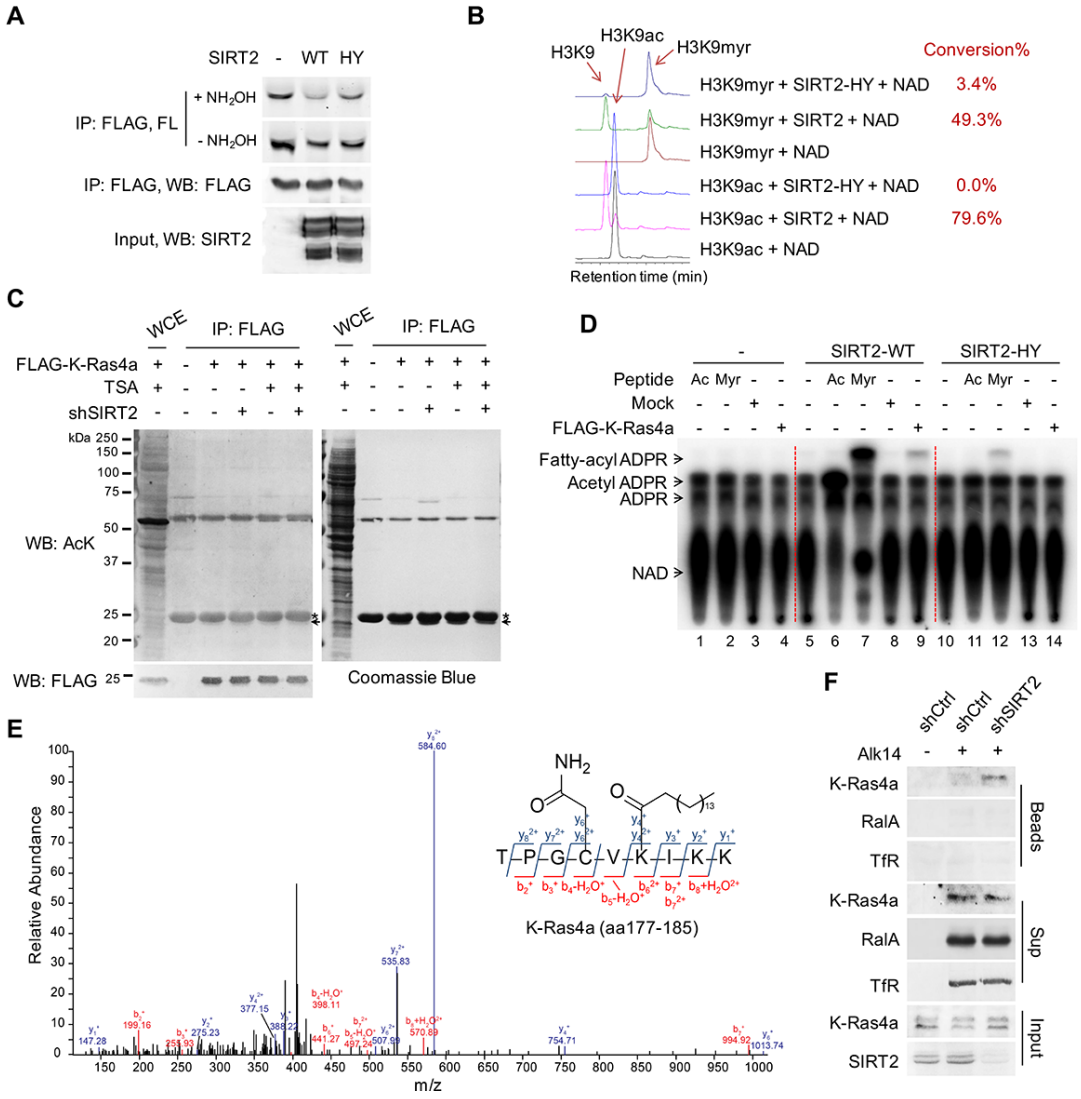

Figure 3.6 SIRT2 removes lysine fatty acylation from K-Ras4a in cells. (**A**) Effect of overexpressing SIRT2-WT and SIRT2-HY catalytic mutant on K-Ras4a fatty acylation level. (**B**) Comparison of the activities of SIRT2-WT and SIRT2-HY on H3K9ac and H3K9myr peptides by HPLC-based *in vitro* assay. The conversion rate is shown on the right. (**C**) Acetylation of K-Ras4a in Ctrl or SIRT2 KD (by shSIRT2-#2) HEK293T cells treated with ethanol or TSA (1 μM) for 1 hr. The "*" points to the light chain of the anti-FLAG antibody, while the arrow points to K-Ras4a. (**D**) Fatty acylated lysine in K-Ras4a detected by formation of ^{32}P-labeled fatty acyl-ADPR using ^{32}P-NAD. (**E**) MS/MS spectrum of triply charged K-Ras4a peptide with palmitoylation on K182. The b- and y-ions are shown along with the peptide sequence. The cysteine residue was carbamidomethylated due to iodoacetamide treatment during sample preparation. (**F**) Lysine fatty acylation of endogenous K-Ras4a in Ctrl and SIRT2 KD (by shSIRT2-#2) HCT116 cells detected by Alk14 labeling and biotin pull-down. Sup, supernatant; Ac, acetyl-H3K9; Myr, myristoyl-H3K9.

To investigate whether K-Ras4a could also be regulated by SIRT2 through deacetylation, we examined its acetylation level using a pan-specific acetyl lysine antibody. Acetylation was not detected on K-Ras4a in either Ctrl KD or SIRT2 KD cells without or with histone deacetylases (HDAC) inhibitor Trichostatin A (TSA) (Fig. 3.6C). We also searched our K-Ras4a MS data and did not find any peptides with lysine acetylation, indicating that SIRT2 likely does not regulate K-Ras4a via deacetylation.

With SIRT2 as a tool, we further confirmed the existence of lysine fatty acylation on K-Ras4a in cells that were not treated with Alk14. We used a previously developed assay that relies on ^{32}P-NAD to detect sirtuin-catalyzed deacylation reactions[30]. When histone H3K9 acetyl (Ac) and myristoyl (Myr) peptides were incubated with SIRT2-WT in the presence of ^{32}P-NAD, the formation of the acyl-ADPR product could be detected by autoradiography after separation using thin-layer chromatography (TLC) (Fig. 3.6D, lanes 6 & 7). In contrast, the SIRT2-HY mutant only generated a tiny amount of the acyl-ADPR product (Fig. 3.6D, lanes 11 & 12). When K-Ras4a isolated from HEK293T cells was treated with SIRT2-WT in the presence of ^{32}P-NAD, a spot corresponding to fatty acyl-ADPR but not acetyl-ADPR was detected (Fig. 2h, lane 9). Control reactions without SIRT2 (Fig. 3.6D, lane 4) or with the HY mutant (Fig. 3.6D, lane 14) did not generate the fatty acyl-ADPR product. These results demonstrate that K-Ras4a contains lysine fatty acylation that can be removed by SIRT2 in the absence of Alk14 supplementation. A peptide carrying palmitoylation, but not myristoylation, on K182 of FLAG-tagged K-Ras4a was detected by MS (Fig. 3.6E), demonstrating that palmitoylation is the major native lysine acylation of K-Ras4a.

We then investigated whether endogenous K-Ras4a is also regulated by SIRT2-catalyzed lysine defatty-acylation. For this purpose, we used the HCT116 human colorectal cancer cell line, in which K-Ras4a was shown to be expressed [19]. Since the commercial antibody against K-Ras4a did not immunoprecipitate K-Ras4a, we enriched fatty acylated proteins labeled with

Alk14 as previously described[31], and detected fatty acylated K-Ras4a using a K-Ras4a-specific antibody. HCT116 cells with Ctrl KD or SIRT2 KD were cultured in the presence of Alk14. Proteins were then extracted and a biotin affinity tag was attached to the Alk14-labeled proteins with click chemistry. The biotin-conjugated proteins were pulled down using streptavidin beads, and subsequently washed with 1% SDS to disrupt protein-protein interaction. Proteins that were only fatty acylated on cysteine residues were then released from the streptavidin beads into the supernatant (Sup) *via* NH_2OH treatment, while proteins with lysine fatty acylation were retained. As shown in Fig. 2i, RalA (Fig. 3.2C) and transferrin receptor (TfR)[32], which are predominantly cysteine fatty acylated, were present in the supernatant but barely detectable from the streptavidin beads, indicating that the NH_2OH treatment was effective. In Ctrl KD cells, K-Ras4a was mainly detected in the supernatant. However, in the SIRT2 KD cells, K-Ras4a was detected both on the streptavidin beads and in the supernatant, indicating that endogenous K-Ras4a possesses lysine fatty acylation that is regulated by SIRT2.

By immunoprecipitation of total Ras protein from Alk14-treated HCT116 cells using a pan-Ras (Y13-259) antibody, we found that endogenous Ras proteins exhibited NH_2OH-resistant fatty acylation (Fig. 3.7A). Moreover, SIRT2 KD increased the NH_2OH-resistant fatty acylation of Ras proteins (Fig. 3.7B). Since SIRT2 KD did not affect lysine fatty acylation of overexpressed H-Ras (Fig. 3.5A & E) and N-Ras (Fig. 3.5D & E), the data suggested that the increase in total Ras lysine fatty acylation observed in SIRT2 KD cells can be attributed to K-Ras4a lysine fatty acylation. This result, together with the detection of K-Ras4a lysine fatty acylation by Alk14 biotinylation, further supports that endogenous K-Ras4a is lysine fatty acylated and is regulated by SIRT2-mediated lysine defatty-acylation.

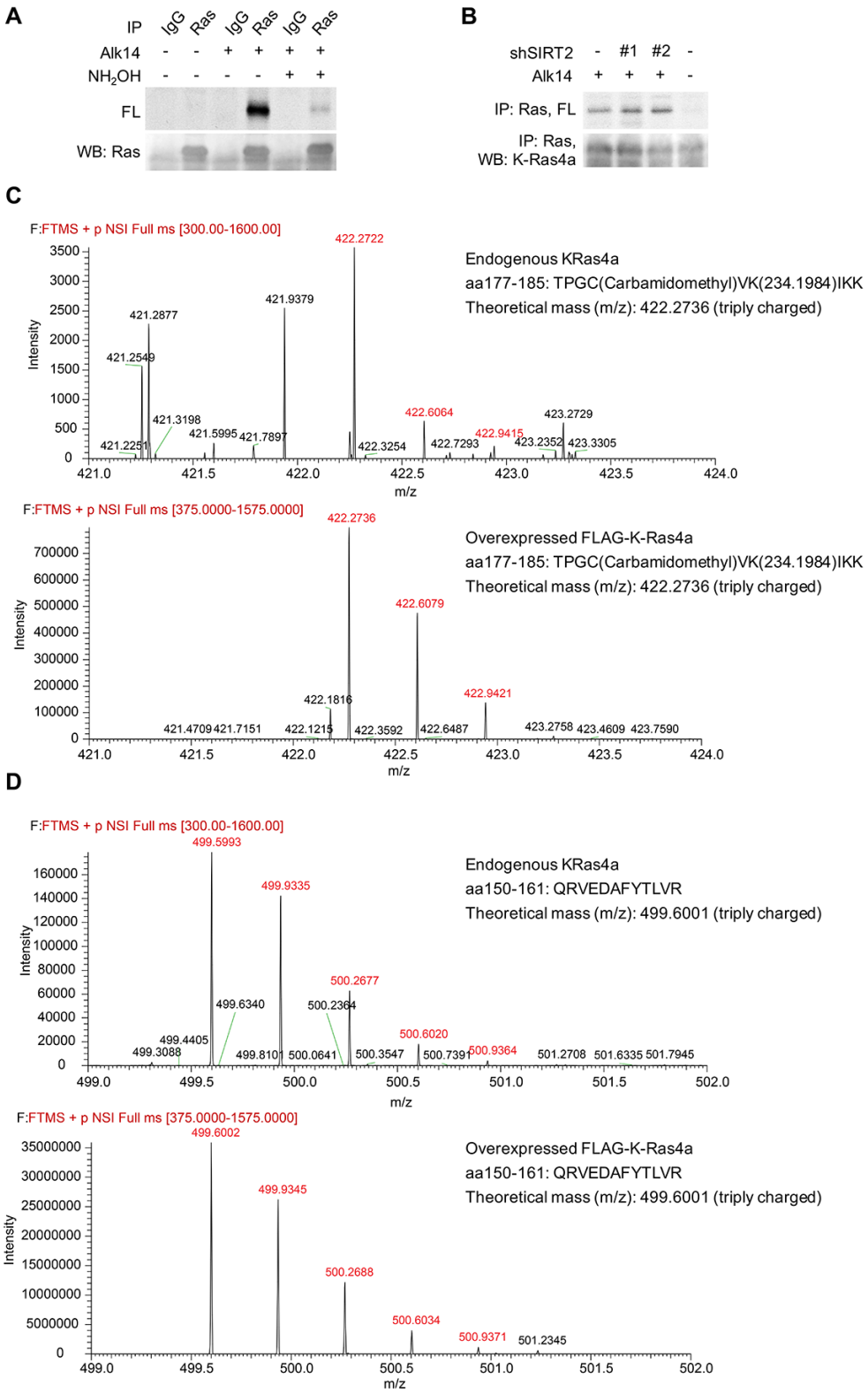

Figure 3.7 Endogenous K-Ras4a is lysine fatty acylated. (**A**) In-gel fluorescence detection of fatty acylation on endogenous total Ras proteins immunoprecipiated from HCT116 cells. (**B**)Effect of SIRT2

KD on fatty acylation of endogenous Ras after NH_2OH treatment. (**C**) Comparison of the MS spectra of Alk14-modified K-Ras4a aa177-185 peptide from endogenous Ras and overexpressed K-Ras4a MS analyses. (**d**) Comparison of the MS spectra of K-Ras4a aa 150-161 peptide from endogenous Ras and overexpressed K-Ras4a MS analyses. The ion intensities for the Alk14-modified aa177-185 and the unmodified aa 150-161 peptides were over 200 times lower than those from overexpressed K-Ras4a.

We also performed MS analysis of endogenous Ras immunoprecipitated from HCT116 cells treated with SIRT2 shRNA and Alk14. We identified a peptide with a primary mass matching the Alk14-modified K-Ras4a aa177-185 peptide, whose exact m/z and isotope pattern were the same as those of overexpressed K-Ras4a (Fig. 3.7C). However, this primary mass did not trigger MS2, which was likely due to low peptide abundance (Fig. 3.7C &D). It has been shown that K-Ras has a much lower expression level than H-Ras and N-Ras because of its rare codon bias[33,34].

SIRT2 was reported to reside predominantly in the cytoplasm[35,36]. The regulation of K-Ras4a lysine fatty acylation by SIRT2 suggested that SIRT2 might also exist at cellular membranes, where K-Ras4a mainly resides. Indeed, by subcellular fractionation, we found that SIRT2 was present in both soluble and membrane fractions (Fig. 3.8A). Co-immunoprecipitation (co-IP) revealed K-Ras4a associated with endogenous SIRT2 (Fig. 3.8B). These results further support that K-Ras4a is a lysine defatty-acylase substrate for SIRT2.

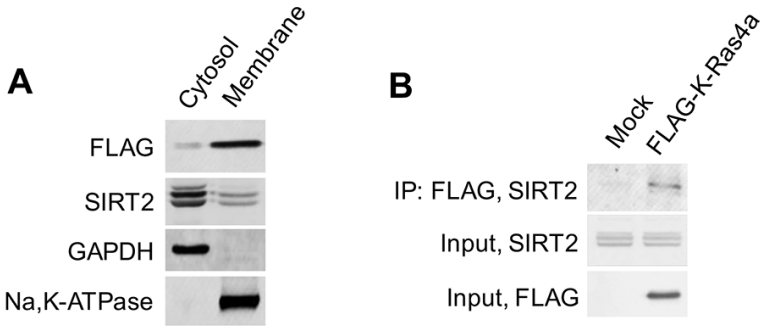

Figure 3.8 SIRT2 interacts with K-Ras4a. (**A**) Subcellular fractionation showing the localization of SIRT2 and FLAG-K-Ras4a. (**B**) Co-IP of FLAG-K-Ras4a with endogenous SIRT2 in HEK293T cells. Representative images from three independent experiments are shown.

2.3 Mapping the fatty acylated lysine residues regulated by SIRT2

MS results suggested that K182 was the preferentially fatty acylated lysine residue on K-Ras4a. However, the lysine 182 to arginine mutant (K182R) exhibited similar lysine fatty acylation levels to that of WT (Fig. 3.9A). As the 3KR (K182/184/185R) but not the 4KR (K169/170/173/176R) mutant significantly decreased K-Ras4a lysine fatty acylation (Fig. 3.2F), we also mutated K184 and K185 to arginine individually. Neither the K184R nor K185R mutation decreased lysine fatty acylation as the 3KR mutant did (Fig. 3.9A). These results suggested that K182, 184 and 185 were likely to be modified redundantly. We suspected that it was hard to pinpoint the exact modification site by mutagenesis because the K182R mutation might enhance fatty acylation on the other two nearby lysine residues. To test this hypothesis, we performed MS analysis of FLAG-K-Ras4a-K182A extracted from Alk14-treated HEK293T cells. We tested the K182A instead of K182R mutant because the K182R mutant would produce a tryptic peptide that is too short to be detected. As expected, the K182A mutation did not affect the overall level of K-Ras4a lysine fatty acylation (Fig. 3.9B). A peptide (amino acids 177-185) fatty acylated on K184 was detected by MS (Fig. 3.9B), which agrees with our hypothesis. It was likely that K185 could also be fatty acylated for the K182R mutant, because the K182/185R mutant slightly but significantly decreased lysine fatty acylation levels compared with the K182R and K185R single mutants (Fig. 3.9A). The K185 fatty acylation was not detected by MS most likely because the modified tryptic peptide was too short and hydrophobic ($K_{fatty\text{-}acyl}C_{prenyl,\ oMe}$). Overall, these data indicate that K182/184/185 are fatty acylated redundantly and that the 3KR mutation is needed to abolish the lysine fatty acylation on the C-terminus of K-Ras4a.

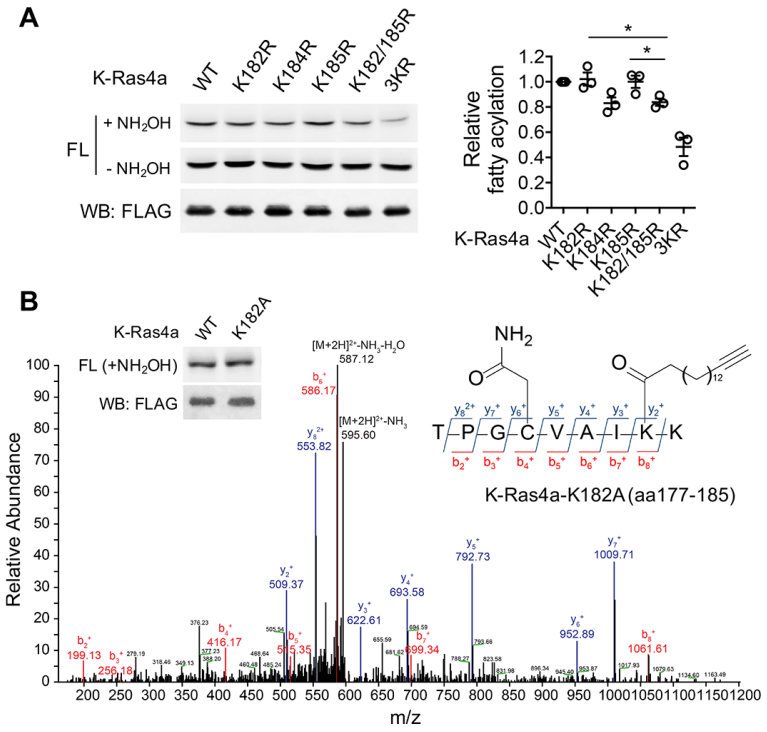

Figure 3.9 K-Ras4a is fatty acylated on lysine 182/184/185. (**A**) Fatty acylation levels of K-Ras4a WT, K182R, K184R, K185R, K182/185R, and 3KR by in-gel fluorescence (left panel) and quantification of fatty acylation levels after NH_2OH treatment relative to that of K-Ras4a WT (right panel). (**B**) MS/MS spectrum of triply charged K-Ras4a-K182A peptide with Alk14 modification on K184. The b- and y-ions are shown along with the peptide sequence. The cysteine residue was carbamidomethylated due to iodoacetamide alkylation during sample preparation. Fatty acylation levels of K-Ras4a WT and K182A with NH_2OH were also shown.

K-Ras4a has been shown to be prenylated on cysteine 186 and palmitoylated on cysteine 180[19]. To examine whether cysteine prenylation or palmitoylation play a role in lysine fatty acylation, we generated cysteine-to-serine C180S and C186S mutants. Mutation of the prenylcysteine (C186S) completely abolished the fatty acylation of K-Ras4a (Fig. 3.10A), which is consistent with the model that prenylation of the cysteine on the CaaX motif of Ras proteins is required for the subsequent fatty acylation[37]. On the other hand, mutation of the palmitoylated cysteine (C180S) led to a substantial but not complete loss of K-Ras4a lysine fatty acylation (Fig. 3.10A). The fatty acylation on the C180S mutant was NH_2OH-resistant and was abolished by combining the C180S and 3KR mutations (Fig. 3.10B), implying that the C180S mutant was fatty acylated on K182/184/185. These data suggest that cysteine

palmitoylation might play an important but nonessential role in the occurrence of lysine fatty acylation. It is possible that cysteine palmitoylation facilitates the lysine fatty acyl transfer reaction, or the delivery of K-Ras4a to where lysine fatty acylation occurs.

We next assessed whether SIRT2 regulates fatty acylation of K-Ras4a on K182/184/185. SIRT2 removed lysine fatty acylation from K-Ras4a WT, the 4KR mutant and the C180S mutant, but not the 3KR mutant *in vitro* (Fig. 3.10C). SIRT2 KD in HEK293T cells increased lysine fatty acylation of K-Ras4a WT and the C180S mutant, but not the 3KR and C180S-3KR mutants (Fig. 3.10D), indicating that fatty acylation on K182/184/185 is regulated by SIRT2.

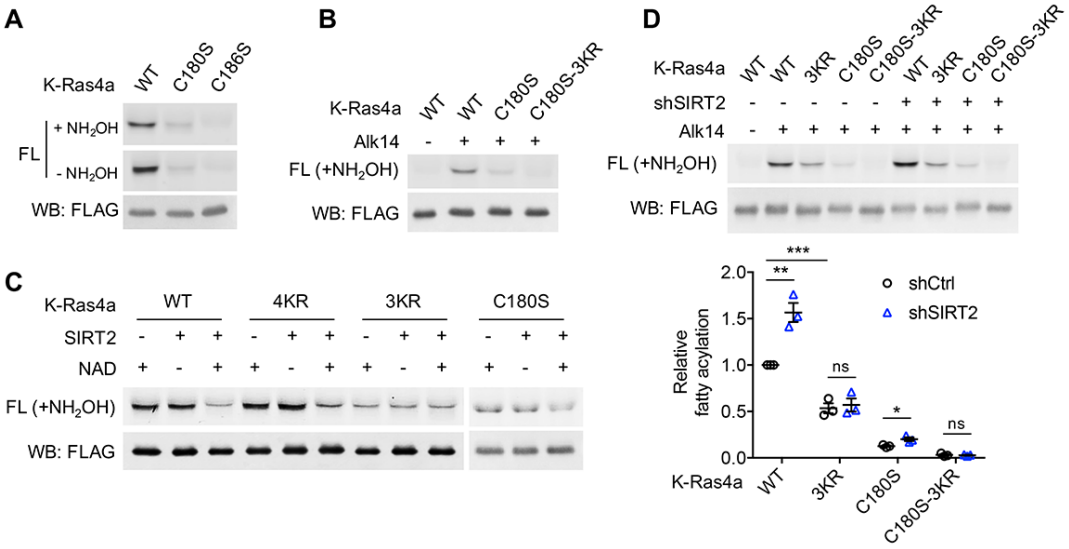

Figure 3.10 SIRT2 regulates lysine fatty acylation of K-Ras4a on K182/184/185. (**A**) Fatty acylation levels of K-Ras4a WT, C180S, and C186S. (**B**) Fatty acylation levels of K-Ras4a WT, C180S and C180S-3KR after NH_2OH treatment. (**C**) In-gel fluorescence detection of fatty acylation of K-Ras4a-WT, -4KR, -3KR and -C180S treated without or with 5 μM SIRT2 and 1 mM NAD *in vitro*. (**D**) Fatty acylation levels of K-Ras4a WT, 3KR, C180S and C180S-3KR after NH_2OH treatment in Ctrl and SIRT2 KD (by shSIRT2-#2) HEK293T cells. Quantification of the fluorescent intensity relative to K-Ras4a WT is shown in the bottom panel. Statistical evaluation was by unpaired two-tailed Student's t test. Error bars represent SEM in three biological replicates. *$P < 0.05$; **$P < 0.01$; ***$P < 0.001$. Representative images from three independent experiments are shown.

2.4 Lysine fatty acylation regulates subcellular localization of K-Ras4a

We next set out to study the effect of lysine fatty acylation on K-Ras4a. A variety of PTMs on Ras proteins, such as cysteine palmitoylation [38,39], phosphorylation[40,41] and ubiquitination[42],

function to deliver the molecule to the right place within the cell. We hypothesized that lysine fatty acylation may also be critical for the correct subcellular distribution of K-Ras4a. To test this hypothesis, we fused *Aequorea coerulescens* Green Fluorescent Protein (GFP) to the N-terminus of K-Ras4a WT and the 3KR mutant and performed live imaging with confocal microscopy in Ctrl and SIRT2 KD HEK293T cells to visualize K-Ras4a localization. The levels of over-expressed K-Ras4a WT and 3KR were equal in Ctrl and SIRT2 KD cells (Fig. 3.11A). We also imaged cells with similar GFP intensity under the same settings to avoid potential false positive observations caused by different levels of expression. In Ctrl KD cells, both K-Ras4a WT and the 3KR mutant displayed predominant localization to the plasma membrane (PM). However, the presence of 3KR on intracellular puncta was noticeably more pronounced compared to WT. SIRT2 KD decreased the intracellular punctate-localized K-Ras4a WT compared to Ctrl KD, whereas it had no effect on the punctate localization of the 3KR mutant (Fig. 3.11B & C), indicating that the effect of the 3KR mutation on K-Ras4a localization was due to lack of lysine fatty acylation. Similar effects of the 3KR mutation were obtained for K-Ras4a in HCT116 cells and for oncogenic K-Ras4a-G12V, which exhibited comparable lysine fatty acylation level to K-Ras4a WT (Fig. 3.11D) in NIH3T3 cells (Fig. 3.11G & F). On the other hand, SIRT2 KD did not affect the intracellular punctate localization of H-Ras (Fig. 3.11B), which is consistent with our observation that H-Ras was not regulated by SIRT2 through lysine defatty-acylation. Taken together, these data indicate that lysine fatty acylation inhibits the intracellular punctate localization of K-Ras4a and SIRT2 promotes this localization by defatty-acylation. In addition, the K-Ras4a-C180S mutant that lacks cysteine palmitoylation and the majority of lysine fatty acylation extensively localized to internal membranes, which was distinct from the punctate localization of the 3KR mutant that is deficient in lysine fatty acylation but retains cysteine palmitoylation (Fig. 3.11G & H). This implies that cysteine

palmitoylation might facilitate the punctate localization of K-Ras4a in the absence of lysine fatty acylation, while lysine fatty acylation inhibits it.

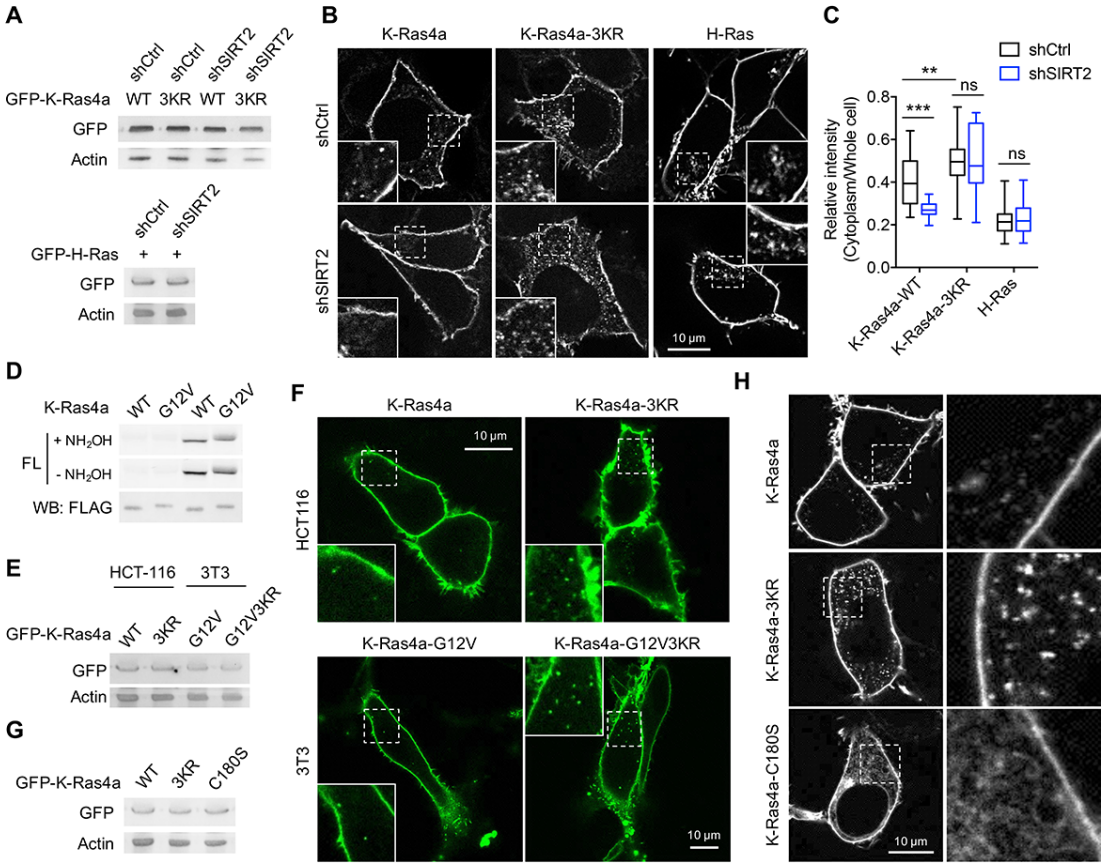

Figure 3.11 Lysine fatty acylation regulates subcellular localization of K-Ras4a. (**A**) Western blot analyses showing equal overexpression of GFP-K-Ras4a WT and 3KR in HEK293T cells with Ctrl and SIRT2 KD. (**B**) Confocal images showing subcellular localization of GFP-K-Ras4a WT, 3KR, and GFP-H-Ras in HEK293T cells with Ctrl or SIRT2 KD (by shSIRT2-#2). Insets are magnifications of the regions enclosed by the white dashed squares. (**C**) Statistical analyses of the relative cytoplasm to whole cell intensity of K-Ras4a WT, 3KR, and H-Ras from (a) (n = 16, 16, 16, 16, 21, 21 for each sample from left to right, respectively). (**D**) Fatty acylation levels of K-Ras4a WT and G12V in HEK293T cells. (**E**) Western blot analyses showing equal protein levels for overexpressed GFP-K-Ras4a-WT and -3KR in HCT116 cells, and GFP-K-Ras4a-G12V and -G12V-3KR in 3T3 cells. (**F**) Live cell imaging of HCT116 cells overexpressing GFP-K-Ras4a-WT and -3KR and NIH 3T3 cells overexpressing GFP-K-Ras4a-G12V and -G12V-3KR. Insets are magnifications of the regions enclosed by the white dashed squares. (**G**) Western blot showing equal protein levels for overexpressed GFP-K-Ras4a-WT, -3KR and -C180S in HEK293T cells. (**H**) Confocal images showing subcellular localization of GFP-K-Ras4a, -3KR, and -C180S. The bottom panels show the magnified images of the regions enclosed by the white dashed squares in the top panels. Statistical evaluation was by two-way ANOVA. *Centre line* of the box plot represents the mean value, box represents the 95 % confidence interval, and whiskers represent the range of the values. $^{**}P < 0.01$; $^{***}P < 0.001$; ns, not significant. Representative images are shown.

It has been shown that Ras proteins associate with and signal from endomembrane compartments, including the endoplasmic reticulum (ER), Golgi, endosomes and lysosome [18,42-48]. Therefore, we next set out to identify the endomembrane compartments where lysine defatty-acylated K-Ras4a is localized. We performed colocalization analyses with a series of membrane compartment markers. Compared with K-Ras4a WT, the 3KR mutant exhibited more pronounced cytoplasmic colocalization with *trans*-Golgi network (TGN) marker STX6, early endosome marker EEA1, recycling endosome marker Rab11 and lysosome marker LAMP1 (Fig. 3.12A & C), but not with the ER marker Sec61, *trans*-Golgi marker GalT and late endosome marker Rab7 (Fig. 3.12B & C). These results suggest that removal of lysine fatty acylation from K-Ras4a promotes its localization to the endomembranes in endocytic pathways, by which it may be routed from early endosome to the lysosome for degradation and to the TGN or recycling endosomes to return to the plasma membrane [49].

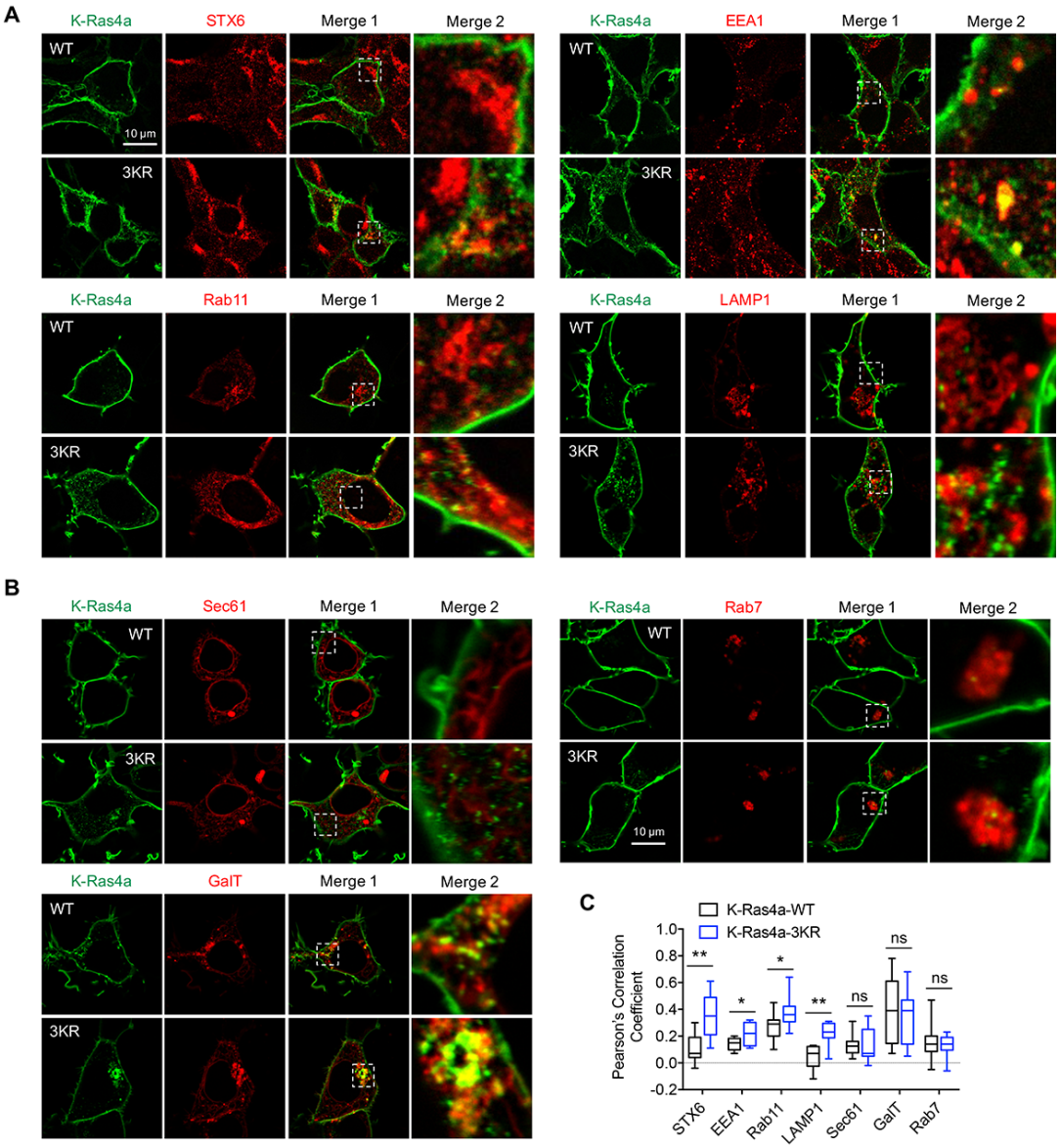

Figure 3.12 Loss of lysine fatty acylation targets K-Ras4a to endomembranes. (**A**) Images showing the colocalization of GFP-K-Ras4a WT or 3KR with STX6, EEA1, Rab11, and LAMP1 in HEK293T cells. Merge 2 shows the magnified white dashed squares-enclosed regions in Merge 1. (**B**) Representative images for examining the colocalization of GFP-K-Ras4a or -3KR with Sec61, GalT, and Rab7 in HEK293T cells. Magnifications of the white dashed squares-enclosed regions in Merge 1 are shown as Merge 2. (**C**) Statistical analyses of the cytoplasmic colocalization of K-Ras4a or -3KR with the indicated intracellular membrane markers from (A & B) using Pearson's coefficient (n = 11, 11, 11, 11, 17, 17, 10, 10, 11, 11, 11, 11, 13, 13 cells for each sample from left to right, respectively). Statistical evaluation was by two-way ANOVA. *Centre line* of the box plot represents the mean value, box represents the 95 % confidence interval, and whiskers represent the range of the values. **P* < 0.05; ***P* < 0.01; ns, not significant. Representative images are shown.

2.5 Lysine fatty acylation regulates transforming activity of K-Ras4a

We next investigated whether lysine fatty acylation also affects the function of K-Ras4a. We assessed the ability of constitutively active K-Ras4a-G12V and the K-Ras4a-G12V-3KR mutant to enable anchorage-independent growth, promote proliferation in monolayer cultures and stimulate migration in Ctrl and Sirt2 KD cells. In Ctrl KD cells, expression of K-Ras4a-G12V-3KR resulted in significantly more colony formation on soft agar than did expression of K-Ras4a-G12V. Furthermore, Sirt2 KD caused a greater decrease in the colony formation induced by K-Ras4a-G12V (75% decrease) than by K-Ras4a-G12V-3KR (45% decrease) (Fig. 3.13). Additionally, Sirt2 KD more potently inhibited K-Ras4a-G12V-mediated colony formation than H-Ras4a-G12V-mediated colony formation (Fig. 3.13), consistent with the fact that SIRT2 regulates lysine fatty acylation of K-Ras4a but not H-Ras or K-Ras4a 3KR. Thus, lysine fatty acylation inhibits the ability of K-Ras4a-G12V to induce anchorage-independent growth of cells and SIRT2 promotes it through defatty-acylation. One caveat of the result, however, was that Sirt2 KD still decreased the colony formation induced by K-Ras4a-G12V-3KR or H-Ras-G12V, whose lysine fatty acylation was not regulated by SIRT2. This is not unexpected because SIRT2 is known to exert tumor-promoting functions by deacetylating various targets[50-58]. Thus, the effect of Sirt2 KD on K-Ras4a-G12V-3KR- and H-Ras-induced transformation might be attributed to other substrates for SIRT2.

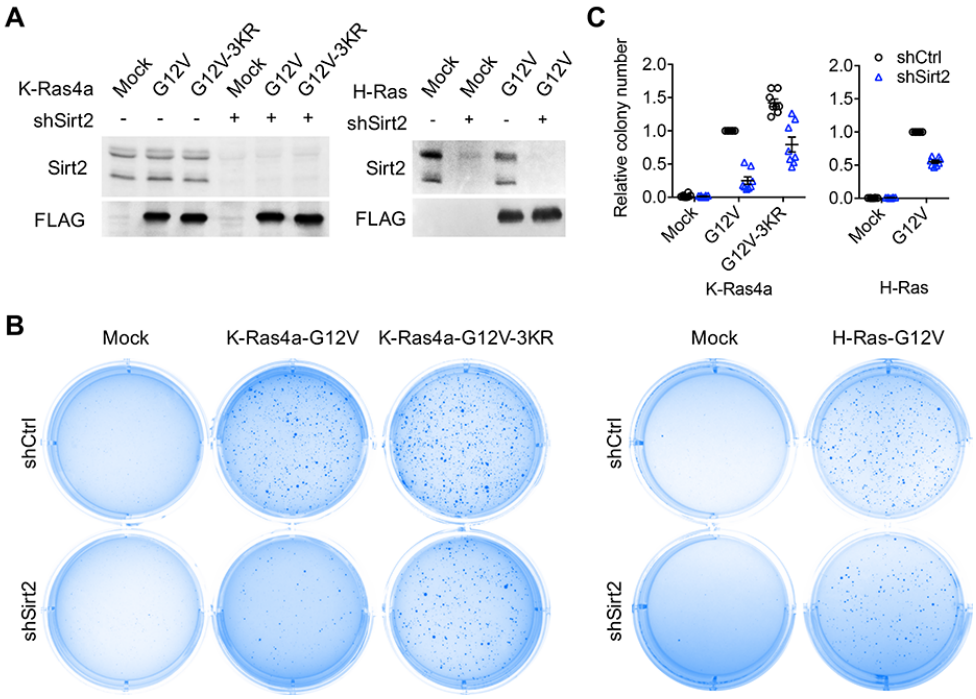

Figure 3.13 SIRT2-dependent lysine defatty-acylation increases K-Ras4a transforming activity. (**A**) Representative western blot analyses of Sirt2, FLAG-K-Ras4a-G12V, FLAG-K-Ras4a-G12V-3KR, FLAG-H-Ras-G12V protein levels in NIH3T3 cells with Ctrl or Sirt2 KD used in (**B** and **C**). (**B**) Anchorage-independent growth of NIH 3T3 cells stably expressing Mock, K-Ras4a-G12V, -G12V-3KR or H-Ras-G12V with Ctrl or Sirt2 KD. (**C**) Quantification of the colony numbers in (**B**) relative to that of the cells expressing K-Ras4a-G12V-shCtrl or H-Ras-G12V-shCtrl. Statistical evaluation was by unpaired two-tailed Student's t test. Error bars represent SEM in eight biological replicates or as indicated. ***$P < 0.001$. Representative images (A, B) from at least three independent experiments are shown.

In monolayer cultures, NIH3T3 cells expressing K-Ras4a-G12V-3KR displayed a higher proliferation rate than those expressing K-Ras4a-G12V. Sirt2 KD inhibited the proliferation of the NIH3T3-K-Ras4a-G12V cells (47% inhibition) slightly more than that of the NIH3T3-K-Ras4a-G12V-3KR (34% inhibition) cells (Fig. 3.14A). Thus, lysine fatty acylation negatively regulates K-Ras4a-G12V-induced cell proliferation under monolayer culture conditions, but the effect was smaller than that on anchorage-independent growth (Fig. 3.13). Results from transwell migration assays revealed that the 3KR mutation did not affect the capability of K-Ras4a-G12V to induce cell migration. Consistent with this finding, Sirt2 KD decreased K-Ras4a-G12V and K-Ras4a-G12V-3KR-mediated cell migration similarly (Fig. 3.14B & C).

Therefore, lysine fatty acylation does not affect the ability of K-Ras4a-G12V to stimulate cell migration.

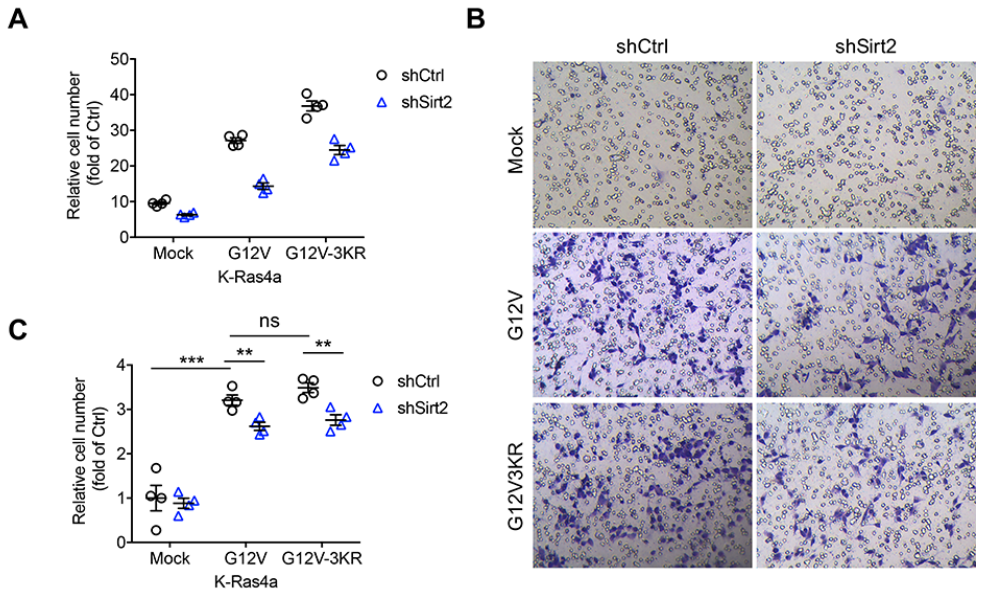

Figure 3.14 Lysine fatty acylation regulates K-Ras4a-G12V-mediated cell proliferation but not migration. (**A**) Effect of Ctrl or Sirt2 KD on proliferation of NIH3T3 cells stably overexpressing Mock, K-Ras4a-G12V or -G12V-3KR. Cell numbers were determined by crystal violet staining 0 or 5 days after the transduction with shCtrl or shSirt2-carrying lentivirus. The y axis represents cell numbers normalized to that of the corresponding shCtrl group on Day 0. (**B**) Representative images of transwell migration assay in NIH3T3 cells stably overexpressing Mock, K-Ras4a-G12V or -G12V-3KR with Ctrl or Sirt2 KD. (**C**) Migration cell numbers in (B) relative to that of Mock with Ctrl KD. Statistical evaluation was done using unpaired two-tailed Student's t test. Error bars represent SEM in four biological replicates. $^{**}P < 0.01$; $^{***}P < 0.001$; ns, not significant.

2.6 A-Raf is involved in the regulation of K-Ras4a by lysine fatty acylation

The dynamic regulation of Ras localization is known to be closely coupled to its signaling output [43,59,60]. We decided to further explore the molecular mechanism underlying the regulation of K-Ras4a-mediated transformation activity by lysine fatty acylation. We first sought to examine whether lysine fatty acylation affects K-Ras4a activation by a pull-down assay with the Ras-binding domain (RBD) of Raf1, which only binds to the GTP-bound form of Ras[43]. Neither the 3KR mutation nor SIRT2 KD affected EGF-stimulated GTP loading of K-Ras4a (Fig. 3.15A & b) or the constitutively GTP-loaded state of K-Ras4a-G12V (Fig. 3.15C & D).

We then determined whether K-Ras4a at endomembranes exists in its GTP-bound state using DsRed-RBD (DsRed fused to the N-terminus of RBD) as a probe. Notably, we observed more colocalization of DsRed-RBD with K-Ras4a on intracellular puncta in cells expressing the 3KR mutant (Fig. 3.15E, F & G) than in cells expressing K-Ras4a WT. Furthermore, SIRT2 KD decreased the colocalization of DsRed-RBD with K-Ras4a WT at intracellular puncta, but not with the 3KR mutant (Fig. 3.15E).

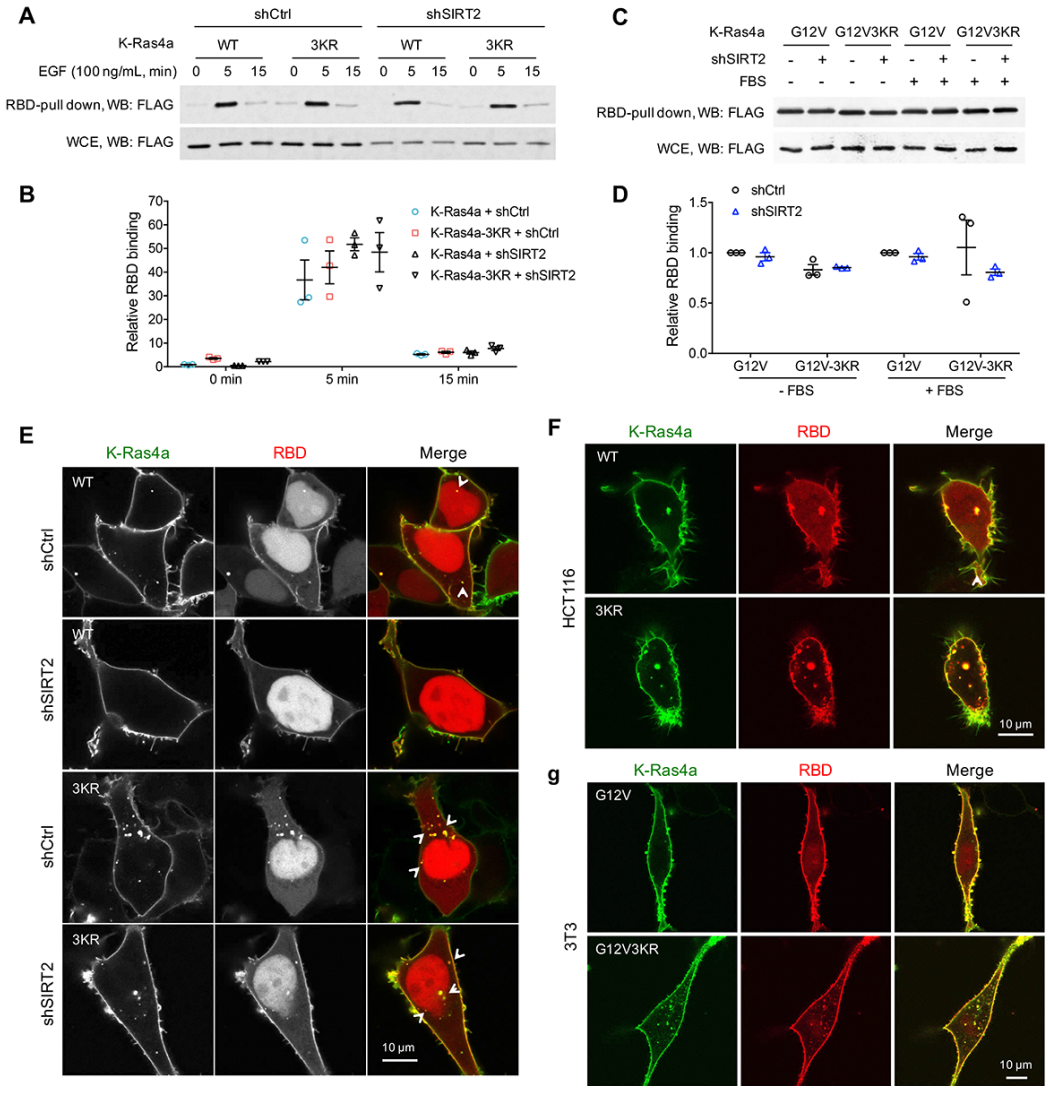

Figure 3.15 Lysine fatty acylation regulates the subcellular localization of active K-Ras4a. (**A**, **B**) RBD pull-down assay in HEK293T cells expressing FLAG-K-Ras4a WT or 3KR with Ctrl or SIRT2 KD (by shSIRT2-#2) (A). Cells were serum-starved overnight and treated with 100 ng/mL EGF for 0, 5 and 15 min. The relative RBD binding with respect to cells expressing K-Ras4a and shCtrl at 0 min was

quantified in (B). (**C**, **D**) RBD pull-down assay in HEK293T cells expressing FLAG-K-Ras4a-G12V or -G12V-3KR with Ctrl or SIRT2 KD (C). Cells were cultured in FBS-free or complete medium for 12 hr before being subjected to RBD pull-down. RBD binding relative to cells expressing K-Ras4a-G12V-shCtrl was quantified in (D). (**E**) Co-localization of GFP-K-Ras4a WT or 3KR with DsRed-RBD in live HEK293T cells with Ctrl or SIRT2 KD. (**F**) Live cell imaging showing the colocalization of GFP-K-Ras4a WT or 3KR with DsRed-RBD in HCT116 cells. (**G**) Live cell imaging showing the colocalization of GFP-K-Ras4a-G12V or -G12V-3KR with DsRed-RBD in NIH3T3 cells. Error bars represent SEM in three biological replicates. The images shown are representative of 80–100% of the cells examined.

The results above suggest that SIRT2-dependent lysine defatty-acylation may promote the localization of activated (GTP-loaded) K-Ras4a at endomembranes, which raises the possibility that lysine defatty-acylation may alter the signaling specificity of K-Ras4a by recruiting different effector proteins to endomembranes. We therefore investigated whether lysine defatty-acylation influenced the binding and activation of the three most well characterized Ras effectors: Raf1, PI3K, and RalGDS[61]. Co-immunoprecipitation demonstrated that neither the 3KR mutation nor Sirt2 KD altered the binding of K-Ras4a-G12V with Raf1, PI3K, or RalGDS (Fig. 3.16 A). We also assessed the capacity of K-Ras4a-G12V and -G12V-3KR in Ctrl and Sirt2 KD cells to activate Raf1, PI3K, and RalGDS signaling pathways using phosphorylated Erk, phosphorylated Akt, and phosphorylated Jnk as reporters, respectively. K-Ras4a-G12V and -G12V-3KR induced comparable levels of Erk activation, which was not affected by Sirt2 KD. Sirt2 KD resulted in a reduction of Akt and Jnk activation, but the effect was similar for both K-Ras4a-G12V and -G12V-3KR (Fig. 3.16B), suggesting other Sirt2 targets that are important for Akt and Jnk activation. These results suggest that SIRT2 catalyzed lysine defatty-acylation of K-Ras4a does not affect the activation of Raf1, PI3K or RalGDS by K-Ras4a.

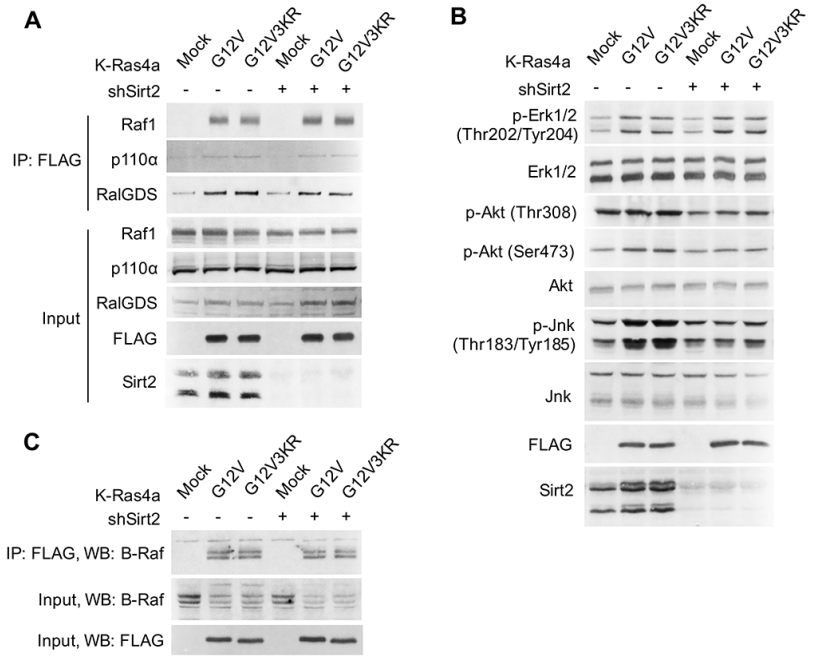

Figure 3.16 Lysine fatty acylation does not affect K-Ras4a signaling through Raf1, PI3K, RalGDS or B-Raf. (**A**) Co-IP of FLAG and Raf1, p110α or RalGDS in NIH3T3 cells stably expressing Mock, FLAG-K-Ras4a-G12V or -G12V-3KR with Ctrl or Sirt2 KD. (**B**) Western blot analyses of phospho-Erk, -Akt and -Jnk in NIH3T3 cells stably expressing Mock, FLAG-K-Ras4a-G12V or -G12V-3KR with Ctrl or Sirt2 KD. (**C**) Co-IP of FLAG and B-Raf in NIH3T3 cells stably expressing Mock, FLAG-K-Ras4a-G12V or FLAG-K-Ras4a-G12V-3KR with Ctrl or Sirt2 KD. Representative images from three independent experiments are shown.

To identify proteins whose binding to K-Ras4a is regulated by lysine fatty acylation, we performed a protein interactome study using stable isotope labeling by amino acids in cell culture (SILAC) (Fig. 3.17). We cultured NIH3T3 cells with stable K-Ras4a-G12V and K-Ras4a-G12V-3KR overexpression in light-isotope- and heavy-isotope-labeled medium, respectively. We then performed FLAG IP, mixed the eluted fractions from both IPs, digested with trypsin and analyzed by MS to identify proteins with Heavy/Light (H/L) ratios > 1.3 or < 0.77, which were candidates that would potentially bind to K-Ras4a-G12V and K-Ras4a-G12V-3KR differently. The experiment was also repeated after swapping the heavy and light SILAC labels. Additionally, to confirm that the effect of the 3KR mutation on the K-Ras4a-G12V interactome was due to the lack of lysine fatty acylation, we also examined the K-Ras4a-G12V

interactome in Ctrl and Sirt2 KD cells with SILAC, which enabled the identification of proteins (H/L > 1.3 or < 0.77) whose binding to K-Ras4a-G12V was regulated by Sirt2.

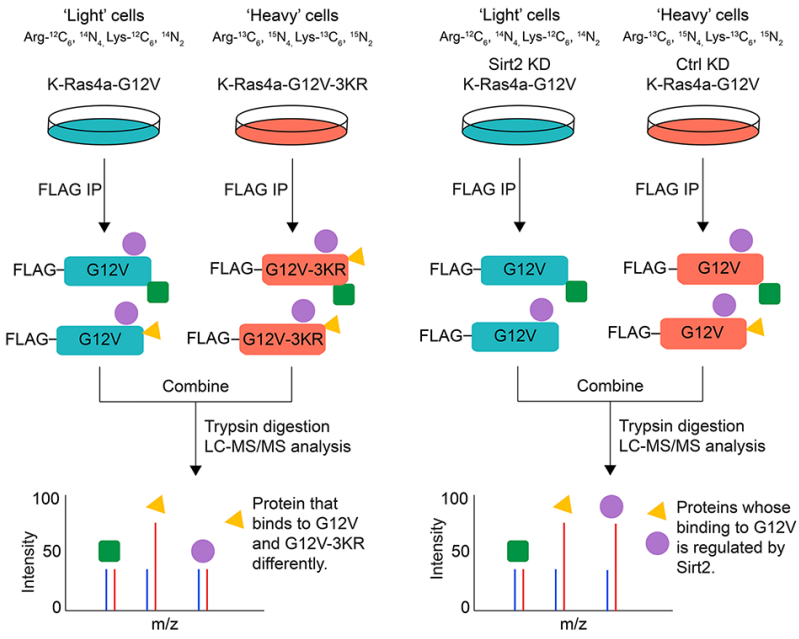

Figure 3.17 Interactome study identifies K-Ras4a-G12V interacting proteins that potentially mediate the effect of lysine fatty acylation. Schematic workflow of the K-Ras4a-G12V SILAC interactome study.

Integration of the three interactome experiments resulted in 175 interacting proteins with at least two unique peptides and H/L ratio. Among them, nine proteins exhibited increased binding to K-Ras4a-G12V-3KR compared to K-Ras4a-G12V, and their interaction with K-Ras4a-G12V was inhibited by Sirt2 KD, suggesting that lysine defatty-acylation enhanced K-Ras4a-G12V interaction with these proteins. On the other hand, one protein showed decreased binding to K-Ras4a-G12V-3KR compared to K-Ras4a-G12V, and its interaction with K-Ras4a-G12V was increased by Sirt2 KD, suggesting that lysine defatty-acylation repressed K-Ras4a-G12V interaction with it (Fig. 3.18A).

Among these 10 proteins, the serine/threonine-protein kinase A-Raf and Apoptosis-inducing factor 1 (Aif), whose interaction with K-Ras4a-G12V might be increased by lysine defatty-acylation, attracted our attention. A-Raf is a member of the Raf family of

serine/threonine-specific protein kinases, acts as a Ras effector and plays an important role in apoptosis [62,63] and tumorigenesis [64-66]. In response to apoptotic stimuli, Aif is released from the mitochondrial intermembrane space into the cytosol and nucleus, where it functions as a proapoptotic factor [67]. Since suppression of apoptosis is linked to Ras-induced transformation[68], it is plausible that A-Raf and Aif are involved in the regulation of K-Ras4a transformation activity by lysine fatty acylation. To test this hypothesis, we first validated the interactome results by co-IP. Although more interaction of Aif with K-Ras4a-G12V-3KR was observed than with K-Ras4a-G12V, Sirt2 KD did not affect the interaction of Aif with either K-Ras4a-G12V or K-Ras4a-G12V-3KR (Fig. 3.18B & C) and was not investigated further. However, a greater interaction of A-Raf with K-Ras4a-G12V-3KR was observed than with K-Ras4a-G12V, and Sirt2 KD significantly decreased the interaction of A-Raf with K-Ras4a-G12V but not with K-Ras4a-G12V-3KR (Fig. 3.18D & E). Thus, we concluded that A-Raf was an effector protein of K-Ras4a that was regulated by lysine fatty acylation and SIRT2. Unlike the effect of Sirt2 KD on K-Ras4a-G12V-A-Raf interaction, Sirt2 KD did not alter H-Ras-G12V-A-Raf interaction (Fig. 3.18D & E). As mentioned earlier, lysine fatty acylation did not affect the binding between C-Raf (Raf1) and K-Ras4a-G12V (Fig. 3.16A). We also assessed the interaction of K-Ras4a-G12V with another Raf family member, B-Raf. Co-IP indicated that neither 3KR mutation nor Sirt2 KD altered the binding of B-Raf to K-Ras4a-G12V (Fig. 3.16C). These results collectively demonstrate that removal of lysine fatty acylation from K-Ras4a by SIRT2 results in its preferential association with A-Raf, but not B-Raf or C-Raf.

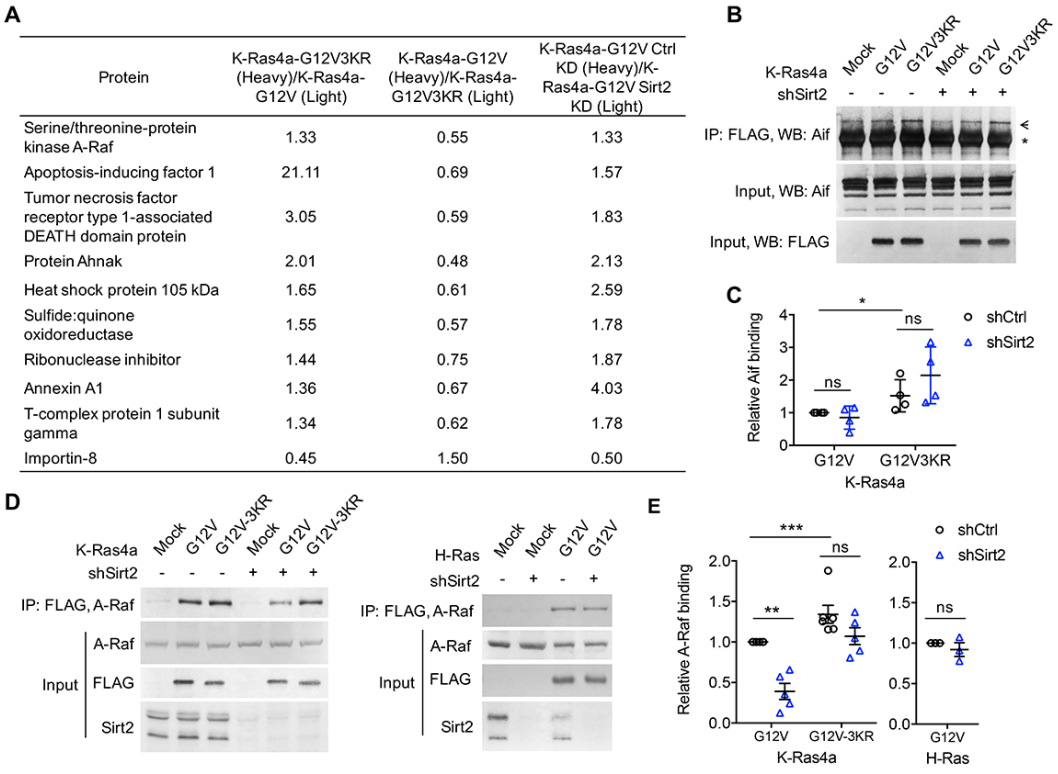

Protein	K-Ras4a-G12V3KR (Heavy)/K-Ras4a-G12V (Light)	K-Ras4a-G12V (Heavy)/K-Ras4a-G12V3KR (Light)	K-Ras4a-G12V Ctrl KD (Heavy)/K-Ras4a-G12V Sirt2 KD (Light)
Serine/threonine-protein kinase A-Raf	1.33	0.55	1.33
Apoptosis-inducing factor 1	21.11	0.69	1.57
Tumor necrosis factor receptor type 1-associated DEATH domain protein	3.05	0.59	1.83
Protein Ahnak	2.01	0.48	2.13
Heat shock protein 105 kDa	1.65	0.61	2.59
Sulfide:quinone oxidoreductase	1.55	0.57	1.78
Ribonuclease inhibitor	1.44	0.75	1.87
Annexin A1	1.36	0.67	4.03
T-complex protein 1 subunit gamma	1.34	0.62	1.78
Importin-8	0.45	1.50	0.50

Figure 3.18 Lysine fatty acylation alters interaction between K-Ras4a and A-Raf. (**A**) List of proteins whose binding to K-Ras4a-G12V may be altered (H/L > 1.3 or < 0.77) by lysine fatty acylation. (**B**) Co-IP of FLAG and Aif in NIH3T3 cells stably expressing Mock, FLAG-K-Ras4a-G12V or -G12V-3KR with Ctrl or Sirt2 KD. The "*" points to the heavy chain of the anti-FLAG antibody, while the arrow points to Aif. (**C**) Quantification of relative Aif binding level in (B) compared to that in cells expressing K-Ras4a-G12V-shCtrl. (**D**) Co-IP of A-Raf with an anti-FLAG antibody in NIH 3T3 cells stably expressing Mock, FLAG-K-Ras4a-G12V, FLAG-K-Ras4a-G12V-3KR, or FLAG-H-Ras-G12V with Ctrl or Sirt2 KD. (**E**) Quantification of relative A-Raf binding levels in (a). Statistical evaluation was by unpaired two-tailed Student's t test. Error bars represent SEM in four biological replicates. *$P < 0.05$; **$P < 0.01$; ***$P < 0.001$; ns, not significant. Representative images are shown.

Our results suggest that SIRT2-mediated lysine defatty-acylation does not affect the magnitude of K-Ras4a activation but promotes endomembrane localization of active K-Ras4a. It has been reported that the efficient activation of certain effector pathways by Ras is dependent on the entry of Ras to the endosomal compartment [42,69]. Therefore, it is plausible that lysine defatty-acylation may facilitate the endomembrane recruitment of A-Raf by K-Ras4a, thereby increasing K-Ras4a oncogenic activity. Live cell imaging revealed that A-Raf colocalized with K-Ras4a-G12V at both the PM and endomembranes. K-Ras4a-G12V-3KR showed more colocalization with A-Raf on the endomembranes than K-Ras4a-G12V did. Sirt2 KD inhibited

the endomembrane recruitment of A-Raf by K-Ras4a-G12V but not that by K-Ras4a-G12V-3KR (Fig. 3.19). These results are in line with our hypothesis. Thus, it is likely that by regulating endomembrane recruitment of A-Raf, K-Ras4a lysine fatty acylation may alter its signaling output through A-Raf, thereby modulating its transforming activity.

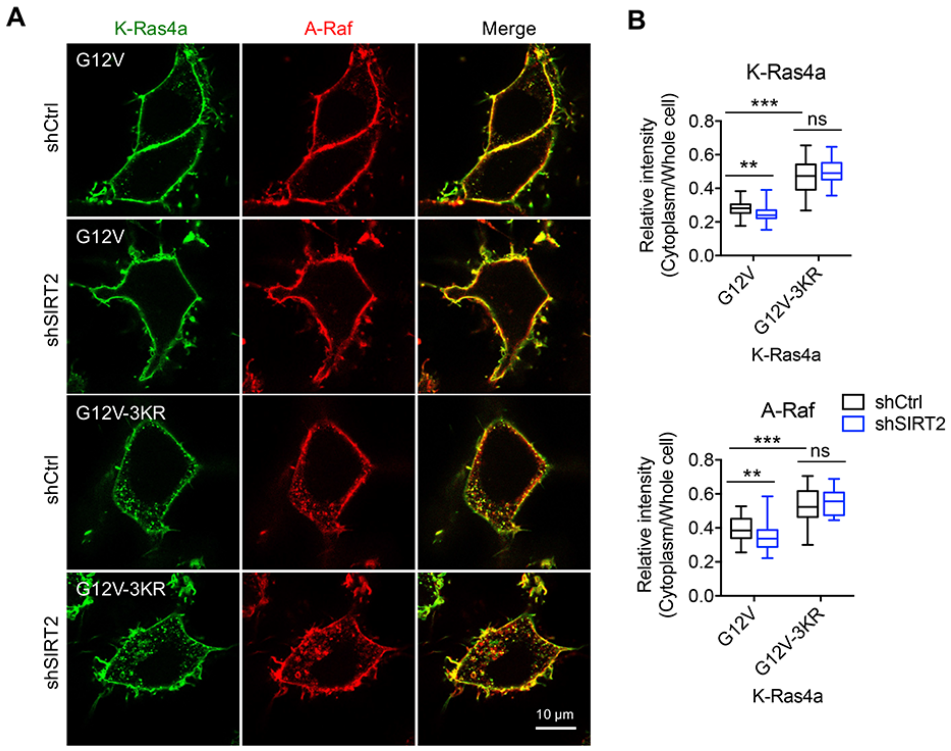

Figure 3.19 Lysine fatty acylation regulates endomembrane recruitment of A-Raf by K-Ras4a. (**A**) Images showing the localization of GFP-K-Ras4a-G12V or -G12V-3KR and DsRed-A-Raf in live HEK293T cells with Ctrl or SIRT2 KD (by shSIRT2-#2). (**B**) Statistical analyses of the relative cytoplasm to whole cell intensity of K-Ras4a and A-Raf from (A) (n = 17 for all samples). Statistical evaluation was by two-way ANOVA. *Centre line* of the box plot represents the mean value, box represents the 95 % confidence interval, and whiskers represent the range of the values. $^{**}P < 0.01$; $^{***}P < 0.001$; ns, not significant. Representative images are shown.

While the functions of B-Raf and C-Raf in Ras-mediated oncogenic transformation have been well elucidated, the role of A-Raf in this process remains obscure[70]. So we next examined whether A-Raf plays a role in K-Ras4a-G12V mediated transformation using the soft agar colony formation assay. Inhibition of A-Raf expression with shRNA (Fig. 3.20A) partially suppressed K-Ras4a-G12V-induced colony formation, indicating that A-Raf is important for K-

Ras4a-G12V mediated transformation. Moreover, A-Raf KD abrogated the 3KR mutation-mediated increase and Sirt2 KD-mediated decrease in the transformation activity of K-Ras4a-G12V (Fig.3.20B & C), suggesting that A-Raf is important for the regulation of K-Ras4a transforming activity by SIRT2-dependent lysine defatty-acylation. These results further support the model that lysine defatty-acylation by SIRT2 enhances the recruitment of A-Raf to K-Ras4a at endomembranes, thereby promoting oncogenic activity of K-Ras4a.

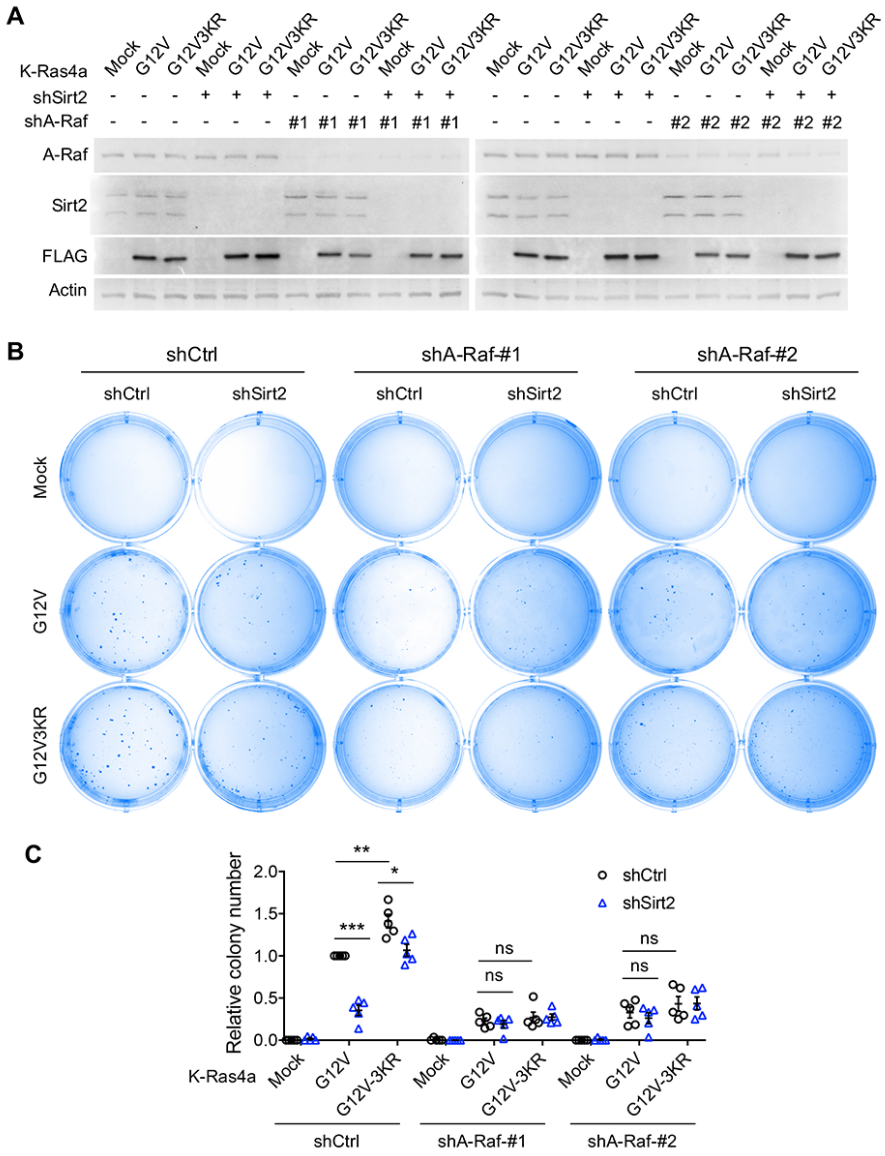

Figure 3.20 A-Raf mediates the regulation of K-Ras4a-G12V transforming activity by lysine fatty acylation. (**A**) Western blot analysis of A-Raf, Sirt2 and FLAG in NIH3T3 cells expressing Mock, FLAG-K-Ras4a-G12V or -G12V-3KR with Ctrl or SIRT2 KD, and Ctrl or A-Raf KD. (**B**) Images showing anchorage-independent growth of NIH3T3 cells stably expressing the K-Ras4a-G12V or -G12V-3KR with Ctrl or Sirt2 KD, and Ctrl or A-Raf KDs. (**C**) Quantification of the relative colony numbers in (B) The y axis represents colony numbers relative to that of the Sirt2 or A-Raf control KD cells expressing K-Ras4a-G12V. Statistical evaluation was by unpaired two-tailed Student's t test. Error bars represent SEM in five biological replicates. *$P < 0.05$; **$P < 0.01$; ***$P < 0.001$; ns, not significant. Representative images are shown.

3. Discussion

Protein lysine fatty acylation was discovered over two decades ago [4-8]. However, very little is known about its functional significance. Our current study furnishes a model where K-Ras4a is fatty acylated on lysine residues at its C-terminal HVR, and the removal of lysine fatty acylation by SIRT2 facilitates its endomembrane localization and interaction with A-Raf, thus enhancing its transforming activity (Fig. 3.21). These findings demonstrate that a Ras protein is modified and regulated by a previously under-appreciated PTM, lysine fatty acylation, which expands not only the regulatory scheme for Ras proteins, but also the biological significance of lysine fatty acylation. Moreover, our study reveals the first lysine defatty-acylation substrate for SIRT2 and uncovers the physiological relevance of SIRT2 as a lysine defatty-acylase[12,14,15].

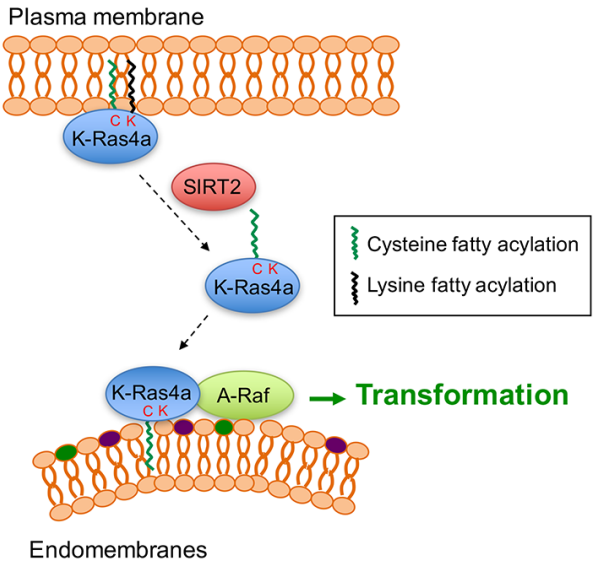

Figure 3.21 Model for the regulation of K-Ras4a by SIRT2-mediated removal of lysine fatty acylation. Removal of lysine fatty acylation by SIRT2 facilitates K-Ras4a to localize to endomembranes and interact with A-Raf, and thus enhances its activity to transform cells.

We found that H-Ras and K-Ras4a possess lysine fatty acylation that could be hydrolyzed by sirtuins *in vitro* or in cells. Although our attempt to detect N-Ras lysine fatty acylation by MS was not successful, the N-Ras-K169/170R (2KR) mutant presented decreased NH_2OH-resisitant fatty acylation compared with WT, suggesting that N-Ras might be lysine fatty acylated (Fig. 3.2C & D). While cysteine palmitoylation of Ras proteins was discovered almost three decades ago[71], lysine fatty acylation of Ras was not identified for several reasons. First, lysine fatty acylation did not emerge as a physiologically significant modification until recent years. Correspondingly, the possibility of lysine fatty acylation on Ras proteins had not been investigated previously. Second, previously people only focused on Ras cysteine palmitoylation because mutations of the palmitoylated cysteine to serine abolished the palmitoylation of H-Ras[72], N-Ras[72] and K-Ras4a[19] based on ^{3}H-palmitic acid labeling. Therefore, lysine fatty acylation of Ras proteins might have been missed based on the mutagenesis results. Similar to, but slightly different from these previous reports, we found that mutating the plamitoylated cysteine of K-Ras4a decreased lysine fatty acylation by nearly 90% (Fig. 2.10A) but not completely. A similar effect of the palmitoylated cysteine to serine mutation was also observed for R-Ras2[25]. Last, although the palmitoylation sites for Ras proteins were characterized with the chemoproteomic approaches based on acyl-biotin exchange (ABE)[23,73] or acyl-resin-assisted capture (acyl-RAC)[3,74], these approaches are cysteine-centric and do not allow identification of amide-linked fatty acylation. Direct site identification of palmitoylation has been challenging owing to the low abundance and high hydrophobicity of the modified peptides, which are easily lost during sample preparation[1]. Our current study highlights the regulation of Ras proteins by lysine fatty acylation and suggests that additional studies are required to understand the regulation of this important class of proteins. Many Ras superfamily small GTPases contain

lysine-rich sequences at their C-termini. It is therefore of great interest to us to investigate whether lysine fatty acylation could act as a general regulatory mechanism for many Ras-related small GTPases.

The discovery of lysine fatty acylation on K-Ras4a raises the question of the relative abundance of lysine versus cysteine fatty acylation. Semi-quantification of the fluorescence intensity from Alk14 labeling results enables us to roughly estimate the stoichiometry of lysine fatty acylation. Based on this, K-Ras4a exhibits nearly 50% of lysine fatty acylation relative to total fatty acylation (Fig. 3.2C). Therefore, the ratio of cysteine palmitoylation to lysine fatty acylation may be close to 1:1 on K-Ras4a. The 3KR mutation decreased K-Ras4a lysine fatty acylation by about 50% (Fig. 3.2F & 3.9A), suggesting that the C-terminal lysine fatty acylation regulated by SIRT2 is around 50% of the lysine fatty acylation and 25% of the total fatty acylation. Regarding endogenous K-Ras4a, by quantifying the K-Ras4a western blot signal from the streptavidin beads and supernatant in Fig. 3.6F, we estimated that about 28% and 50% of the fatty acylated K-Ras4a is lysine fatty acylated in Ctrl KD and SIRT2 KD HCT116 cells, respectively. Unfortunately, precise quantitation of protein fatty acylation still remains a significant unsolved challenge and we could not determine the ratio of fatty acylated versus unmodified K-Ras4a.

To study the physiological function of K-Ras4a lysine fatty acylation, we utilized the K-Ras4a-3KR mutant in combination with SIRT2 KD. The lysine-to-arginine mutant maintains the positive charge of the polybasic patch, which makes it a good lysine fatty acylation-deficient mimic. Recently, Zhou *et al.* reported that lysine and arginine residues are not equivalent in determining the membrane lipid binding specificity of K-Ras4b C-terminus, which raises the possibility that the effect of 3KR mutation might not be solely due to lack of lysine fatty acylation[75]. Likewise, changes in the SIRT2 KD cells could be mediated through other substrates for SIRT2. Therefore, it is critical to employ both the 3KR mutant and SIRT2 KD to

rule out these possibilities. SIRT2 KD enhances the lysine fatty acylation of K-Ras4a WT but not 3KR mutant. Thus, if a biological effect is due to lysine fatty acylation, SIRT2 should have a great impact on the effect of K-Ras4a WT than that of the 3KR mutant. Of note, H-Ras, which shares similar properties with K-Ras4a, but is not a lysine defatty-acylase target for SIRT2, also serves as a good control for the effect of SIRT2 KD. Indeed, SIRT2 KD repressed the endomembrane localization, transforming activity, and A-Raf binding of K-Ras4a WT more than that of K-Ras4a 3KR or H-Ras, indicating that SIRT2-dependent lysine defatty-acylation facilitates endomembrane localization of K-Ras4a, enhances its interaction with A-Raf, and thus promotes cellular transformation.

Goodwin *et al.* previously reported that cysteine depalmitoylated H-Ras and N-Ras traffic to and from the Golgi complex by a nonvesicular mechanism, and suggested a model where cysteine palmitoylation traps Ras on membranes, enabling Ras to undergo vesicular transport [76]. In line with this, Tsai *et al.* [19] and we observed that the K-Ras4a-C180S mutant, which possesses no cysteine palmitoylation and little lysine fatty acylation localizes to ER/Golgi-like internal membranes (Fig. 3.11H). Differently, we found that removal of the lysine fatty acylation by SIRT2, which results in K-Ras4a with only cysteine palmitoylation, promotes endomembrane localization of K-Ras4a (Fig. 3.11B). This evidence supports the model that cysteine palmitoylation enables K-Ras4a to undergo vesicular transport, whereas lysine fatty acylation blocks K-Ras4a translocation from the PM to endomembranes (Fig. 3.21). Furthermore, the C180S mutant suppressed K-Ras4a-G12V-mediated anchorage-independent growth and activation of MAPK signaling[19,20]. In contrast, the 3KR mutant increased K-Ras4a-G12V-mediated anchorage-independent growth (Fig. 3.13), exhibited no effect on MAPK signaling (Fig. 3.16), but activated A-Raf instead (Fig. 3.18). Considering the possibility that lysine fatty acylation largely relies on cysteine palmitoylation to occur, it is likely that the

reversible lysine fatty acylation adds a layer of regulation for K-Ras4a above that of cysteine palmitoylation.

In the GTP-bound active form, Ras proteins bind directly to the Ras binding domain (RBD) of Raf, then form secondary interactions with a cysteine-rich domain (CRD). Although the RBD and CRD are highly conserved in all Raf isozymes, there is evidence for different binding affinities for Ras proteins to the individual Raf proteins[77,78]. For example, Weber *et al.* reported that A-Raf presents significantly lower binding affinities to H-Ras-G12V as compared to C-Raf because the Ras-binding interface of C-Raf differs from A-Raf by a conservative arginine to lysine exchange at residue 59 or 22 respectively[79]. Furthermore, Williams *et al.*[80] and Fischer *et al.*[81] found that farnesylation of H-Ras is required for its binding to C-Raf but not B-Raf, implying the involvement of Ras C-terminal PTM in the regulating Ras-Raf interactions. Based on these previous studies, it is likely that the C-terminal PTM of K-Ras4a regulates its interaction with Raf isozymes and that lysine fatty acylation may inhibit the binding of K-Ras4a to A-Raf but not to B-Raf and C-Raf.

Mutations that activate Ras are found in about 30% of all human tumors screened. *KRAS* mutations, which affects both K-Ras4a and K-Ras4b, occur most frequently, accounting for 86% of *RAS*-driven cancers[82]. Though K-Ras4a is homologous to the transforming cDNA identified in Kirsten rat sarcoma virus[83], its function and regulation is less characterized compared to K-Ras4b. Recent studies showed that K-Ras4a is widely expressed in human cancers, suggesting that K-Ras4a plays a significant role in *KRAS*-driven tumors[19,20]. Our findings reveal that K-Ras4a is regulated by SIRT2-dependent lysine defatty-acylation. Depletion of SIRT2 increased lysine fatty acylation and diminished oncogenic transforming activity of K-Ras4a, suggesting that interference with K-Ras4a lysine fatty acylation could be an approach to anti-K-Ras therapy.

The seven mammalian sirtuins, SIRT1-7, are implicated in various biological pathways and are considered potential targets against a number of human diseases[55]. So far, the known biological functions of sirtuins have been mainly attributed to their deacetylase activities. Although sirtuins are increasingly recognized as lysine deacylases in addition to deacetylases, the biological significance of sirtuins as lysine deacylases remains largely unknown[84]. Our work here identifies the first physiological defatty-acylation substrate for SIRT2. Since protein acyl lysine modifications likely use acyl-CoA molecules as the acyl donors, the cellular metabolic state can affect acyl lysine PTMs by altering the concentration of acyl-CoA molecules. Sirtuins requires NAD as a co-substrate and the NAD level is regulated by cellular metabolism. Thus SIRT2 may provide an additional link between K-Ras4a signaling and cellular metabolism. Given that Ras proteins play critical roles in many human cancers, SIRT2, as a Ras regulator, may be an important therapeutic target for cancer, which is consistent with several recent reports[50,53,54,57,58,85-87]. The physiological and pathophysiological roles of SIRT2 thus merit further investigation.

4. Methods

Reagents, antibodies and plasmids. Chemicals from commercial sources were obtained in the highest purity available. Alk14, Rhodamin-N_3 and Biotin-N_3 were synthesized as previously reported[88]. Trichostatin A (TSA, T8552), protease inhibitor cocktail (P8340), phosphatase inhibitor cocktail (P0044), Azide-PEG3-biotin (762024), Tris[(1-benzyl-1H-1,2,3-triazol-4-yl)methyl]amine (TBTA, 678937), Tris(2-carboxyethyl)phosphine (TCEP, 75259), hydroxylamine (NH_2OH, 159417), NAD (NAD100-RO), Puromycin (P8833), Crystal Violet (C0775), low-melting point agarose (A0701), triple FLAG peptide (F4799), L-lysine (L9037), L-arginine (A8094), [$^{13}C_6$, $^{15}N_2$]-L-lysine (608041) and [$^{13}C_6$, $^{15}N_4$]-L-arginine (608033) were purchased from Sigma-Aldrich. The anti-human SIRT1 (05-1243), anti-RalA (ABS223) and

anti-Ras (Y13-259, OP01A) antibodies were from EMD Chemicals Inc. The anti-SIRT2 (ab134171), Transferrin Receptor (ab84036) antibodies were from Abcam. The anti-SIRT2 (12650), Phospho-Erk1/2 (Thr202/204) (9101), Erk1/2 (4696), Phospho-Akt (Thr308) (9275), Phospho-Akt (Ser473) (9271), Akt (4691), Phospho-SAPK/JNK (Thr182/Tyr185) (4668), SAPK/JNK (9252), Syntaxin 6 (STX6, 2869), EEA1 (3288) antibodies were purchased from Cell Signaling Technology. The anti-β-Actin (sc-4777), K-Ras4a (sc-522), A-Raf (sc-408), B-Raf (sc-166), C-Raf (sc-227), Na/K-ATPase (sc-21712), GAPDH (sc-47724), the normal rat IgG (sc-2026) and the goat anti-mouse/rabbit/Rat IgG-horseradish peroxidase-conjugated antibodies were purchased from Santa Cruz Biotechnology. The anti-Acetyl Lysine antibody (ICP0380) was obtained from Immunechem. The anti-FLAG M2 antibody conjugated with horseradish peroxidase (A8592) and the anti-FLAG M2 affinity gel (A2220) were from Sigma-Aldrich. Enzyme-linked chemiluminescence (ECL) plus (32132) western blotting detection reagent, Cy3-conjugated goat anti-rabbit IgG (H+L) secondary antibody (A10520) and the high capacity Streptavidin agarose (20357) were purchased from Thermo Fisher Scientific. FuGene 6 (E2692) transfection reagent and sequencing grade modified trypsin (V5111) were purchased from Promega. ^{32}P-NAD^{+} was purchased from PerkinElmer. Saponin (S0019-25G) was from TCI America. Sep-Pak C18 cartridge was purchased from Waters.

The pLKO.1-puro lentiviral shRNAs constructs for luciferase and human SIRT1, SIRT2, and mouse SIRT2 were purchased from Sigma-Aldrich. Luciferase shRNA (SHC007), human SIRT1 shRNAs (#1, TRCN0000018980, #2, TRCN0000018981), human SIRT2 shRNAs (#1, TRCN0000040219, #2, TRCN0000310335), mouse SIRT2 shRNA (TRCN0000012118), mouse A-Raf shRNAs (#1, TRCN0000022612, #2, TRCN0000022610) were used. The human *K-RAS4A* expression vector with N-terminal FLAG tag was obtained by RT-PCR amplification of *K-RAS4A* and subcloning *via* EcoRI and SalI sites into pCMV5 vector. The human *K-RAS4A* lentiviral vector was obtained by inserting FLAG-*K-RAS4A* into pCDH-CMV-MCS-EF1-Puro

vector between the EcoRI and NotI sites. The human *H-RAS* lentiviral vector was obtained by inserting FLAG-*HRAS* into pCDH-CMV-MCS-EF1-Puro vector between the EcoRI and BamHI sites. The GFP-K-Ras4a and GFP-H-Ras expression vectors were constructed by inserting *K-RAS4A and H-RAS* cDNA into pGFP1-C1 vector between the BglII and SalI sites, respectively. The human *STX6* expression vector with N-terminal FLAG tag was constructed by inserting FLAG-STX6 cDNA into pCMV-tag-4a vector between the EcoRI and XhoI sites. To generate the expression vector for human SIRT2 with C-terminal FLAG tag, full-length human *SIRT2* cDNA was amplified by PCR and inserted into pCMV-tag-4a vector between the BamHI and XhoI sites. The expression vectors for H-Ras, N-Ras, K-RAS4A mutants and SIRT2-H187Y were generated by QuikChange site-directed mutagenesis[89]. The DsRed cDNA without stop codon was inserted using NotI and BamHI sites into pCMV-tag-4a to generate pCMV-tag-4a-DsRed-C vector that enables cloning of gene of interest with N-terminal DsRed. The DsRed-RBD expression vector was constructed by inserting cDNA coding the Ras-binding domain of human Raf1 (aa51-131) into pCMV-tag-4a-DsRed-C vector between EcoRV and XhoI sites. The DsRed-A-Raf expression vector was generated by inserting mouse *Araf* cDNA into pCMV-tag-4a-DsRed-C vector using BamHI and EcoRI sites. DsRed-GalT plasmid[90] was obtained from Dr. Yuxin Mao (Cornell Univeristy, Ithaca, NY). Expression vectors for mCherry-Sec61 beta (Addgene plasmid #49155)[91], mCherry-Rab11 (Addgene plasmid #55124), DsRed-Rab7 (Addgene plasmid #12661)[92] and Lamp1-RFP (Addgene plasmid #1817)[93] were gifts from Gia Voeltz, Michael Davidson, Richard Pagano and Walther Mothes, respectively.

Cell culture, transfection and transduction. Human HEK293T cells were grown in DMEM media (11965-092, Gibco) with 10% heat inactivated (HI) fetal bovine serum (FBS, 26140079, Gibco). Mouse embryonic fibroblast NIH3T3 cells were grown in DMEM media supplemented with non-essential amino acids (11140050, Gibco) and 15% HI FBS. Human HCT116 cells were grown in McCoy's 5A media (16600082, Gibco) with 10% HI FBS. The

cell lines were purchased from American Type Culture Collection (ATCC). The cell lines were not further authenticated after purchase from ATCC. All cell lines were tested for and showed no mycoplasma contamination.

For SILAC experiment, 'light' NIH3T3 cells were maintained in DMEM media for SILAC (88420, Thermo Fisher Scientific) supplemented with 100 mg/L [$^{12}C_6$, $^{14}N_2$]-L-lysine, 100 mg/L [$^{12}C_6$, $^{14}N_4$]-L-arginine and 15% dialyzed FBS (26400036, Thermo Fisher Scientific); 'heavy' NIH3T3 cells were cultured in DMEM media for SILAC supplemented with 100 mg/L [$^{13}C_6$, $^{15}N_2$]-L-lysine, 100 mg/L [$^{13}C_6$, $^{15}N_4$]-L-arginine and 15% dialyzed FBS. Cells were cultured in SILAC media for at least six doubling times to achieve maximum incorporation of 'labeled' amino acids into proteins before the interactome study was performed.

To transiently overexpress proteins of interest in cells, the expression vectors were transfected into cells using FuGene 6 according to the manufacturer's protocol. Empty vector was transfected as a negative control. Lentiviral infection for overexpressing H-Ras, K-Ras4a WT and mutants or knocking down SIRT1, SIRT2 and A-Raf was performed as previously described [9,53]. Puromycin (3 μg/mL for NIH3T3 cells, 1.5 μg/mL for HEK293T cells) was added to the cell culture media to select NIH3T3 cells with stable overexpression of Mock (pCDH empty vector control), K-Ras4a-G12V, K-Ras4a-G12V-3KR or H-Ras-G12V as well as HEK293T cells with stable luciferase KD (Ctrl KD), SIRT1 KD, or SIRT2 KD.

Immunoprecipitation of Alk14-labeled proteins of interest. HEK293T cells (parental cells, luciferase KD, SIRT1 KD, or SIRT2 KD) were transiently transfected to express FLAG-tagged protein of interest overnight. The cells were then cultured with fresh medium containing 50 μM Alk14 for 6 h. Cells were collected and lysed in 1% NP-40 lysis buffer (25 mM Tris-HCl pH 8.0, 150 mM NaCl, 10% glycerol, 1% Nonidet P-40) with protease inhibitor cocktail. The supernatant was collected after centrifugation at 16,000g for 20 min at 4 °C. Protein

concentration was determined by Bradford assay (23200, Thermo Fisher Scientific). 0.5-1 mg cell lysate was incubated with 10 μL suspension of anti-FLAG M2 affinity gel for 2 h at 4 °C. The affinity gel was then centrifuged at 500 *g* for 2 min at 4 °C, washed three times with 1 mL IP washing buffer (25 mM Tris-HCl pH 8.0, 150 mM NaCl, 0.2% Nonidet P-40) and used for further experiments.

Detection of fatty acylation on protein of interest by on-beads click chemistry and in-gel fluorescence. The immunopurified protein with Alk14 labeling was suspended in 20 μL IP washing buffer for click chemistry. Rh-N_3 (3 μL of 1 mM solution in DMF, final concentration 150 μM) was added to the above suspension, followed by the addition of TBTA (1 μL 10 mM solution in DMF, final concentration 500 μM), $CuSO_4$ (1 μL of 40 mM solution in H_2O, final concentration 2 mM), and TCEP (1 μL of 40 mM solution in H_2O, final concentration 2 mM). The click chemistry reaction was allowed to proceed at room temperature for 30 min. The reaction mixture was mixed with 10 μL of 6 × protein loading buffer and heated at 95 °C for 10 min. After centrifugation at 16,000 g for 2 min at room temperature, 15 μL of the supernatant was treated with NH_2OH (pH 8.0, 1 μL of 5 M solution in H_2O, final concentration 300 mM) or equivalent volume of water (negative control) at 95 °C for 7 min. The samples were resolved by SDS-PAGE. Rhodamine fluorescence signal was recorded by Typhoon 9400 Variable Mode Imager (GE Healthcare Life Sciences, Piscataway, NJ) with setting of Green (532 nm)/580BP30 PMT 500 V (normal sensitivity). Fiji software[94] was used for quantification of the fluorescence intensity. Signal intensity of in-gel fluorescence was normalized with respect to that of the corresponding FLAG western blot.

Defatty-acylation of K-Ras4a by sirtuins *in vitro*. The *Plasmodium falciparum* Sir2A (PfSir2A)[26], the human SIRT1[95], SIRT2[53], SIRT3[95] and SIRT6[9] were expressed as previously described. The immunoprecipated Ras with Alk14 labeling on anti-FLAG affinity gel was suspended in 25 μl of assay buffer (50 mM Tris-HCl, pH 8.0, 100 mM NaCl, 2 mM $MgCl_2$, 1

mM DTT) with 10 μM of PfSir2A or 5 μM of SIRT1, SIRT2, SIRT3, SIRT6 or the corresponding amount of BSA and with or without 1 mM NAD and incubated at 37 °C for 30 min (SIRT2) or 1 h (PfSir2A, SIRT1, 3 and 6). The reaction was stopped by washing the affinity gel using 1 mL of IP washing buffer for 3 times. On-bead click chemistry and in-gel fluorescence were carried out as described above.

High-performance liquid chromatography (HPLC)-based SIRT2 activity assay. SIRT2 or SIRT2-H187Y (1 μM) was incubated in 60 μL of reaction buffer (20 mM Tris, pH 8.0, 1 mM DTT, 1 mM NAD) with 32 μM acetyl H3K9, myristoyl H3K9, or myristoyl K-Ras4a-C180 peptides, respectively, at 37°C for 10 min (deacetylation) or 20 min (demyristoylation). Reactions was quenched with 60 μL ice-cold acetonitrile and spun down at 18,000 g for 10 min to remove the precipitated protein. The supernatant was then analyzed by HPLC on a Kinetex XB-C18 column (100 A, 75 mm × 4.6 mm, 2.6 μm, Phenomenex). The peak areas were integrated and the conversion rate was calculated from the ratio of the free H3K9 peptide peak area over the total peak areas of the substrate and product peptides.

Western blot. Western blot analysis was performed as described previously[9]. The proteins of interest were detected using ECL plus and visualized using the Typhoon 9400 Variable Mode Imager (GE Healthcare). Quantification of signal intensity from western blots was done using Fiji software. To assess the effect of lysine fatty acylation on the signaling output of K-Ras4a-G12V through Erk, Akt and Jnk, NIH3T3 cells stably expressing Mock, FLAG-K-Ras4a-G12V or -G12V-3KR were infected with lentivirus carrying luciferase (Ctrl) or mouse Sirt2 shRNA for 3 days, collected and lysed in 1% NP-40 lysis buffer with protease inhibitor cocktail and phosphatase inhibitor cocktail. Cell lysates were then subjected to western blot for the analyses of indicated proteins.

To detect acetyl lysine on K-Ras4a, HEK293T cells with stable Ctrl KD or SIRT2 KD were transfected with empty vector or pCMV5-*K-RAS4A* overnight. The cells were then treated with ethanol or trichostatin A (TSA, 1 μM) for 1 hr. The cells were collected and lysed in 1% NP-40 lysis buffer with protease inhibitor cocktail. Cell lysates (~3 mg), with/without overexpression of K-Ras4a, were incubated with 10 μL of anti-FLAG M2 affinity gel suspension for 2 h at 4 °C. The affinity gel was washed three times with 1 mL of IP washing buffer and then heated in 15 μL of 2 × protein loading buffer at 95 °C for 10 min. The supernatant was then resolved by SDS-PAGE and the acetylation of K-Ras4a was examined by western blot using anti-acetyllysine antibody after transfer to a PVDF membrane. Total cell lysates from TSA-treated HEK293T cells were used as a positive control for the acetyllysine blot. After recording the acetyl-lysine signal, the PVDF membrane was stained with Coomassie blue to detect K-Ras4a protein. A western blot using anti-FLAG antibody was carried out in parallel to demonstrate equal loading of K-Ras4a.

Subcellular fractionation. HEK293T cells were transfected with pCMV5-*K-RAS4a* and cultured for overnight before being collected. Cell pellets were re-suspended in subcellular fraction buffer (250 mM Sucrose, 20 mM HEPES, pH 7.4, 10 mM KCl, 1.5 mM $MgCl_2$, 1 mM EDTA, 1 mM EGTA and 1 mM DTT) containing protease inhibitor cocktail and homogenized on ice by 10 passes through a 25-gauge syringe needle. Nuclei and intact cells were removed by centrifugation at 3,000 rpm for 5 min. Mitochondrial fraction was removed by centrifuging the postnuclear supernatant at 8,000 rpm for 5 min. The supernatant was ultracentrifuged at 40,000 rpm for 1 hr. The resulting supernatant (cytosol fraction) was concentrated through the filter. The pellet (membrane fraction) was washed with subcellular fraction buffer, re-centrifuged for 45 min and dissolved in 4% SDS lysis buffer (4% SDS, 50 mM triethanolamine pH 7.4, and 150 mM NaCl). Equivalent portions of the cytosol and membrane fractions were then subjected to western blot analyses.

Co-Immunoprecipitation. To examine the interaction between FLAG-tagged K-Ras4a and SIRT2, HEK293T cells transfected with empty vector or pCMV5-FLAG-*K-RAS4A* were cultured overnight, collected and lysed in 1% NP-40 lysis buffer with protease inhibitor cocktail. To examine the interaction between FLAG-tagged K-Ras4a-G12V/K-Ras4a-G12V-3KR or H-Ras-G12V and A-Raf/B-Raf/C-Raf (Raf1)/p110α/RalGDS, NIH3T3 cells stably expressing Mock, FLAG-K-Ras4a-G12V, -G12V-3KR, or FLAG-H-Ras-G12V were infected with lentivirus carrying luciferase (Ctrl) or mouse Sirt2 shRNA for 3 days, collected and lysed in 1% NP-40 lysis buffer with protease inhibitor cocktail. For both experiments, total cell lysates (2 mg of total protein for detecting SIRT1/2, 50 μg for A-Raf and c-Raf, 1 mg for B-Raf, p110α and RalGDS, determined by Bradford assay) were incubated with 10 μL suspension of anti-FLAG M2 affinity gel for 2 hr at 4 °C. The resulting affinity gel was washed three times with 1 mL IP washing buffer and heated in protein loading buffer (2 × final concentration) at 95 °C for 10 min. Western blot was then performed to detect levels of the indicated proteins.

Detection of lysine fatty acylation on K-Ras4a using the ^{32}P-NAD assay. The ^{32}P-NAD assays were carried out as described previously with minor modification[30]. HEK293T cells were transfected with empty pCMV5 vector or pCMV5-*K-RAS4A* overnight and lysed in 1% NP-40 lysis buffer with protease inhibitor cocktail. For each reaction, cell lysates (3 mg of total protein, determined by Bradford assay) were incubated with 10 μL suspension of anti-FLAG M2 affinity gel for 2 hr at 4 °C. The affinity gel was washed three times with 1 mL of IP washing buffer. The resulting anti-FLAG affinity gel or the synthetic acetyl and myristoyl H3K9 peptides[30] (25 μM, positive control) were mixed with 10 μL solutions containing 1 μCi ^{32}P-NAD, 50 mM Tris-HCl pH 8.0, 150 mM NaCl, 1 mM DTT. The reactions were incubated with 1 μM BSA (negative control), SIRT2, or SIRT2-H187Y at 37°C for 30 min. A total of 2 μL of each reaction were spotted onto silica gel TLC plates and developed with 7:3 ethanol:ammonium bicarbonate (1 M aqueous solution). After development, the plates were air-dried and exposed to a

PhosphorImaging screen (GE Healthcare). The signal was detected using Typhoon 9400 Variable Mode Imager (GE Healthcare).

Biotin pull-down of lysine fatty acylated endogenous K-Ras4a. The assay was carried out as previously described with some modifications [31]. Briefly, HCT116 cells were infected with lentivirus carrying luciferase (Ctrl) or SIRT2 shRNA for 3 days and treated without or with Alk14 (50 μM) for 6 hrbefore being collected. Total proteins were then extracted using 1% NP-40 lysis buffer with protease inhibitor cocktail. 10 mg of total protein extract was subjected to click reaction with 100 μM Biotin-N_3, 500 μM TBTA, 1 mM $CuSO_4$ and 1 mM TCEP in a final volume of 5 mL. The reaction was allowed to proceed at room temperature for 1 hr. Proteins were precipitated by adding 4 volumes of ice-cold methanol, 3 volumes of water, and 1.5 volumes of chloroform. Precipitated proteins were pelleted by centrifugation (4,500× g, 20 min, 4 °C), washed twice with 50 mL of ice-cold methanol and air-dried. The protein pellet was suspended in 4% SDS buffer (4% SDS, 50 mM triethanolamine pH 7.4, and 150 mM NaCl, 10 mM EDTA). The solubilized protein mixture was diluted to 1% SDS with 1% Brij 97 (in 50 mM triethanolamine pH 7.4, and 150 mM NaCl) and incubated with streptavidin agarose (0.2 ml slurry for 1 mg of protein) for 1 hrat room temperature. The streptavidin beads were washed three times with 10 mL of 1% SDS in PBS buffer. The streptavidin beads were incubated with 1 M NH_2OH (pH 8.0) in 300 μL of 1% SDS PBS buffer for 1 hrat room temperature to elute proteins with only cysteine fatty acylation. The resulting supernatant was concentrated to 20 μL final volume using the Amicon Ultra-0.5 Centrifugal Filter (UFC501008, EMD Millipore). The resulting streptavidin beads were washed three times with 1% SDS PBS buffer. Both the concentrated supernatant and washed beads were heated in protein loading buffer (2 × final concentration) at 95 °C for 10 min and subjected to western blot analyses.

Confocal microscopy. Cells were seeded in 35-mm glass bottom dishes (MatTek) and transfected with relevant constructs overnight.

For live cell imaging, cells were incubated in the Live Cell Imaging Solution (A14291DJ, Thermo Fisher Scientific) and imaged with a Zeiss 880 confocal/multiphoton inverted microscope (Carl Zeiss MicroImaging, Inc., Thornwood, NY) in a humidified metabolic chamber maintained at 37 °C and 5% CO_2. For time-lapse movies, 60 single section images were recorded at 1 sec intervals for 1 min.

For immunofluorescence, cells were rinsed with 1 × PBS twice and fixed with 4% paraformaldehyde (v/v in 1 × PBS) for 15 min. The fixed cells were washed twice with 1 × PBS, permeabilized and blocked with 0.1% Saponin/5% BSA/1 × PBS for 30 min. The cells were then incubated overnight at 4 °C in dark with indicated primary antibody at 1/50 - 1/100 dilution (in 0.1% Saponin/5% BSA/1 × PBS). Cells were washed with 0.1% Saponin/1 × PBS three times and incubated with Cy3-conjugated goat anti-rabbit IgG (H+L) secondary antibody at 1/1000 dilution (in 0.1% Saponin/5% BSA/1 × PBS) at room temperature in dark for 1 hr. Samples were washed with 0.1% Saponin/1 × PBS three times and mounted with Fluoromount-G® (0100-01) from SouthernBiotech before imaging with Zeiss LSM880 inverted confocal microscopy. Images were processed with Fiji software.

For colocalization analyses of GFP-K-Ras4a WT or -3KR with various intracellular membrane markers, live cell imaging was performed for colocalization with mCherry-Sec61, DsRed-GalT, mCherry-Rab11, DsRed-Rab7 and Lamp1-RFP; immunofluorescence was performed for colocalization with STX6 (1/50 dilution for anti-STX6 antibody) and EEA1 (1/100 dilution for anti-EEA1 antibody).

Quantitative analyses of colocalization and fluorescence intensity. Fiji software was used for quantification. To quantify the degree of cytoplasmic colocalization, background was subtracted, then the cytoplasm area was selected and quantified for each cell examined. Pearson's correlation coefficient[96] was calculated using Fiji plug-in Coloc2 program

(http://fiji.sc/Coloc_2) on a single plane between the two indicated fluorescent signals. To quantify fluorescence intensity, background was subtracted and the cytoplasm area or the whole cell was selected for integrated signal intensity quantification. Relative cytoplasm with respect to whole cell fluorescence intensity was presented.

Soft agar colony formation assay. To assess the effect of Ctrl or Sirt2 KD on K-Ras4a-G12V, -G12V-3KR or H-Ras-G12V-mediated anchorage-independent growth, NIH3T3 cells with stable overexpression of Mock, K-Ras4a-G12V or -G12V-3KR were infected with Ctrl shRNA- or Sirt2 shRNA-carrying lentivirus for 6 hrand cultured in complete medium for another 72 hrbefore being seeded for soft agar colony formation assay.

To determine the effect of Ctrl or A-Raf KD, NIH3T3 cells with stable overexpression of Mock (pCDH empty vector control), K-Ras4a-G12V or -G12V-3KR were first infected with Ctrl shRNA- or Sirt2 shRNA-carrying lentivirus for 6 hr and then with Ctrl shRNA- or A-Raf shRNAs for another 6 hr. The infected cells were then cultured in complete medium for another 72 hr before being seeded for soft agar colony formation assay.

0.6% base low-melting point agarose (LMP) and 0.3% top LMP were prepared by mixing 1.2% LMP in H_2O and 0.6% LMP in H_2O, respectively, with 2 × complete medium in 1:1 (v/v) ratio. 1.5 mL of 0.6% base LMP was added to each well of 6-well plate and allowed to solidify for 30 min at room temperature. Then 5.0×10^3 cells were resuspended in 0.3% LMP top LMP and plated onto 6-well plate pre-coated with the base LMP. 150 μL of complete medium was added on top of the 0.3% LMP and refreshed every 3 days. After 14 days of culture, colonies were stained with 0.1% crystal violet (m/v in 25% methanol) for 30 min, rinsed with 50% methanol, and counted.

Cell proliferation assay. NIH3T3 cells with stable overexpression of Mock, K-Ras4a-G12V, or -G12V-3KR were seeded in 12-well plate at a density of 1.5×10^4 cells/well 24 hr

before being infected with luciferase (Ctrl) shRNA- or Sirt2 shRNA-carrying lentivirus for 0 or 5 days. After knocking down Sirt2 for the indicated time, cells were washed with 1 × PBS, fixed with ice-cold methanol for 10 min and then stained with 0.25% crystal violet (m/v, in 25% methanol) for 10 min. The stained cells were washed with running distilled water, air-dried and solubilized in 200-800 μL of 0.5% SDS in 50% ethanol. Absorbance of the resulting solution was measured at 550 nm.

Transwell migration assay. NIH3T3 cells with stable overexpression of Mock, K-Ras4a-G12V or -G12V-3KR were infected with Ctrl shRNA- or Sirt2 shRNA-carrying lentivirus for 6 hr and cultured in complete medium for another 72 hr. Cells were cultured in serum-free medium for 12 hr before the assay. The assay was performed in 24-well Transwell plate with 8 mm polycarbonate sterile membrane (Corning Incorporated). Cells were plated in the upper chamber (20,000 cells/insert) in 200 μL of serum-free medium. Inserts were then placed in wells containing 600 μL of medium supplemented with 10% FBS. 12 hr later, cells on the upper surface of the filter were detached with a cotton swab and cells on the lower surface of the filters were fixed with ice-cold methanol for 10 min and stained with 0.1% crystal violet for 15 min. The cells were then rinsed with distilled water, photographed and counted. Migration was quantified by counting the migrated cells in ten random microscopic fields.

Active Ras pull-down and detection. Ras activity was determined using a Ras binding domain of Raf1 (RBD) pull-down assay kit (16117, Thermo Fisher Scientific) by following the manufacturer's instructions. Briefly, to determine RBD binding of K-Ras4a WT and -3KR in Ctrl or SIRT2 KD cells, HEK293T cells expressing FLAG-K-Ras4a WT or 3KR were infected with luciferase (Ctrl) shRNA- or human SIRT2 shRNA-carrying lentivirus for 6 hr and cultured in complete medium for another 72 hr. Cells were then serum-starved overnight and treated with 100 ng/mL EGF for 0, 5 and 15 min. At the end of treatment, cells were rinsed with ice-cold 1 × PBS and scraped on ice in lysis buffer containing 25mM Tris pH 7.2, 150 mM NaCl, 5 mM

$MgCl_2$, 1% NP-40 and 5% glycerol and 1 × protease inhibitor cocktail. The samples were collected, vortexed, incubated on ice for 5 min and centrifuged at 16,000 g at 4 °C for 15 min to remove cellular debris. Protein concentration was measured by Bradford assay. Equal amounts of lysate (500 μg) were incubated with RBD-coated agarose beads at 4 °C for 1 hr. The beads were then washed three times with ice-cold lysis buffer, boiled for 5 min at 95 °C, and active Ras was analysed by western blot using Ras-specific antibodies (16117, Thermo Scientific). For comparison to total Ras protein, 1% of total lysates used for pull-down was analysed by immunoblot.

To determine RBD binding of K-Ras4a-G12V and -G12V-3KR in Ctrl or SIRT2 KD cells, HEK293T cells were transfected with pCMV5-FLAG-K-Ras4a-G12V or -G12V-3KR and infected with luciferase (Ctrl) shRNA- or human SIRT2 shRNA-carrying lentivirus 12 hr after the transfection. 72 hr later, cells were cultured in FBS-free or complete medium for another 12 hr before being subjected to RBD pull-down as described above.

K-Ras4a interactome by SILAC. Three SILAC experiments were performed to determine K-Ras4a-G12V or -G12V-3KR interacting proteins: (1) NIH3T3 cells stably overexpressing FLAG-K-Ras4a-G12V cultured in DMEM with [$^{12}C_6$, $^{14}N_2$]-L-lysine and [$^{12}C_6$, $^{14}N_4$]-L-arginine as "light" cells, and NIH3T3 cells stably overexpressing FLAG-K-Ras4a-G12V-3KR cultured in DMEM with [$^{13}C_6$, $^{15}N_2$]-L-lysine and [$^{13}C_6$, $^{15}N_4$]-L-arginine as "heavy" cells. (2) NIH3T3 cells stably overexpressing FLAG-K-Ras4a-G12V-3KR cultured in DMEM with [$^{12}C_6$, $^{14}N_2$]-L-lysine and [$^{12}C_6$, $^{14}N_4$]-L-arginine as "light" cells, and NIH3T3 cells stably overexpressing FLAG-K-Ras4a-G12V cultured in DMEM with [$^{13}C_6$, $^{15}N_2$]-L-lysine and [$^{13}C_6$, $^{15}N_4$]-L-arginine as "heavy" cells. The second group served as the reverse SILAC of the first group. (3) NIH3T3 cells stably overexpressing FLAG-K-Ras4a-G12V and transiently transduced with luciferase (Ctrl) shRNA cultured in DMEM with [$^{13}C_6$, $^{15}N_2$]-L-lysine and [$^{13}C_6$, $^{15}N_4$]-L-arginine as "heavy" cells, and NIH3T3 cells stably overexpressing FLAG-K-Ras4a-G12V and transiently

transduced with mouse Sirt2 shRNA cultured in DMEM with [$^{12}C_6$, $^{14}N_2$]-L-lysine and [$^{12}C_6$, $^{14}N_4$]-L-arginine as “light” cells.

Cells were collected and lysed in 1% NP-40 lysis buffer containing protease inhibitor cocktail. Protein concentration was quantified by Bradford assay, and 8 mg of total protein from each sample was subjected to FLAG IP to enrich FLAG-K-Ras4a-G12V or -G12V-3KR with its interacting proteins. After washing the FLAG resin five times with IP washing buffer, the resins from ‘heavy’ and ‘light’ cells were mixed. Enriched proteins on the resin were eluted with triple FLAG peptide following the manufacturer’s protocol. Eluted proteins were precipitated with methanol/chloroform/water (4/1.5/3 volume ratio with the sample volume set as 1), and the protein pellets were washed twice with 1 mL ice-cold methanol. The protein pellets were air dried for 10-15 min, and subjected to disulfide reduction and protein denaturation in 100 µL of buffer containing 6 M urea, 10 mM DTT and 50 mM Tris-HCl pH 8.0 at room temperature for 1 hr. Then iodoacetamide (final concentration 40 mM) was added to alkylate the proteins at room temperature for 1 hr. Subsequently, DTT (final concentration 40 mM) was added to stop alkylation at room temperature for 1 hr. The samples were then diluted 7 times with buffer containing 1 mM $CaCl_2$ and 50 mM Tris-HCl pH 8.0 and digested with 2 µg trypsin at 37˚C for 12 hr. Trypsin digestion was quenched with 0.2 % trifluoroacetic acid. Then the mixture was desalted using Sep-Pak C18 cartridge following the manufacturer’s protocol and subjected to liquid chromatography (LC)-MS/MS analysis.

The lyophilized peptides were reconstituted in 2% acetonitrile (ACN) with 0.5% formic acid (FA) and analyzed by LTQ-Orbitrap Elite mass spectrometer coupled with nanoLC. Reconstituted peptides were injected onto Acclaim PepMap nano Viper C18 trap column (5 µm, 100 µm × 2 cm, Thermo Dionex) for online desalting and then separated on C18 RP nano column (5 µm, 75 µm × 50 cm, Magic C18, Bruker). The flow rate was 0.3 µL/min, and the

gradient was 5-38% ACN with 0.1% FA from 0-120 min, 38-95% ACN with 0.1% FA from 120-127 min, and 95% ACN with 0.1% FA from 127-135 min. The Orbitrap Elite was operated in positive ion mode with spray voltage 1.6 kV and source temperature 275 ˚C. Data-dependent acquisition (DDA) mode was used by one precursor ions MS survey scan from m/z 375 to 1800 at resolution 120,000 using FT mass analyzer, followed by up to 10 MS/MS scans at resolution 15,000 on 10 most intensive peaks. Collision-induced dissociation (CID) parameters were set with isolation width 2.0 m/z and normalized collision energy at 35%. All data were acquired in Xcalibur 2.2 operation software. MS1 and MS2 data were processed using Sequest HT software within the Proteome Discoverer 1.4.1.14 (PD 1.4, Thermo Scientific).

Detection of lysine fatty acylation on Ras by mass spectrometry. To detect H-Ras lysine fatty acylation, HEK293T cells were transfected with pCMV5-H-Ras for 24 hr and treated with 50 μM Alk14 for another 6 hr. To detect K-Ras4a lysine fatty acylation, HEK293T cells with stable SIRT2 KD were transfected with pCMV5-FLAG-K-Ras4a for 24 hr and treated with or without 50 μM Alk14 for another 6 hr. Cells were collected and lysed in 1% NP-40 lysis buffer with protease inhibitor cocktail. FLAG IP was then performed with 50 mg of total protein lysate to purify FLAG-K-Ras4a or Flag-H-Ras. After washing the FLAG resin three times with IP washing buffer, H-Ras or K-Ras4a was eluted by heating at 95 ºC for 10 min in buffer containing 1% SDS and 50 mM Tris-HCl pH 8.0. After centrifuging at 15,000 g for 2 min, the supernatant was transferred to a new tube and was treated with 300 mM NH_2OH pH 7.4 at 95 ºC for 10 min. The Ras protein was then precipitated by methanol/chloroform and processed (disulfide reduction, denaturing, alkylation and neutralization) as described above. The resultant Ras protein was digested with 2 μg of trypsin at 37˚C for 2 hr in a glass vial (to avoid absorption of the fatty acylated peptide by plastics). Then desalting was done using Sep-Pak C18 cartridge following the manufacturer's protocol.

For the LC-MS/MS analysis of the digested peptides, the same settings described for the SILAC experiment were applied except the LC gradient was 5-95% ACN with 0.1% FA from 0-140 min. The settings for identifying Alk14 modification in Sequest were: two miscleavages for full trypsin with fixed carbamidomethyl modification of cysteine residue, dynamic modifications of 234.198 Da (Alk14) on lysine residue, N-terminal acetylation, methionine oxidation and deamidation of asparagine and glutamine residues. The peptide mass tolerance and fragment mass tolerance values were 15 p.p.m. and 0.8 Da, respectively.

Detection of lysine fatty acylation on endogenous Ras in HCT116 cells. HCT116 cells (parental cells, or cells infected with shCtrl/shSIRT2-carrying lentivirus for 3 days) were cultured with fresh medium containing 50 μM Alk14 for 6 h. Cells were collected and lysed using the same method described above. Pan-Ras immunoprecipitation was performed using pan-Ras (Y13-259) antibody by following manufacturer's protocol. The lysine fatty acylation on endogenous Ras was detected by on-beads click chemistry and in-gel fluorescence using the same method described above. To directly detect lysine fatty acylation on endogenous Ras by mass spectrometry, 200 mg of total lysates from HCT116 cells with SIRT2 KD was used for pan-RAS immunoprecipitation, followed by denaturation, alkylation, neutralization, trypsin digestion and LC-MS/MS analysis using the same method described above.

Statistical analysis. Quantitative imaging data were expressed in box plot as indicated in figure legends. Statistical evaluation of imaging data was done using two-way ANOVA. Other quantitative data were expressed as mean ± SEM (standard error of the mean, shown as error bar). Differences between two groups were examined using unpaired two-tailed Student's t test. The *P* values were indicated (*$P < 0.05$, ** $P < 0.01$, and *** $P < 0.001$). *P* values < 0.05 were considered statistically significant. No statistical tool was used to pre-determine sample size. No blinding was done, no randomization was used, and no sample was excluded from analysis.

5. References

1. Peng, T., Thinon, E. & Hang, H.C. Proteomic analysis of fatty-acylated proteins. *Curr Opin Chem Biol* **30**, 77-86 (2016).
2. Tate, E.W., Kalesh, K.A., Lanyon-Hogg, T., Storck, E.M. & Thinon, E. Global profiling of protein lipidation using chemical proteomic technologies. *Curr Opin Chem Biol* **24**, 48-57 (2015).
3. Lanyon-Hogg, T., Faronato, M., Serwa, R.A. & Tate, E.W. Dynamic Protein Acylation: New Substrates, Mechanisms, and Drug Targets. *Trends Biochem Sci* **42**, 566-581 (2017).
4. Hedo, J.A., Collier, E. & Watkinson, A. Myristyl and palmityl acylation of the insulin receptor. *J Biol Chem* **262**, 954-7 (1987).
5. Stevenson, F.T., Bursten, S.L., Fanton, C., Locksley, R.M. & Lovett, D.H. The 31-kDa precursor of interleukin 1 alpha is myristoylated on specific lysines within the 16-kDa N-terminal propiece. *Proc Natl Acad Sci U S A* **90**, 7245-9 (1993).
6. Bursten, S.L., Locksley, R.M., Ryan, J.L. & Lovett, D.H. Acylation of monocyte and glomerular mesangial cell proteins. Myristyl acylation of the interleukin 1 precursors. *J Clin Invest* **82**, 1479-88 (1988).
7. Pillai, S. & Baltimore, D. Myristoylation and the post-translational acquisition of hydrophobicity by the membrane immunoglobulin heavy-chain polypeptide in B lymphocytes. *Proc Natl Acad Sci U S A* **84**, 7654-8 (1987).
8. Stevenson, F.T., Bursten, S.L., Locksley, R.M. & Lovett, D.H. Myristyl acylation of the tumor necrosis factor alpha precursor on specific lysine residues. *J Exp Med* **176**, 1053-62 (1992).
9. Jiang, H. et al. SIRT6 regulates TNF-a secretion through hydrolysis of long-chain fatty acyl lysine. *Nature* **496**, 110-113 (2013).
10. Jiang, H., Zhang, X. & Lin, H. Lysine fatty acylation promotes lysosomal targeting of TNF-alpha. *Sci Rep* **6**, 24371 (2016).
11. Zhang, X. et al. Identifying the functional contribution of the defatty-acylase activity of SIRT6. *Nat Chem Biol* **12**, 614-20 (2016).
12. Feldman, J.L., Baeza, J. & Denu, J.M. Activation of the protein deacetylase SIRT6 by long-chain fatty acids and widespread deacylation by mammalian sirtuins. *J Biol Chem* **288**, 31350-6 (2013).
13. Bao, X. et al. Identification of 'erasers' for lysine crotonylated histone marks using a chemical proteomics approach. *Elife* **3**(2014).
14. Teng, Y.B. et al. Efficient demyristoylase activity of SIRT2 revealed by kinetic and structural studies. *Sci Rep* **5**, 8529 (2015).
15. Liu, Z. et al. Integrative chemical biology approaches for identification and characterization of "erasers" for fatty-acid-acylated lysine residues within proteins. *Angew Chem Int Ed Engl* **54**, 1149-52 (2015).
16. Tong, Z. et al. SIRT7 Is an RNA-Activated Protein Lysine Deacylase. *ACS Chem Biol* **12**, 300-310 (2017).
17. Malumbres, M. & Barbacid, M. RAS oncogenes: the first 30 years. *Nat Rev Cancer* **3**, 459-65 (2003).
18. Hancock, J.F. Ras proteins: different signals from different locations. *Nat Rev Mol Cell Biol* **4**, 373-84 (2003).
19. Tsai, F.D. et al. K-Ras4A splice variant is widely expressed in cancer and uses a hybrid membrane-targeting motif. *Proc Natl Acad Sci U S A* (2015).
20. Zhao, H. et al. Roles of palmitoylation and the KIKK membrane-targeting motif in

leukemogenesis by oncogenic KRAS4A. *J Hematol Oncol* **8**, 132 (2015).
21. To, M.D. et al. Kras regulatory elements and exon 4A determine mutation specificity in lung cancer. *Nat Genet* **40**, 1240-4 (2008).
22. Nishimura, A. & Linder, M.E. Identification of a novel prenyl and palmitoyl modification at the CaaX motif of Cdc42 that regulates RhoGDI binding. *Mol Cell Biol* **33**, 1417-29 (2013).
23. Kang, R. et al. Neural palmitoyl-proteomics reveals dynamic synaptic palmitoylation. *Nature* **456**, 904-9 (2008).
24. Swaney, D.L., Wenger, C.D. & Coon, J.J. Value of using multiple proteases for large-scale mass spectrometry-based proteomics. *J Proteome Res* **9**, 1323-9 (2010).
25. Zhang, X., Spiegelman, N.A., Nelson, O.D., Jing, H. & Lin, H. SIRT6 regulates Ras-related protein R-Ras2 by lysine defatty-acylation. *Elife* **6**(2017).
26. Zhu, A.Y. et al. Plasmodium falciparum Sir2A preferentially hydrolyzes medium and long chain fatty acyl lysine. *ACS Chem Biol* **7**, 155-9 (2012).
27. North, B.J. & Verdin, E. Mitotic regulation of SIRT2 by cyclin-dependent kinase 1-dependent phosphorylation. *J Biol Chem* **282**, 19546-55 (2007).
28. Hoff, K.G., Avalos, J.L., Sens, K. & Wolberger, C. Insights into the sirtuin mechanism from ternary complexes containing NAD+ and acetylated peptide. *Structure* **14**, 1231-40 (2006).
29. Jackson, M.D., Schmidt, M.T., Oppenheimer, N.J. & Denu, J.M. Mechanism of nicotinamide inhibition and transglycosidation by Sir2 histone/protein deacetylases. *J Biol Chem* **278**, 50985-98 (2003).
30. Du, J. et al. Sirt5 is an NAD-dependent protein lysine demalonylase and desuccinylase. *Science* **334**, 806-809 (2011).
31. Wilson, J.P., Raghavan, A.S., Yang, Y.-Y., Charron, G. & Hang, H.C. Proteomic analysis of fatty-acylated proteins in mammalian cells with chemical reporters reveals S-acylation of histone H3 variants. *Mol. Cell. Proteomics* **10**(2011).
32. Omary, M.B. & Trowbridge, I.S. Covalent binding of fatty acid to the transferrin receptor in cultured human cells. *J Biol Chem* **256**, 4715-8 (1981).
33. Lampson, B.L. et al. Rare codons regulate KRas oncogenesis. *Curr Biol* **23**, 70-5 (2013).
34. Ali, M. et al. Codon bias imposes a targetable limitation on KRAS-driven therapeutic resistance. *Nat Commun* **8**, 15617 (2017).
35. North, B.J. & Verdin, E. Interphase nucleo-cytoplasmic shuttling and localization of SIRT2 during mitosis. *PLoS One* **2**, e784 (2007).
36. Inoue, T. et al. SIRT2, a tubulin deacetylase, acts to block the entry to chromosome condensation in response to mitotic stress. *Oncogene* **26**, 945-57 (2007).
37. Wright, L.P. & Philips, M.R. Thematic review series: lipid posttranslational modifications. CAAX modification and membrane targeting of Ras. *J Lipid Res* **47**, 883-91 (2006).
38. Choy, E. et al. Endomembrane trafficking of ras: the CAAX motif targets proteins to the ER and Golgi. *Cell* **98**, 69-80 (1999).
39. Rocks, O. et al. An acylation cycle regulates localization and activity of palmitoylated Ras isoforms. *Science* **307**, 1746-52 (2005).
40. Ballester, R., Furth, M.E. & Rosen, O.M. Phorbol ester- and protein kinase C-mediated phosphorylation of the cellular Kirsten ras gene product. *J Biol Chem* **262**, 2688-95 (1987).
41. Bivona, T.G. et al. PKC regulates a farnesyl-electrostatic switch on K-Ras that promotes its association with Bcl-XL on mitochondria and induces apoptosis. *Mol Cell* **21**, 481-93 (2006).

42. Jura, N., Scotto-Lavino, E., Sobczyk, A. & Bar-Sagi, D. Differential modification of Ras proteins by ubiquitination. *Mol Cell* **21**, 679-87 (2006).
43. Chiu, V.K. et al. Ras signalling on the endoplasmic reticulum and the Golgi. *Nat Cell Biol* **4**, 343-50 (2002).
44. Lu, A. et al. A clathrin-dependent pathway leads to KRas signaling on late endosomes en route to lysosomes. *J Cell Biol* **184**, 863-79 (2009).
45. Howe, C.L., Valletta, J.S., Rusnak, A.S. & Mobley, W.C. NGF signaling from clathrin-coated vesicles: evidence that signaling endosomes serve as a platform for the Ras-MAPK pathway. *Neuron* **32**, 801-14 (2001).
46. Misaki, R. et al. Palmitoylated Ras proteins traffic through recycling endosomes to the plasma membrane during exocytosis. *J Cell Biol* **191**, 23-9 (2010).
47. Apolloni, A., Prior, I.A., Lindsay, M., Parton, R.G. & Hancock, J.F. H-ras but not K-ras traffics to the plasma membrane through the exocytic pathway. *Mol Cell Biol* **20**, 2475-87 (2000).
48. Fivaz, M. & Meyer, T. Reversible intracellular translocation of KRas but not HRas in hippocampal neurons regulated by Ca2+/calmodulin. *J Cell Biol* **170**, 429-41 (2005).
49. Grant, B.D. & Donaldson, J.G. Pathways and mechanisms of endocytic recycling. *Nat Rev Mol Cell Biol* **10**, 597-608 (2009).
50. Zhou, W. et al. The SIRT2 Deacetylase Stabilizes Slug to Control Malignancy of Basal-like Breast Cancer. *Cell Rep* **17**, 1302-1317 (2016).
51. He, X. et al. SIRT2 activity is required for the survival of C6 glioma cells. *Biochem. Biophys. Res. Comm.* **417**, 468-472 (2012).
52. Liu, P.Y. et al. The histone deacetylase SIRT2 stabilizes Myc oncoproteins. *Cell Death Differ.* **20**, 503-514 (2013).
53. Jing, H. et al. A SIRT2-Selective Inhibitor Promotes c-Myc Oncoprotein Degradation and Exhibits Broad Anticancer Activity. *Cancer Cell* **29**, 297-310 (2016).
54. Zhao, D. et al. Lysine-5 acetylation negatively regulates lactate dehydrogenase A and is decreased in pancreatic cancer. *Cancer cell* **23**, 464-476 (2013).
55. Jing, H. & Lin, H. Sirtuins in epigenetic regulation. *Chem Rev* **115**, 2350-75 (2015).
56. Hu, J., Jing, H. & Lin, H. Sirtuin inhibitors as anticancer agents. *Future Med Chem* **6**, 945-66 (2014).
57. Wang, Y.P. et al. Regulation of G6PD acetylation by SIRT2 and KAT9 modulates NADPH homeostasis and cell survival during oxidative stress. *EMBO J* **33**, 1304-20 (2014).
58. Xu, S.N., Wang, T.S., Li, X. & Wang, Y.P. SIRT2 activates G6PD to enhance NADPH production and promote leukaemia cell proliferation. *Sci Rep* **6**, 32734 (2016).
59. Dekker, F.J. et al. Small-molecule inhibition of APT1 affects Ras localization and signaling. *Nat Chem Biol* **6**, 449-56 (2010).
60. Chandra, A. et al. The GDI-like solubilizing factor PDEdelta sustains the spatial organization and signalling of Ras family proteins. *Nat Cell Biol* **14**, 148-58 (2011).
61. Berndt, N., Hamilton, A.D. & Sebti, S.M. Targeting protein prenylation for cancer therapy. *Nat Rev Cancer* **11**, 775-91 (2011).
62. Rauch, J. et al. Heterogeneous nuclear ribonucleoprotein H blocks MST2-mediated apoptosis in cancer cells by regulating A-Raf transcription. *Cancer Res* **70**, 1679-88 (2010).
63. Rauch, J. et al. Differential localization of A-Raf regulates MST2-mediated apoptosis during epithelial differentiation. *Cell Death Differ* **23**, 1283-95 (2016).
64. Lee, W. et al. The mutation spectrum revealed by paired genome sequences from a lung cancer patient. *Nature* **465**, 473-7 (2010).

65. Imielinski, M. et al. Oncogenic and sorafenib-sensitive ARAF mutations in lung adenocarcinoma. *J Clin Invest* **124**, 1582-6 (2014).
66. Nelson, D.S. et al. Somatic activating ARAF mutations in Langerhans cell histiocytosis. *Blood* **123**, 3152-5 (2014).
67. Hangen, E., Blomgren, K., Benit, P., Kroemer, G. & Modjtahedi, N. Life with or without AIF. *Trends Biochem Sci* **35**, 278-87 (2010).
68. Pylayeva-Gupta, Y., Grabocka, E. & Bar-Sagi, D. RAS oncogenes: weaving a tumorigenic web. *Nat Rev Cancer* **11**, 761-74 (2011).
69. Roy, S., Wyse, B. & Hancock, J.F. H-Ras signaling and K-Ras signaling are differentially dependent on endocytosis. *Mol Cell Biol* **22**, 5128-40 (2002).
70. An, S. et al. A-Raf: A new star of the family of raf kinases. *Crit Rev Biochem Mol Biol* **50**, 520-31 (2015).
71. Buss, J.E. & Sefton, B.M. Direct identification of palmitic acid as the lipid attached to p21ras. *Mol Cell Biol* **6**, 116-22 (1986).
72. Hancock, J.F., Magee, A.I., Childs, J.E. & Marshall, C.J. All ras proteins are polyisoprenylated but only some are palmitoylated. *Cell* **57**, 1167-77 (1989).
73. Drisdel, R.C. & Green, W.N. Labeling and quantifying sites of protein palmitoylation. *Biotechniques* **36**, 276-85 (2004).
74. Forrester, M.T. et al. Site-specific analysis of protein S-acylation by resin-assisted capture. *J Lipid Res* **52**, 393-8 (2011).
75. Zhou, Y. et al. Lipid-Sorting Specificity Encoded in K-Ras Membrane Anchor Regulates Signal Output. *Cell* **168**, 239-251 e16 (2017).
76. Goodwin, J.S. et al. Depalmitoylated Ras traffics to and from the Golgi complex via a nonvesicular pathway. *J Cell Biol* **170**, 261-72 (2005).
77. Wellbrock, C., Karasarides, M. & Marais, R. The RAF proteins take centre stage. *Nat Rev Mol Cell Biol* **5**, 875-85 (2004).
78. Matallanas, D. et al. Raf family kinases: old dogs have learned new tricks. *Genes Cancer* **2**, 232-60 (2011).
79. Weber, C.K. et al. Mitogenic signaling of Ras is regulated by differential interaction with Raf isozymes. *Oncogene* **19**, 169-76 (2000).
80. Williams, J.G. et al. Elucidation of binding determinants and functional consequences of Ras/Raf-cysteine-rich domain interactions. *J Biol Chem* **275**, 22172-9 (2000).
81. Fischer, A. et al. B- and C-RAF display essential differences in their binding to Ras: the isotype-specific N terminus of B-RAF facilitates Ras binding. *J Biol Chem* **282**, 26503-16 (2007).
82. Cox, A.D., Fesik, S.W., Kimmelman, A.C., Luo, J. & Der, C.J. Drugging the undruggable RAS: Mission possible? *Nat Rev Drug Discov* **13**, 828-51 (2014).
83. Shimizu, K. et al. Structure of the Ki-ras gene of the human lung carcinoma cell line Calu-1. *Nature* **304**, 497-500 (1983).
84. Bheda, P., Jing, H., Wolberger, C. & Lin, H. The Substrate Specificity of Sirtuins. *Annu Rev Biochem* (2016).
85. Wilking-Busch, M.J., Ndiaye, M.A., Huang, W. & Ahmad, N. Expression Profile of SIRT2 in Human Melanoma and Implications for Sirtuin-Based Chemotherapy. *Cell Cycle*, 0 (2017).
86. Shah, A.A., Ito, A., Nakata, A. & Yoshida, M. Identification of a Selective SIRT2 Inhibitor and Its Anti-breast Cancer Activity. *Biol Pharm Bull* **39**, 1739-1742 (2016).
87. Moniot, S. et al. Development of 1,2,4-Oxadiazoles as Potent and Selective Inhibitors of the Human Deacetylase Sirtuin 2: Structure-Activity Relationship, X-Ray Crystal Structure and Anticancer Activity. *J Med Chem* (2017).
88. Charron, G. et al. Robust fluorescent detection of protein fatty-acylation with

chemical reporters. *J Am Chem Soc* **131**, 4967-75 (2009).
89. Liu, H. & Naismith, J.H. An efficient one-step site-directed deletion, insertion, single and multiple-site plasmid mutagenesis protocol. *BMC Biotechnol* **8**, 91 (2008).
90. Luo, X. et al. Structure of the Legionella Virulence Factor, SidC Reveals a Unique PI(4)P-Specific Binding Domain Essential for Its Targeting to the Bacterial Phagosome. *PLoS Pathog* **11**, e1004965 (2015).
91. Zurek, N., Sparks, L. & Voeltz, G. Reticulon short hairpin transmembrane domains are used to shape ER tubules. *Traffic* **12**, 28-41 (2011).
92. Choudhury, A. et al. Rab proteins mediate Golgi transport of caveola-internalized glycosphingolipids and correct lipid trafficking in Niemann-Pick C cells. *J Clin Invest* **109**, 1541-50 (2002).
93. Sherer, N.M. et al. Visualization of retroviral replication in living cells reveals budding into multivesicular bodies. *Traffic* **4**, 785-801 (2003).
94. Schindelin, J. et al. Fiji: an open-source platform for biological-image analysis. *Nat Methods* **9**, 676-82 (2012).
95. Du, J., Jiang, H. & Lin, H. Investigating the ADP-ribosyltransferase activity of sirtuins with NAD analogues and 32P-NAD. *Biochemistry* **48**, 2878-90 (2009).
96. Adler, J. & Parmryd, I. Quantifying colocalization by correlation: the Pearson correlation coefficient is superior to the Mander's overlap coefficient. *Cytometry A* **77**, 733-42 (2010).

CHAPTER 4

SUMMARY AND FUTURE PERSPECTIVES

SIRT2 has been closely implicated in cell cycle regulation, stress response, metabolism and differentiation by deacetylating a wide variety of substrates. Targeting SIRT2 for cancer treatment, however, was a topic of debate due to conflicting reports and lack of potent and specific inhibitors. My work in Chapter 2 demonstrated that TM is as a highly potent and selective mechanism-based SIRT2 inhibitor and exhibits broad anticancer activity in part by decreasing the protein level of c-Myc. SIRT2 has been reported by several groups to have lysine defatty-acylase activities in addition to the deacetylase activity, but the substrates and physiological function for its defatty-acylase activity were unknown. In Chapter 3, I identified a Ras protein, K-Ras4a, as a SIRT2 lysine defatty-acylase target and elucidated that the SIRT2-dependent defatty-acylation promotes the oncogenic activity of K-Ras4a. Here I summarize the lessons I learned from these studies and the questions to be addressed in the future.

1. Lessons learned

Phenotype of genetic knockout (KO) mice may not predict the effect of small molecule inhibitors.

A previous study showed that *Sirt2* KO mice tend to develop tumors earlier than wildtype mice [1]. Another study reported that although the spontaneous tumor development phenotype was not observed, tumor development upon DNA damage did increase in *Sirt2* KO mice [2]. So, it was surprising that the SIRT2-selective inhibitor, TM, can inhibit the proliferation of many cancer cell lines tested. I further confirmed with several experiments that SIRT2 inhibition produces the anticancer effects. This suggests the phenotype of genetic knockout mice may not predict the effect of small molecule inhibitors. Sometimes depletion of a protein genetically and

small molecule inhibition may produce different effect. Therefore, getting potent and selective inhibitors is the ultimate way to demonstrate whether a protein is a good anticancer target or not.

Removal of palmitoylation could promote Ras function.

Palmitoylation has been shown to be essential for the plasma membrane association and function of H-Ras and N-Ras. Studies with nonpalmitoylated variants of H-Ras and N-Ras also supports the importance of palmitoylation in RAS-driven tumorigenesis[3,4]. However, my study in Chapter 3 reveals that lysine fatty acylation (palmitoylation) impedes the transforming activity of K-Ras4a, which seemed counter-intuitive. Actually, it has been demonstrated that the dynamic de/reacylation cycle promotes Ras redistribution to cellular membranes where it is active and that depalmitoylation inhibitors inhibit Ras function. Therefore, it is possible that lysine fatty acylation blocks the dynamic acylation cycle of K-Ras4a. Removal of lysine fatty acylation by SIRT2 may facilitate the distribution of K-Ras4a to endomembranes where it recruits A-Raf to promote oncogenic transformation.

Targeting the vulnerabilities of cancer.

Myc hyperactivation or overexpression and K-Ras mutations are among the most common drivers of human cancer. Thus, both Myc and K-Ras are highly pursued cancer drug targets. Despite intensive studies, it remains challenging to target Myc or K-Ras directly. One possible approach to treat Myc- or K-Ras-driven cancers is to identify the 'Achilles' heel' target that is not inherently tumorigenic but essential for the cancer cells to survive. My studies in Chapter 2 suggest that SIRT2 inhibition is a way to target c-Myc indirectly. SIRT2 inhibitor up-regulates the transcription of several c-Myc E3 ubiquitin ligases that promote c-Myc degradation, and thus inhibits cancer cell proliferation. In other word, the survival of certain c-Myc-driven cancer cells relies on SIRT2. In Chapter 3, I demonstrated that SIRT2 promotes K-Ras4a-induced oncogenic transformation, suggesting that SIRT2 inhibition may produce therapeutic benefit in

K-Ras-driven cancers. Therefore, the dependence on SIRT2 may be a vulnerability of Myc- or K-Ras-driven cancer cells, and thus offer an attractive approach for the development of novel anticancer therapeutics.

2. Questions to be addressed and future directions

How does SIRT2 regulate expression of E3 ligases of c-Myc?

In Chapter 2, I showed that TM upregulates several E3 ligases of c-Myc in MCF-7 cells (sensitive to TM) but not in BT-549 cells (resistant to TM). It is unclear how SIRT2 regulates the expression of these E3 ligases and why such regulation was not observed in BT-549 cells. Understanding the mechanism may point out new ways to target c-Myc and also help to predict what tumors may be sensitive to SIRT2 inhibition. Since SIRT2 inhibition by TM affects transcriptional levels of the E3 ligases and SIRT2 is known to act as a histone deacetylase to repress gene expression[2,5], it is possible that SIRT2 could be recruited to the promoter regions of the genes for the E3 ligases to inhibit their expression through histone deacetylation in MCF-7 but not in BT-549 cells. To test this hypothesis in the future, chromatin immunoprecipitation (ChIP) coupled to quantitative real-time PCR and interactome study could be performed to compare chromatin localization and interacting proteins of SIRT2 in the two cell lines. Presumably, the different mechanisms for the chromatin recruitment of SIRT2 could be ascribed to the susceptibility of cells to SIRT2 inhibitor.

What is the stoichiometry of K-Ras4a lysine fatty acylation?

Determining the stoichiometry of lysine fatty acylation would be crucial for us to better understand its functional consequences. Semi-quantification of the fluorescence intensity from Alk14 metabolic labeling results enabled us to roughly estimate the stoichiometries for cysteine palmitoylation and lysine fatty acylation. However, this estimation may not be accurate due to our limited knowledge on the site occupancy of fatty acylation and possible palmitoylation loss

during sample preparation. In the future, development of mass spectrometry analysis that allows precise quantitation of protein lysine fatty acylation will help to address this question and thus will greatly advance our understanding of the complex regulation of Ras proteins by lysine fatty acylation.

How does recruitment of A-Raf to endomembranes promote K-Ras4a-induced transformation?

In Chapter 3, my results indicated that A-Raf is required for the regulation of K-Ras4a by SIRT2-mediated lysine defatty-acylation. I also demonstrated that lysine defatty-acylation promotes the association between K-Ras4a and A-Raf at endomembranes. However, it is unclear how binding of A-Raf to K-Ras4a at endomembranes promote K-Ras4a function. Unlike B-Raf and C-Raf, which are the other two members of the Raf serine/threonine kinase family and promote cellular transformation by activating MEK/ERK MAPK pathway, A-Raf has weak MEK kinase activity and is a less understood Ras effector protein[6]. In line with this, lysine fatty acylation did not affect the activation of ERK, which is downstream of MEK. Therefore, there may be other mechanisms involved in the effect of A-Raf. To elucidate the mechanism, quantitative phosphoproteomics can be conducted to identify A-Raf kinase substrates and compare the phosphorylation status of A-Raf substrates when K-Ras4a WT or the 3KR mutant is expressed. Alternatively, interactome study can be employed to search for A-Raf interacting partners that are regulated by K-Ras4a lysine fatty acylation.

Proteome-wide identification of defatty-acylation substrates for SIRT2.

To better understand the physiological relevance of the defatty-acylase activity of SIRT2, more substrates need to be identified and the corresponding function of lysine fatty acylation need to be investigated. SILAC-based quantitative proteomics coupled with Alk14 metabolic labeling can be conducted to discover SIRT2 targets. Briefly, SIRT2 WT and KO (or KD) cells are cultured in light and heavy medium, respectively, in the presence of Alk14. Proteins are then

extracted and a biotin affinity tag is attached to the Alk14-labeled proteins with click chemistry. The biotin-conjugated proteins are pulled down using streptavidin beads. The proteins with only cysteine fatty acylation can be removed by on-beads hydroxylamine. Samples are then on-beads digested with trypsin and submitted for mass spectrometry analysis. My previous attempts using this method did not lead to successful identification of SIRT2 substrates. The top hits were found to have either no fatty acylation or only cysteine palmitoylation. High background and lack of modification site information are the two major problems of the previous methodology.

In the future, optimization could be done in the following ways. Firstly, one SILAC sample with SIRT2 KO (or KD) cells treated without Alk14 and with Alk14 should be included to rule out proteins that bind to streptavidin beads. Secondly, stringent hydroxylamine treatment and washes could help to remove more proteins with only cysteine fatty acylation and the interacting proteins of the real SIRT2 substrates. Thirdly, RNA-sequencing of the SIRT2 WT and KO (or KD) cells can be performed in parallel to rule out proteins that are regulated by SIRT2 in the transcriptional level. Lastly, biotin-N_3 with a cleavable liner, which allows cleavage to release the captured proteins or peptides on streptavidin beads, could be used. Thus, all the peptides labeled with Alk14 will contain a tag that can be treated as a modification with a unique mass shift for precise location of the modified lysine residue.

Functional contribution of the defatty-acylase activity of SIRT2.

As I have demonstrated with my doctoral studies, SIRT2 possesses not only deacetylase activity, but also defatty-acylase activity. Previous studies have highlighted the functional significance of the SIRT2 deacetylase. My study in Chapter 3 underscores the functional significance of SIRT2 defatty-acylase. However, the multiple enzymatic functions of SIRT2 make it very difficult to dissect the contribution of any certain enzymatic activity by genetically manipulating SIRT2 level in cells. Identification of SIRT2 mutants that have either deacetylase activity or defatty-acylase activity will greatly help us to study the specific function of

deacetylase or defatty-acylase activity of SIRT2. Previous studies in our laboratory have shown that mutating a glycine residue that is conserved in SIRT1-6 to alanine in SIRT6 results in a SIRT6 mutant that has only defatty-acylation activity and lacks deacetylation activity in cells[7]. Moreover, the crystal structure of SIRT2 in complex with a thiomyristoyl peptide BHJH-TM1[8] (PDB 4R8M) revealed that the myristoyl group is accommodated by a hydrophobic pocket. Based on these previous studies, mutating the conserved glycine residue or the key residues in the acyl-binding pocket may provide the best chance to differentiate SIRT2 defatty-acylase activity from deacetylase activity.

Development of inhibitors that target the defatty-acylase activity of SIRT2.

The emerging biological functions, especially cancer relevance, of SIRT2 as a lysine defatty-acylase suggests that inhibitors targeting the defatty-acylase activity of SIRT2 merit further investigation. My studies in Chapter 2 showed that the fatty acylation levels of many proteins were elevated when SIRT2 was knocked down, but not when SIRT2 inhibitor TM was used (Fig. 2.7). Furthermore, TM exerted little effect on the lysine fatty acylation of K-Ras4a, suggesting that TM may selectively target the deacetylase activity of SIRT2. Considering that low K_m value of SIRT2 for fatty acyl substrate, SIRT2 may preferentially bind to fatty acyl substrate rather than TM. Therefore, increasing binding affinity to SIRT2 could be an approach to obtain defatty-acylase inhibitors. Alternatively, as TM binds to SIRT2 in cells, targeted degradation of SIRT2 protein could be achieved by coupling TM to proteolysis-targeting chimera (PROTAC) technology.

3. Reference

1. Kim, H.S. et al. SIRT2 maintains genome integrity and suppresses tumorigenesis through regulating APC/C activity. *Cancer Cell* **20**, 487-99 (2011).
2. Serrano, L. et al. The tumor suppressor SirT2 regulates cell cycle progression and genome stability by modulating the mitotic deposition of H4K20 methylation. *Genes Dev* **27**, 639-53 (2013).

3. Chiu, V.K. et al. Ras signalling on the endoplasmic reticulum and the Golgi. *Nat Cell Biol* **4**, 343-50 (2002).
4. Cuiffo, B. & Ren, R. Palmitoylation of oncogenic NRAS is essential for leukemogenesis. *Blood* **115**, 3598-605 (2010).
5. Eskandarian, H.A. et al. A role for SIRT2-dependent histone H3K18 deacetylation in bacterial infection. *Science* **341**, 1238858 (2013).
6. An, S. et al. A-Raf: A new star of the family of raf kinases. *Crit Rev Biochem Mol Biol* **50**, 520-31 (2015).
7. Zhang, X. et al. Identifying the functional contribution of the defatty-acylase activity of SIRT6. *Nat Chem Biol* **12**, 614-20 (2016).
8. He, B., Hu, J., Zhang, X. & Lin, H. Thiomyristoyl peptides as cell-permeable Sirt6 inhibitors. *Org Biomol Chem* **12**, 7498-502 (2014).